A study of cosmic ray anisotropies in the heliosphere

GODFREY SIBUSISO NKOSI (Hons. B.Sc.)

Thesis accepted in partial fulfillment of the requirements for the degree Magister Scientiae in Physics at the North-West University

Supervisor: Prof. M. S. Potgieter

Assistant Supervisor: Dr. S. E. S. Ferreira

December 2006

Potchefstroom

South Africa

Abstract

The three-dimensional (3D) steady-state electron modulation model of Ferreira (2002), based on Parker (1965) transport equation, is used to study the modulation of the 7 MeV galactic and Jovian electron anisotropies in the inner heliosphere. The Jovian electrons are produced in Jupiter's magnetosphere which is situated at ~ 5 AU in the ecliptic plane. The propagation of these particles is mainly described by the diffusion tensor applicable for the inner heliosphere. Some of the elements of the diffusion tensor are revisited in order to establish what contribution they make to the three-dimensional anisotropy vector and its components in the inner heliosphere. The 'drift' term is neglected since the focus of this study is on low-energy electrons. The effects on the electron anisotropy of different scenarios when changing the solar wind speed from minimum to maximum activity is illustrated. The effects on both the galactic and Jovian electron anisotropy of changing the polar perpendicular coefficient, in particular, are illustrated. It is shown that the computed Jovian electron anisotropy dominates the galactic anisotropy close to the Jovian electron source at ~ 5 AU, as expected, testifying to the validity of the 3D model. For the latitudinal anisotropy, the polar perpendicular diffusion plays a dominant role for Jovian electrons close to the source, with the polar gradient becoming the dominant factor away from the electron source. Of all three anisotropy components, the azimuthal anisotropy is dominant in the equatorial plane close to the source. It is found that there is a large azimuthal gradient close to the source because the low-energy electrons tend to follow the heliospheric magnetic field more closely than higher energy particles. The transition of the solar wind speed from minimum to intermediate to maximum solar activity condition was used to illustrate the modulation of the magnitude of the 7 MeV total anisotropy vector along the Ulysses trajectory. It was found that during the two encounters with the planet a maximum anisotropy of 38% was computed but with different anisotropy-time peaks as the approach to Jupiter was different.

Keywords: Cosmic rays, galactic electrons, Jovian electrons, heliospheric modulation, solar wind, solar activity, transport processes, perpendicular diffusion, cosmic ray anisotropy.

Samevatting

Die drie-dimensionele (3D) stasionêre toestand model vir die modulasie van elektrone van Ferreira (2002), en gebaseer op die transport vergelyking van Parker (1965), is gebruik vir hierdie studie. Die fokus is op die modellering van die 7 MeV galaktiese en Jupiter elektron anisotropie vir die binneste heliosfeer. Die Joviaanse elektrone word in Jupiter se magnetosfeer geproduseer wat by ~ 5 AU in die ekliptiese vlak voorkom. Die voortplanting van hierdie deeltjies word grootliks deur die diffusie- tensor soos van toepassing op die binneste heliosfeer beskryf. Van die elemente van die diffusie-tensor word herbeskou ten einde te bepaal tot watter mate hulle bydra tot die 3D anisotropie-vektor vir lae-energie-elektrone. Die dryfterm is verwaarloos wat 'n goeie aanname is vir hierdie elektrone. Die effek wat die veranderende sonwind het op die elektron anisotropie wanneer dit met sonaktiwiteit verander, is bestudeer. Dit is bevind dat die berekende Joviaanse elektron anisotropie die galaktiese anisotropie domineer naby die bron van elektrone soos wat verwag is. Dit getuig van die geldigheid van die 3D model. Die breedtegraadse anisotropie vir Joviaanse elektrone word grootliks bepaal deur die poolwaartse loodregte diffusie-koëffisiente naby die bron en deur die poolgradiënt wanneer weg beweeg word van die bron. Die asimutale anisotropie is die dominerende komponent in die ekwatoriale vlak omdat die asimutale gradiënt naby die bron baie groot is want hierdie elektrone beweeg meestal langs die magnetiese veldlyne. Die oorgang van die sonwindspoed van son-minimum tot son-maksimum aktiwiteit is gebruik om te illustreer hoe die modulasie die grootte van die 7 MeV totale anisotropie-vektor langs Ulysses-ruimtetuig se baan verander. Die eindresultaat is dat die maksimum waarde van 38% vir die 7 MeV totale anisotropie-vektor bereken is vir die twee episodes waar die ruimtetuig die planeet genader het. Die wyse waarop die intensiteit-tyd pieke in die anisotropie-vektor voorkom verskil egter.

Nomenclature

2D	Two-Dimensional
3D	Three-Dimensional
ADI	Alternating Direction Implicit
AU	Astronomical units = 1.49×10^8 km
CIRs	Corotating Interaction Regions
CME	Coronal Mass Ejection
COSPIN	Cosmic and Solar Particle Investigation
CRs	Cosmic Rays
DCs	Diffusion Coefficients
EPHIN	Electron-Proton Helium Instrument
ESA	European Space Agency
GCRs	Galactic Cosmic Rays
HCS	Heliospheric Current Sheet
HMF	Heliospheric Magnetic Field
KET	Kiel Electron Telescope
LIS	Local Interstellar Spectra
LISM	Local Interstellar Medium
NASA	National Aeronautic and Space Agency
SEPs	Solar Energetic Particles
SOHO	Solar and Heliospheric Observatory
SWOOPS	Solar Wind Observation Over The Polar regions of the Sun
TPE	Transport Equation
TS	Termination Shock

Contents

Chapter 1

Introduction

Galactic cosmic rays (GCRs) are high-energy charged particles with energies larger than ~ 1 MeV that is transported into our solar system and to Earth from the Galaxy. The study of cosmic ray modulation is about the transport of these energetic particles in the region influenced magnetohydrodynamically by the Sun, called the heliosphere. The modulation of cosmic rays (CRs) in the heliosphere is described by the Parker (1965) transport equation which contains all relevant physical processes. Apart from galactic cosmic ray electrons, there is another electron population which is produced in Jupiter's magnetosphere located at ~ 5 AU in the ecliptic plane known as " Jovian electrons" with energies up to at least ~ 30 MeV (Simpson et al., 1974; Teegarden et al., 1974; Chenette et al., 1974) and is of importance for this study. In this study the focused is on modelling the anisotropies of these low-energy electrons in the inner heliosphere (≤ 10 AU).

Since its launch in October 1990 Ulysses has sampled the heliosphere between the Earth and Jupiter in three dimensions continuously and has made excellent observations of CR nuclei and electrons of various energies (Heber et al., 2002). Ulysses observations have also indicated the presence of low-energy electron 'jets' with extraordinary anisotropies off the equatorial plane as far as 2.2 AU from Jupiter. They were observed during the direct encounter in 1992 and during the close encounter in 2004, in the 3-10 MeV range as events with sharp intensity increases and decreases, a strong field-aligned anisotropy, and durations of up to a few hours. These observations are very interesting features of the Jovian electron intensity-time profiles and are important in evaluating and testing the propagation modulation models.

A three-dimensional (3D), steady-state, electron modulation model (Ferreira, 2002) which describes the relevant physical process of the heliospheric transport and modulation of low-energy (< 30 MeV) Jovian and galactic electrons is used to study the three components of the anisotropy vector for these low-energy electrons in the inner heliosphere. This has not been done with a comprehensive 3D model before. The purpose

is to establish what the well-known modulation processes and mechanisms contribute to the electron anisotropy.

Recently Ferreira (2001a) and Moeketsi (2004) established the relationship between the latitudinal dependence of the solar wind speed and heliospheric perpendicular diffusion, and how the transition was made between solar maximum and solar minimum. The effects of this introduced latitude dependence on low-energy (~ 7 MeV) Jovian and galactic electron modulation were illustrated between the model solution and the 3-10 MeV KET observations.

The main focus of this work is to study the three components of the anisotropy vector, in particular the role that polar perpendicular diffusion plays in determining the electron anisotropy in the inner heliosphere for low-energy (~ 7 MeV) Jovian and galactic electrons.

The structure and chapters of this work are as follows:

Chapter 2: This chapter gives an introduction to cosmic rays and the heliosphere, with all the concepts and definitions used in this study. Lastly the Ulysses mission is discussed together with the Kiel Electron Telescope (KET) which has provided exceptional observational electron data.

Chapter 3: In this chapter, the propagation and modulation of the low-energy (3-30 MeV) electrons, in particular the Jovian electrons in the inner heliosphere are discussed. It begins with an introduction to the sources of these low-energy electrons, followed by a brief overview of the 3D electron propagation models. Lastly, a brief discussion on the modulation and source spectrum of Jovian electrons is given.

Chapter 4: This chapter begins with an introduction to the cosmic ray transport equation (Parker, 1965) which combines the four major processes that cosmic rays undergo when entering the heliosphere. The diffusion tensor is discussed as used in this work.

Chapter 5: A short description of the 3D steady-state electron modulation model (Ferreira, 2002) used in this study is given. The effect of changing the grid size in the radial direction in the model is given.

Chapter 6: The transition of the average solar wind speed from solar minimum to intermediate to solar maximum activity conditions, with corresponding scenarios of the

heliospheric polar diffusion, are illustrated for the modulation of the low-energy electron differential intensities and gradients in the inner heliosphere.

Chapter 7: The chapter begins by introducing the reader to the anisotropy vector components. The effect of polar perpendicular diffusion on Jovian and galactic electron anisotropy components is illustrated. The different scenarios for the enhancement of perpendicular diffusion assumed to correspond to different solar activity conditions are illustrated for the anisotropy components. Lastly, these different scenarios are used to study the modulation of Jovian electron anisotropy along the Ulysses trajectory.

Chapter 8: In this final chapter a summary and conclusions are given.

This work was personally presented during the South African Institute of Physics conferences (SAIP) in Pretoria (July 2005) and in Cape Town (July 2006). This work also formed part of the poster presentation at the 29th International Cosmic Ray Conference in Pune, India by Potgieter et al. (2005).

Chapter 2

Cosmic rays, the Sun and the Heliosphere

2.1 Introduction

Within the heliosphere and nearby interstellar space exist energetic charged particle populations of a very wide energy range. With most of our heliosphere as well as interstellar space still unexplored it is likely that new aspects of the characteristics of these energetic particle populations will be identified in future. It is well established that dynamic, magnetized plasmas of all astrophysical scales are frequently the source of large fluxes of energetic ions and electrons. The composition, energy spectra, temporal and spatial variation and arrival directions of these different components contains information on the location of these plasmas, their dynamics as well as the nature of the medium traversed by the particles.

This chapter gives an overview of the basic features and knowledge of cosmic rays and the heliosphere. It starts with the description of cosmic rays, the Sun, the solar wind plasma, heliosphere and the heliospheric magnetic field (HMF), the current sheet and the solar cycle variations. The Ulysses space mission is discussed as related to the Kiel Electron Telescope (KET) instrument which provides a wide range of observations of cosmic rays in particular of electron data at low-energies.

2.2. Cosmic rays in the heliosphere

Cosmic rays (CRs) are charged energetic particles, which after being accelerated to very high velocities at supernova shocks propagate throughout the galaxy. These particles were discovered on Earth by Victor Hess during the historic balloon flights between 1911 and 1912 when it was shown that the origin of these particles was extraterrestrial. These particles were called 'cosmic rays' by Millikan in 1925. By 1930, Compton and Clay had shown that these particles were electrically charged (for a review see, Simpson, 1997). CRs are defined to be fully ionized energetic particle with kinetic energy E greater than a

few hundred keV to as high as 3 x 10^{21} eV. Those that are detected on Earth consist of ~ 97% protons, ~ 2% electrons and positrons and ~ 1% heavier nuclei (e.g., Longair, 1990: Simpson, 1992). CRs can be divided into different populations:

(1) Galactic cosmic rays (GCRs) originate from far outside our solar system. These particles are accelerated during supernova explosions, and it is generally believed that subsequent blast waves are responsible for the acceleration (see detailed review by Jones and Ellison, 1991).

(2) Solar energetic particles (SEPs) originating from solar flares (e.g., Forbush, 1946). Coronal mass ejection (CMEs) and the interplanetary medium can also produce these energetic particles. SEPs may have energies up to several hundred MeV but are usually observed at Earth only for several hours when occurring.

(3) Anomalous cosmic rays (ACRs) are formed due to ionization of the interstellar neutral atoms relatively close to the Sun which then get transported to and accelerated at the solar wind termination shock (e.g., Garcia-Munoz et al., 1973; Fisk et al.,1974; Fichtner, 2001a)

Jovian electrons originate from Jupiter's magnetosphere. It was discovered with the fly by of the Pioneer 10 spacecraft in 1973 that the Jovian magnetosphere at ~ 5 AU in the equatorial region is a relatively strong source of electrons with energies up to at least ~ 30 MeV (Simpson et al., 1974; Teegarden et al., 1974; Chenette et al., 1974).

2.3. The Sun, solar wind and solar activity

Our nearest star, the Sun is located at an average distance of 1 AU from the planet Earth. The Sun has a differential rotation period which increases in latitude from an average value of ~ 25 days at the equator to ~ 32 days near the polar regions. The Sun's chemical composition is mainly hydrogen (~ 90%) and helium (~ 10%) with traces of heavier elements. The interior of the Sun is divided into four zones.

(1) The core. This is the high density, high temperature region at the center of the Sun, where thermonuclear energy production takes place. The core extends from

the center of the Sun and contains half of the solar mass. Practically all the Sun's energy production takes place in this region.

(2) The radiative zone. The energy produced in the core is transported through the core and the radiative zone by gamma ray diffusion.

(3) The convective zone. This zone is located in the uppermost 30% of the solar interior. In this region the solar material is convectionally unstable, because the radial temperature gradient is large.

(4) The atmosphere. The solar atmosphere consists of four layers. The lowest is the thin and dense photosphere which emits most of the sunlight and the temperature is about 5 770 K. The next layer is the chromosphere, where the temperature increases from 4 200 K to ~ 10^4 K. The chromosphere is followed by a very narrow transition layer where the temperature increases from ~ 10^4 K to ~ 10^6 K. The uppermost layer of the solar atmosphere is the solar corona. This region extends into the interplanetary space where it becomes the solar wind.

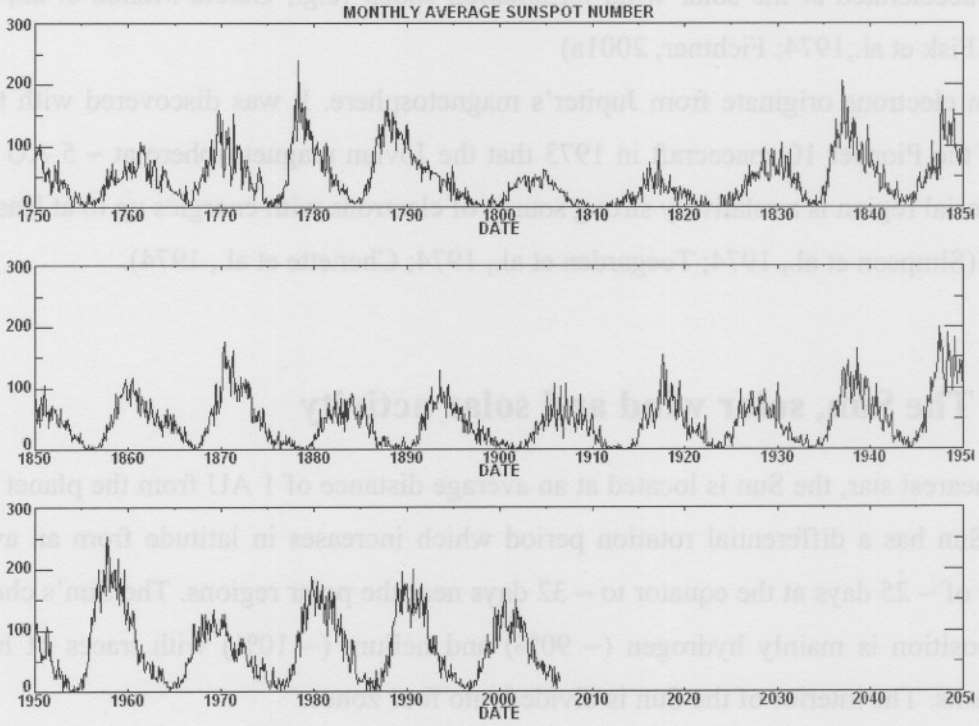

Figure (2.1): Monthly averaged sunspot number from the year 1749 up to 2005 (adapted from http://solarscience.msfc.nasa.gov/SunspotCycle.shtml).

Visible on the photosphere of the Sun are sunspots, dark areas of irregular shape that are cooler than the surrounding solar surface and strong magnetic fields are also associated with them. Detailed records of the sunspot numbers, which are direct indication of the level of solar activity have been kept since 1749 and are shown in Figure (2.1) up to the end of 2005. From these monthly averages, it is evident that the Sun has a quasi-periodic ~ 11 year cycle called the solar activity cycle. Every 11 years the Sun goes through a period of fewer and smaller sunspots called solar minimum followed by a period of larger and more sunspots called solar maximum.

The solar wind (originally called "solar corpuscular radiation") was first proposed by Bierman, as reviewed by Fichtner (2001a) to account for the behavior of the comet tails that always pointed directly away from the Sun regardless of the position of the comet. Bierman's estimates of the solar wind speed, V, ranged between 400 – 1000 km.s^{-1} which where remarkable accurate. However, the name 'solar wind' was first introduced by Parker (1958). It was observationally confirmed in 1959 by the Soviet Lunar 3 spacecraft and has been the object of study ever since (for a review see, Marsch et al., 2003).

Observations made over many years showed that V is not uniform over all latitude and can be divided into the fast solar wind and the slow solar wind. The basic reason is that the Sun's magnetic field dominates the original outflow of the solar wind (e.g., Smith, 2000). If the solar magnetic field is perpendicular to the radial outflow of the solar wind it can prevent the outflow. This is usually the case at low latitudes where the Sun's magnetic field lines are parallel to the surface of the Sun. These field lines are in the form of loops which begin and end on the surface and stretch around the Sun to form the streamer belts as shown in Figure (2.2). These streamer belts are regarded as the most plausible sources of the slow solar wind speed which has typical average velocity of up to $V = 400$ km.s^{-1}(e.g., Schwenn, 1983; Marsch, 1991; Phillips et al., 1995; McComas, et al., 1998; McComas et al., 2002a). Other indications are that the slow solar wind speed may arise from the edges of large coronal holes or from smaller coronal holes (e.g., Hundhausen, 1977; McComas, 2000; McComas et al., 2002a). In the region where the solar magnetic fields are directly radial outward, such as at the solar polar regions, the magnetic field will assist rather than oppose the coronal outflow.

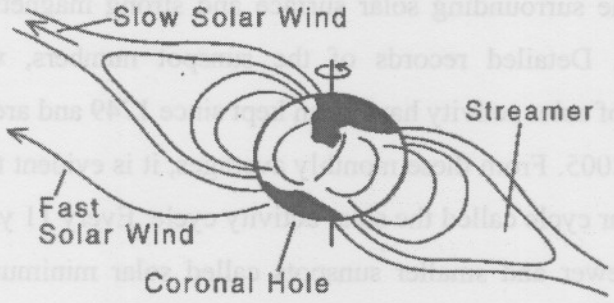

Figure (2.2): The solar magnetic field sketched for the declining phase of the solar cycle illustrating polar coronal holes (shade regions) and streamers as sources of fast and slow solar wind speed (adapted from Suess et al., 1998).

The fast solar wind speed with a characteristic speed of up to $V = 800$ km.s^{-1} are associated with polar coronal holes at the higher heliographic latitudes (e.g., Krieger et al., 1973; Nolte et al., 1976; Zirker, 1977; McComas, 2000; McComas et al., 2002b; Neugebauer et al., 2002, 2003; Hu et al., 2003) illustrated in Figure (2.2). In these regions the magnetic field lines are open and frozen into the solar wind and carried into the interplanetary space. These magnetic field lines affect the transport of the CRs in the heliosphere. The fast solar wind from the polar region can sometimes extend close to the equator and overtake the earlier emitted slow stream resulting in corotating interaction regions (CIRs); for review, see Odstrcil (2003).

The latitudinal dependence of V during solar minimum activity has been confirm by Ulysses observations (e.g., Phillips et al., 1994; 1995) and is shown in Figure (2.3) as six hour averages during the fast pole to pole transit (fast latitude scan) of the Ulysses spacecraft. Ulysses is the first spacecraft to explore both equator and polar regions of the Sun and its mission is discussed in section 2.8. Evident from Figure (2.3) are significant variations of V with heliolatitude where Ulysses has observed a high solar wind speed, 700 – 800 km.s^{-1}, at latitudes $\geq 20^0$ S. In the $\sim 20^0$ S to the $\sim 20^0$ N band it observed medium to slow speeds, increasing again to 700 – 800 km.s^{-1} at $\sim 20^0$ N, thus confirming the existence of the fast and slow solar wind streams during solar minimum. For solar maximum no well defined high speed solar wind is observed (e.g., Richardson et al., 2001).

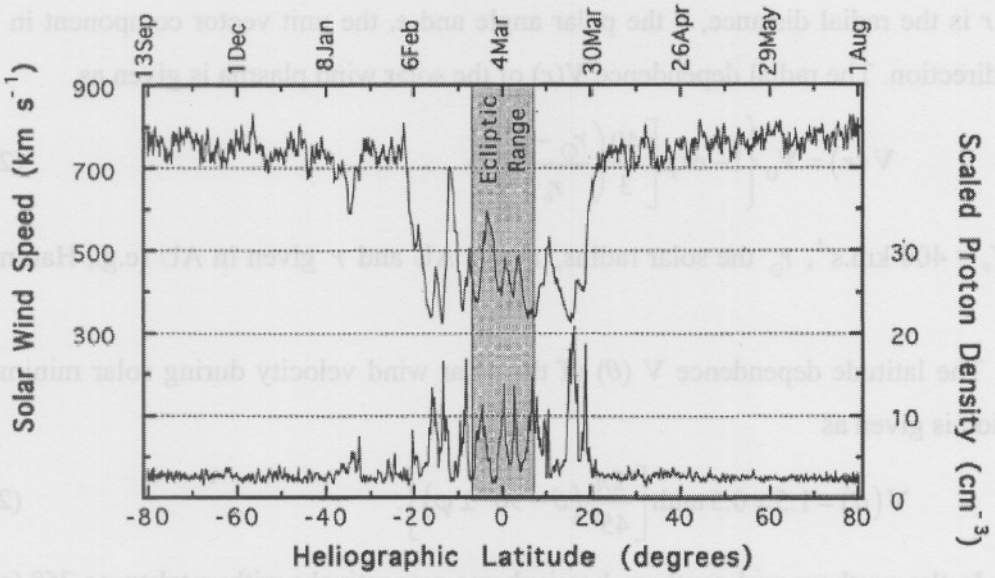

Figure (2.3): Solar wind speed and density from pole to pole. The upper data plot shows the relatively structureless wind with speeds in excess of 700 km.s^{-1} above ± 20^0 heliolatitude. At lower heliolatitude, the wind has a lot of structure and average speeds of ~ 400 km.s^{-1}. The density (bottom trace) has been corrected for radial dependence by multiplying by r^2. This scale density is basically anticorrelated with the speed, being low in the fast wind and highly variable, in the slow wind (where high density peaks correlate with low speed minima). The vertical lines show the range of latitudes (± 7.25^0) surveyed by previous in-ecliptic spacecraft and indicate the enormous increase in heliolatitude coverage made possible by Ulysses (adapted from Phillips et al., 1995).

The radial dependence of V between 0.1 AU and 1.0 AU was studied by e.g., Kojima et al. (1991) and Sheeley et al. (1997). They have found that both the low and high speed winds accelerate within 0.1 AU of the Sun and become a steady flow at 0.3 AU. Using measurements from Pioneer 10 and 11 and Voyager 1 and 2, Gazis et al. (1994) and Richardson et al., (2001) have found that the average solar wind speed does not vary with distance up to 50 AU. However, it does show solar cycle dependence with values about 20% higher during solar minimum than during solar maximum. At solar maximum there is a mixture of high and low speed winds in the region of the equator (Gazis et al., 1991; McComas et al., 2002a).

The average solar wind velocity **V** is modeled as

$$\mathbf{V}\,(r,\theta) = \mathbf{V}(r,\theta)\;\mathbf{e}_r = \mathbf{V}(r)\,\mathbf{V}(\theta)\,\mathbf{e}_r, \tag{2.1}$$

where r is the radial distance, θ the polar angle and $\mathbf{e}_r$ the unit vector component in the radial direction. The radial dependence $\mathbf{V}(r)$ of the solar wind plasma is given as

$$\mathbf{V}(r) = \mathbf{V}_o\left\{1-\exp\left[\frac{40}{3}\left(\frac{r_\odot - r}{r_o}\right)\right]\right\}, \tag{2.2}$$

with $\mathbf{V}_o$ = 400 km.s^{-1}, $r_\odot$ the solar radius, r_0 = 1 AU and r given in AU (e.g., Hattingh, 1998).

The latitude dependence $\mathbf{V}\,(\theta)$ of the solar wind velocity during solar minimum condition is given as

$$\mathbf{V}(\theta) = 1.5 \mp 0.5\tanh\left[\frac{2\pi}{45^\circ}\left(\theta - 90^\circ \pm \varphi\right)\right]. \tag{2.3}$$

In the northern and southern hemispheres respectively with φ taken as 35° (e.g., Hattingh, 1998). For solar maximum condition no latitudinal dependence is assume, so that

$$\mathbf{V}\,(\theta) = \mathbf{V}_o. \tag{2.4}$$

Figure (2.4), panel (a) shows the latitude dependence of $\mathbf{V}$ as a function of radial distance for $r \geq 0.3$ AU for both solar maxima and minima. $\mathbf{V}$ = 800 km.s^{-1} in the fast solar wind speed region and in the slow solar wind region $\mathbf{V}$ = 400 km.s^{-1} for solar minimum conditions. For solar maximum condition, $\mathbf{V}$ = 400 km.s^{-1} for all θ. Figure (2.4), panel (b) shows $\mathbf{V}$ as a function of r for both the fast and slow solar wind streams. From this follows that the acceleration of the solar wind occurs rather rapidly close to the Sun and reaches a constant speed ~ 0.3 AU away from the Sun for both solar wind streams.

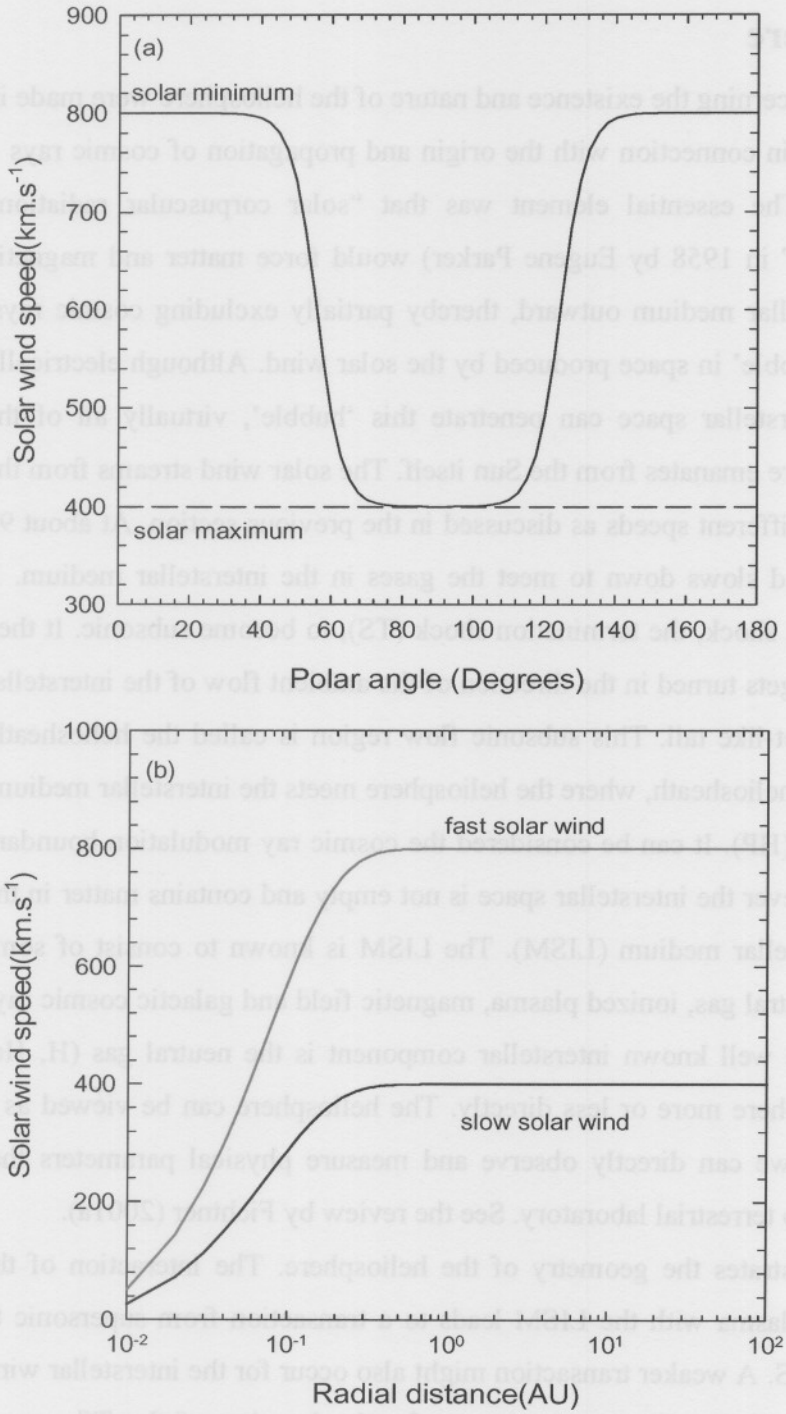

Figure (2.4): Panel (a) shows the modelled solar wind speed V as a function of polar angle θ for $r \geq 0.3$ AU, for solar maximum and solar minimum. Panel (b) shows the modelled V as a function of radial distance r for both the fast and slow solar wind streams. In the fast speed region $V = 800$ km.s^{-1} and in the slow solar wind speed region $V = 400$ km.s^{-1}.

2.4 The heliosphere

The first suggestions concerning the existence and nature of the heliosphere were made in 1955 by Leverett Davis in connection with the origin and propagation of cosmic rays – see Fichtner (2001a). The essential element was that "solar corpuscular radiation" (termed the "solar wind" in 1958 by Eugene Parker) would force matter and magnetic flux in the local interstellar medium outward, thereby partially excluding cosmic rays. The heliosphere is a 'bubble' in space produced by the solar wind. Although electrically neutral atoms from interstellar space can penetrate this 'bubble', virtually all of the material in the heliosphere emanates from the Sun itself. The solar wind streams from the Sun in all directions at different speeds as discussed in the previous section. At about 90 AU, this supersonic wind slows down to meet the gases in the interstellar medium. It must first pass through a shock, the termination shock (TS), to become subsonic. It then slows down further and gets turned in the direction of the ambient flow of the interstellar medium to form a comet-like tail. This subsonic flow region is called the heliosheath. The outer surface of the heliosheath, where the heliosphere meets the interstellar medium, is called the heliopause (HP). It can be considered the cosmic ray modulation boundary of the heliosphere. However the interstellar space is not empty and contains matter in the form of the local interstellar medium (LISM). The LISM is known to consist of some combination of dust, neutral gas, ionized plasma, magnetic field and galactic cosmic rays (e.g., Smith, 2001). The well known interstellar component is the neutral gas (H, He) which enters the heliosphere more or less directly. The heliosphere can be viewed as a huge laboratory where we can directly observe and measure physical parameters that cannot be scaled down to terrestrial laboratory. See the review by Fichtner (2001a).

Figure (2.5) illustrates the geometry of the heliosphere. The interaction of the supersonic solar wind plasma with the LISM leads to a transaction from supersonic to subsonic speeds at the TS. A weaker transaction might also occur for the interstellar wind at the heliospheric bow shock. Previous estimates for the location of the TS ranged between ~ 70 AU and ~ 100 AU (e.g., Stone et al., 1996; Whang and Burlaga, 2000). This position depends also on solar activity. Recently, Voyager 1 observed the TS at 94 AU (Stone et al., 2005). In this study the TS is not considered because the focus is on modulation of low energy electrons in the inner heliosphere ($r < 10$ AU).

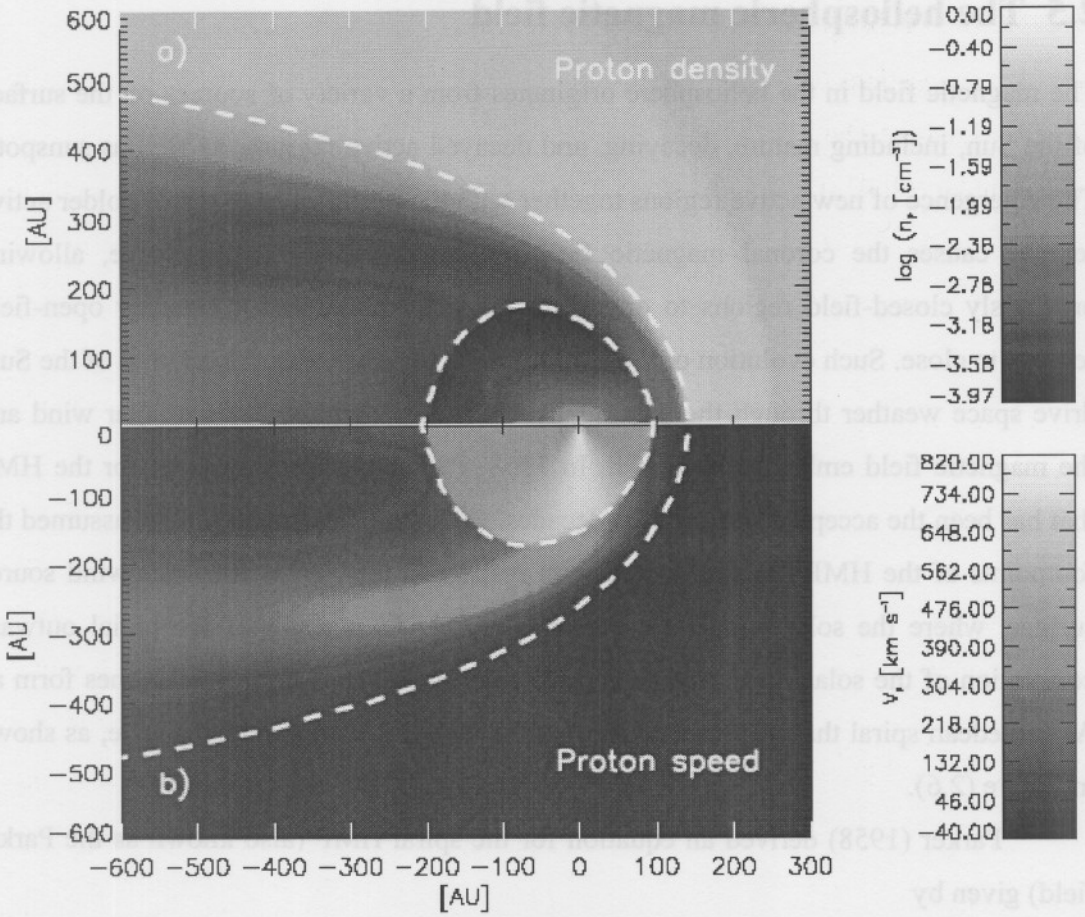

Figure (2.5): Contour plot of the heliosphere showing the computed proton number density (top) and proton speed (bottom). Shown by the dashed lines are the positions of the termination shock and the heliopause (adapted from Ferreira and Scherer, 2004).

The heliopause it believed to lie between 100 and 150 AU from the Sun in the direction in which the Sun is moving, but much further out downstream (e.g., Scherer and Ferreira, 2004). Additionally, the heliopause probably fluctuates in response to changes in the ISM and solar wind conditions. The thickness of the heliopause is still unknown but could be tens of AU. Upstream of the heliopause, in the LISM, theory suggests the existence of a bow shock where the interstellar wind first reacts to its impending 'collision' with the Sun's magnetic field.

2.5 The heliospheric magnetic field

The magnetic field in the heliosphere originates from a variety of sources on the surface of the Sun, including mature, decaying, and decayed active regions, as well as sunspots. The emergence of new active regions together with the dispersal of flux from older active regions causes the coronal magnetic field topology to continually evolve, allowing previously closed-field regions to open into the heliosphere and previously open-field regions to close. Such evolution of the coronal field, together with the rotation of the Sun, drive space weather through the continually changing conditions of the solar wind and the magnetic field embedded within it. In 1958, Parker put forth a model for the HMF that has been the accepted standard for decades. In this model, Parker (1958) assumed the footpoints of the HMF remains rooted with respect to the Sun at the solar wind source surface, where the solar wind flow becomes radial. As a result of the radial outward convection of the solar wind plasma and the rotation of the Sun, the field lines form an Archimedean spiral that lies on the cones of the constant heliographic latitude, as shown in Figure (2.6).

Parker (1958) derived an equation for the spiral HMF (also known as the Parker field) given by

$$\mathbf{B} = \frac{B_0 r_0^2}{r^2}\left(\mathbf{e}_r - \tan\psi \mathbf{e}_\phi\right), \tag{2.5}$$

where $\mathbf{B}$ is the HMF with components in the radial $\mathbf{e}_r$ and azimuthal $\mathbf{e}_\phi$ directions respectively, B_0 is the magnitude of the HMF an average ~ 5 nT at Earth, r_0 = 1 AU, and the direction of the HMF lines at a certain position.
It is mathematically expressed as

$$\psi = \arctan\left[\frac{\Omega(r - r_\odot)}{V}\right], \tag{2.6}$$

with Ω the angular velocity of the Sun about its rotational axis, $r_\odot$ the solar radius and V the solar wind speed. The spiral angle ψ is the angle between the radial direction and the average HMF at a certain position. It indicates how tightly wound is the spiral structure of the HMF lines.

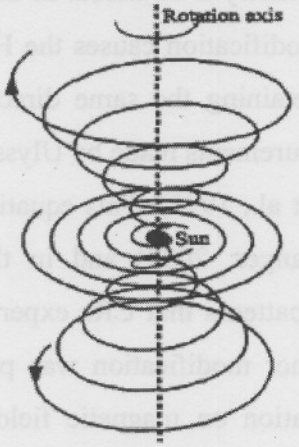

Figure (2.6): A three-dimensional (3D) representation by Hattingh (1998) of the Parker HMF spiral structure with the Sun at the centre. Spirals rotate around the polar axis for $\theta = 45^0$, $\theta = 90^0$ and $\theta = 135^0$.

At high latitudes the spiral angle is less tightly wound and the fields are nearly radial. Substituting equation (2.6) into (2.5) yields

$$B = \frac{B_0 r_0^2}{r^2}\sqrt{1+\left[\frac{\Omega(r-r_\odot)\sin\theta}{V}\right]^2}, \qquad (2.7)$$

for the magnitude of the Parker HMF throughout the heliosphere. The polar angle $\theta = 0^0$ at the polar axis of the Sun with $\theta = 90^0$ at the equatorial plane. However, at high latitude the geometry of HMF is not just an ordinary Parker spiral as argued by Jokipii and Kóta (1989). The solar surface, where the feet of the field lines occur is not a smooth surface, but a granular turbulent surface that keeps changing with time, especially in the polar regions. This may cause the footpoint of the polar field lines to wonder randomly, creating transverse components in the field and thus causing temporal deviation from smooth Parker geometry. The effect of the more turbulent magnetic field in these regions is to increase the mean magnetic field strength. Thus Jokipii and Kóta (1989) suggested a modification to Equation (2.7) so that

$$B = \frac{B_0 r_0^2}{r^2}\sqrt{1+\left[\frac{\Omega(r-r_\odot)\sin\theta}{V}\right]^2+\left(\frac{r\delta_m}{r_\odot}\right)}, \qquad (2.8)$$

for $\delta_m = 0$ the standard Parker geometry is obtained. In this work it is assumed that $\delta_m = 0.002$ (Haasbroek, 1993). This modification causes the HMF to vary as $1/r$ throughout most of the heliosphere while retaining the same direction as the Parker field. This modification is supported by measurements made by Ulysses of HMF in the polar regions of the heliosphere (e.g., Balogh et al., 1995). This equation is used in most modulation models (e.g., Ferreira, 2002; Langer, 2004) and in this work. A purpose of this modification is to alter the drift patterns that CRs experience by reducing them in the heliospheric polar regions. Another modification was proposed by Smith and Bieber (1991) who based their modification on magnetic field data. This modification also changes the geometry of the magnetic field strength over the poles. For an implementation of this modification model see Haasbroek (1997). An alternative model for HMF has been proposed by Fisk (1996) based on the argument that the Sun does not rotate rigidly, but rather differentially with the solar poles rotating ~ 20% faster than the solar equator (e.g., Snodgrass, 1983). As a result of the complexity of this field, it is not incorporated in the numerical modulation model used in this study. For more information from cosmic ray point of view about this field the reader is referred to Kóta and Jokipii (1997, 1999), van Niekerk (2000), Burger and Hattingh (2001), Krüger (2005), and references therein. For a recent review, see Burger (2005).

2.6 Heliospheric current sheet

The existence of a heliospheric current sheet (HCS), originally called an interplanetary sector boundary, and has been known since it was first identified by Wilcox and Ness (1965). The HCS separates regions of the solar wind where the magnetic field points toward or away from the Sun. Since the magnetic and the rotational axis are not aligned, the rotation of the Sun causes the HCS to have a warped or wavy structure. The angle between the Sun's rotational axis and the magnetic axis is known as the tilt angle α where larger α corresponds to a larger latitudinal extend of the HCS (for a recent review, see Smith, 2001). The waviness of the HCS is correlated to the solar activity of the Sun. During solar maximum, the α increases to as much as $\alpha \approx 75^0$ and during solar minimum

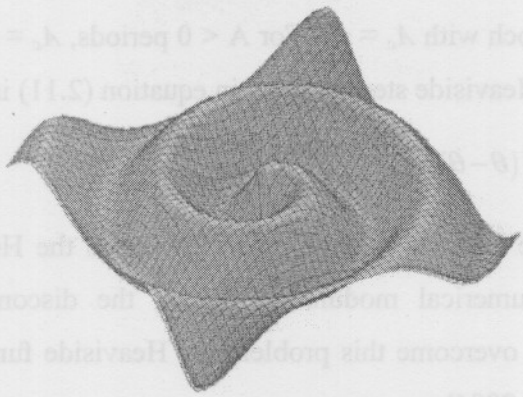

Figure (2.7): A schematic 3D idealization of the HCS configuration for the first 10 AU when $\alpha = 25^0$. The Sun is in the centre. (From Ferreira, 2002).

the axis of the magnetic equator and the heliographic equator becomes nearly aligned, causing relatively small current waviness with $\alpha \sim 5^0$ to 10^0. The wavy structure of the HCS is carried out radially by the solar wind plasma shown in Figure (2.7). The figure shows a 3D idealization of the HCS for the first 10 AU when $\alpha = 25^0$. The HCS plays an important role in CR modulation affecting the drift motions (Jokipii et al., 1977; Potgieter and Moraal, 1985). Because the HMF above and below the HCS is oppositely directed, CRs experience particle drifts along the HCS. Fully three dimensional simulations of CR transport with a realistic three-dimensional HCS have been done by e.g. Kóta and Jokipii (1983) and Hattingh and Burger (1995b). For a constant and radial solar wind speed, the HCS satisfies the equation given by Jokipii and Thomas (1981):

$$\theta' = \frac{\pi}{2} + \sin^{-1}\left\{\sin\alpha \sin\left[\phi + \frac{\Omega(r-r_0)}{V}\right]\right\}, \tag{2.9}$$

for small values of α this equation can be reduced to

$$\theta' = \frac{\pi}{2} + \alpha \sin\left[\phi + \frac{\Omega(r-r_0)}{V}\right], \tag{2.10}$$

to include the polarity of the HMF, Equation (2.5) is modified so that

$$\mathbf{B} = A_c \frac{B_0 r_0^2}{r^2}(\mathbf{e}_r - \tan\psi \mathbf{e}_\phi)\left[1 - 2H(\theta - \theta')\right], \tag{2.11}$$

with θ' the polar angle of the HCS and $A_c = \pm 1$ a constant determining the polarity of the HMF which alternates every 11 years in value. Periods when the magnetic fields lines are

directed outward in the northern hemisphere and inward in the southern hemisphere are called A > 0 polarity epoch with A_c = +1. For A < 0 periods, A_c = -1 and the direction of the HMF reverses. The Heaviside step function in equation (2.11) is given by

$$H(\theta-\theta')=\begin{cases}0 & \text{when} \quad \theta<\theta' \\ 1 & \text{when} \quad \theta>\theta', \end{cases} \tag{2.12}$$

This function causes the HMF to change polarities across the HCS. If this function is used directly in the numerical modulation model, the discontinuity causes severe numerical problems. To overcome this problem the Heaviside function is approximated (Hattingh, 1998; Langer, 2004):

$$H(\theta-\theta')\approx \tanh\left[2.75(\theta-\theta')\right]. \tag{2.13}$$

2.7 Solar cycle variations

As mentioned in the beginning of this chapter, the measurement of sunspot number shown in Figure (2.1) indicates that the Sun has a quasi-periodic ~ 11 year cycle called the solar activity cycle. Every 11 years the Sun goes through a period of fewer and smaller sunspots called solar minimum followed by a period of larger and more sunspots called solar maximum. The effect of solar cycle variations in the Sun's magnetic dipole angle have considerable effects on the structure of the HCS with the tilt angle α following the changes in magnetic dipole angle of the Sun which is nearly aligned with the Sun's rotational axis near solar minimum and almost equatorial at solar maximum (Hoeksema, 1992). Figure (2.8) shows α from the first value recorded in 1976 until recently. Two different models for α are shown namely the "classic" and the "new" model.

It is evident that α varies from small to a larger value between solar minimum and solar maximum (shaded-band) tracing out the 11 year solar cycle. For a discussion of the modulation effects caused by the differences between the two approaches, see Ferreira and Potgieter (2004). Interesting is that the duration of extreme solar maxima (shaded-regions) differs.

The record of the long-term solar modulation of CRs in the heliosphere, e.g. recorded by the Hermanus neutron monitor, shows a clear 11-year modulation cycle

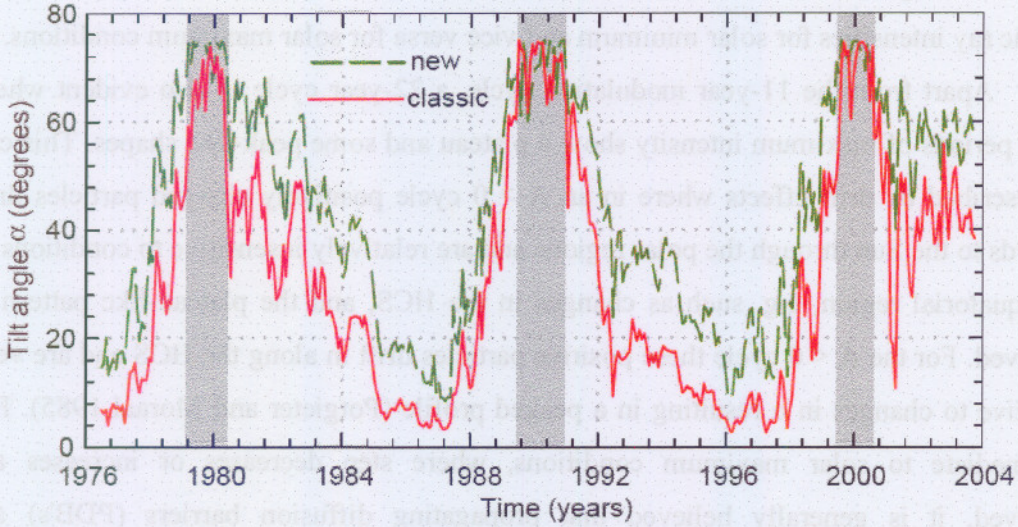

Figure (2.8): The tilt angle α from the first value recorded in 1976 until recently. Two different models for tilt angles are shown namely "classic" (dashed line) and "new" (solid line). The "classic" model uses a line-of-sight boundary condition and the "new" model uses radial boundary condition at the photosphere. (Wilcox Solar Obsevatory:http://sun.stanford.edu; see also Hoeksema, 1992). The shaded parts indicate periods of the reversal of the HMF polarity.

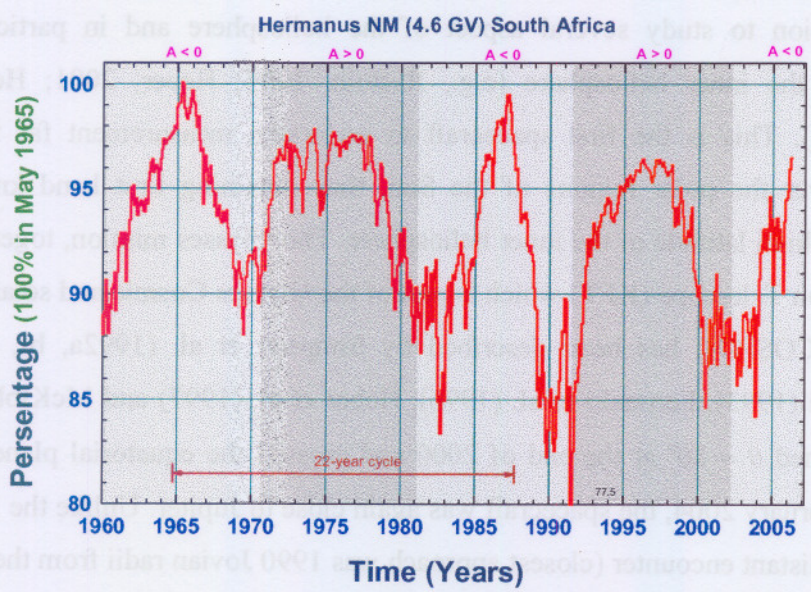

Figure (2.9): The long-term modulation of galactic cosmic rays as monitored by Hermanus neutron monitor in South Africa with a cutoff rigidity of 4.6 GV.

depicted in Figure (2.9). This cycle is anti-correlated with solar activity, with maximum cosmic ray intensities for solar minimum and vice versa for solar maximum conditions.

Apart from the 11-year modulation cycle, a 22-year cycle is also evident where some periods of maximum intensity show a plateau and some peak-like shapes. This can be described by drift effects where in an $A > 0$ cycle positively charged particles drift inwards to the Sun through the polar regions and are relatively insensitive to conditions in the equatorial region, e.g. such as changes in the HCS, and the plateau-like pattern is observed. For the $A < 0$ cycle these positive particles drift in along the HCS and are very sensitive to changes in α resulting in a peaked profile (Potgieter and Moraal 1985). For intermediate to solar maximum conditions, where step decreases or increases are observed, it is generally believed that propagating diffusion barriers (PDB's) are responsible for cosmic ray modulation.

2.8 The Ulysses mission

A joint European Space Agency (ESA) and National Aeronautic and Space Administration (NASA) mission, Ulysses, named after a Greek legend, is one of the most important mission to study several aspect of the heliosphere and in particular CR modulation in the inner heliosphere (e.g., Rastoin, 1995; Heber, 2001; Heber and Marsden, 2001). This is the first spacecraft to undertake measurement far from the ecliptic and over the polar regions of the Sun, thus obtaining first hand knowledge concerning the high latitude of the inner heliosphere. The Ulysses mission, together with the Kiel Electron Telescope (KET) which is part of the Ulysses Cosmic and solar Particle Investigation (COSPIN) has been described by Simpson et al. (1992a, b), Marsden (1993), Wenzel (1993), Ferrando et al. (1996), Heber et al. (1997) and McKibben et al. (2003). It reached $\theta \approx 80^{0}$ at the end of 2000 and crossed the equatorial plane in May 2001. On 5 February 2004, the spacecraft was again close to Jupiter. Unlike the 1992 fly-by, this was a distant encounter (closest approach was 1990 Jovian radii from the planet's centre, compared with 6 Jovian radii in 1992). Another difference between the two fly-bys is that the spacecraft approached the planet from high southern heliolatitudes. This

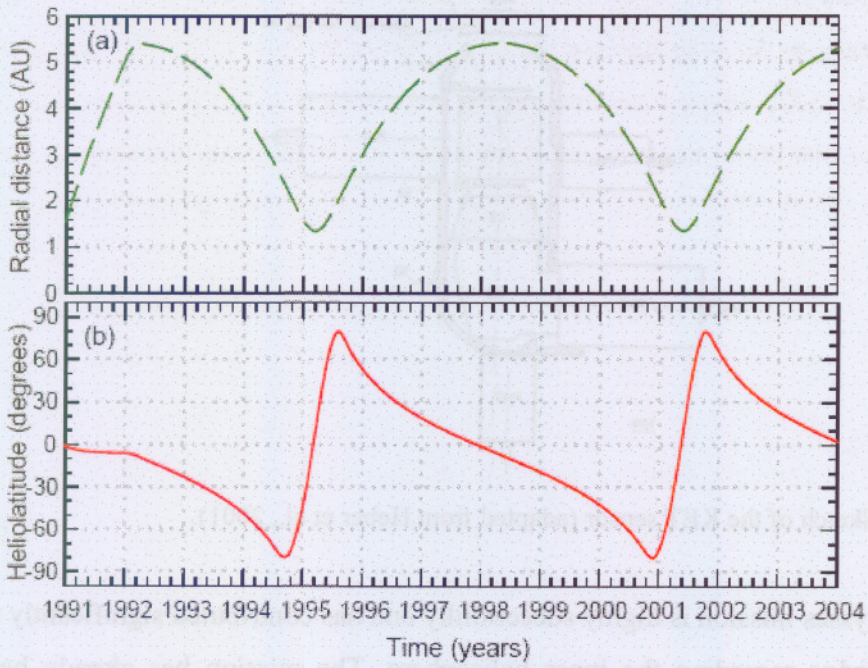

Figure (2.10): Trajectory of the Ulysses spacecraft in (a) radial distance (AU) and (b) heliolatitude (θ in degrees) coordinates from launch in 1990 until the end of 2005.

difference became apparent in the radio data from the Unified Radio and Plasma Wave (URAP) experiment on board Ulysses, which in February and March 2003 detected an intense radio emission from Jupiter at levels well above those seen in 1993 when Ulysses was a comparable distance from the planet (~ 2.8 AU). Details of the Ulysses trajectory can be found on the Ulysses homepage: http://helio.estec.esa.nl/ulysses/.

Onboard Ulysses are nine scientific instruments of which the KET provides a wide range of e.g. electron fluxes from about 2.5 MeV to 6 GeV. In this study the 3 – 10 MeV (~ 7 MeV) electrons are of importance. See Heber (2001).

Figure (2.11) shows a sketch of the KET sensor. The telescope is described in Simpson et al., (1992) and consists of two parts: (1) the entrance telescope with the semiconductor detectors D1 and D2, the Cherenkov detector C1, and the anti-coincidence A, and (2) the calorimeter, a lead fluoride Cherenkov detector C2, in which an electromagnetic shower can develop, and a scintillation detector S2, which counts the number of charged particles leaving C2.

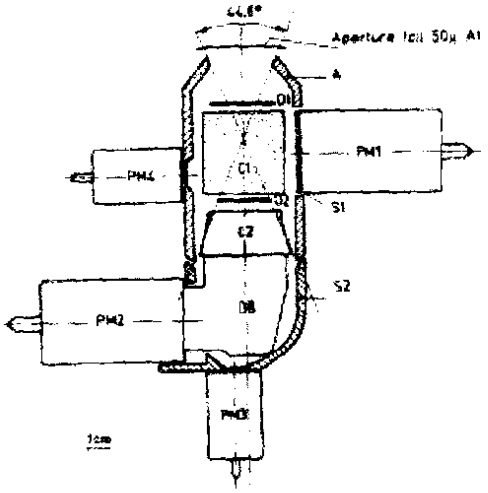

Figure (2.11): Sketch of the KET sensor (adapted from Heber et al., 2001).

The Ulysses mission is highly successfully and has contributed significantly to the current knowledge regarding the inner heliosphere. The mission has already been in progress for 15 years and in February 2004 the mission was extended until March 2008.

Then the operating time will have reached about 17 years and in December 2006 the spacecraft will pass close to the Sun for the third time. Thus, Ulysses will be measuring the next solar minimum, which should begin at the end of 2005. This extension is the third in the history of the joint ESA – NASA mission. For reviews, see the following publications: Marsden (1995; 2001), Balogh et al., (2001), Smith et al., (2003).

2.9 Summary

In this chapter a brief introduction was given of the basic concepts used in the heliospheric modulation of CRs that are used in this study, including the origin of GCRs, the Sun, the solar wind, the heliosphere, the HMF, the HCS, the tilt angle and solar cycle variations. The Ulysses mission was also discussed as related to KET.

Chapter 3

Low-energy electrons in the inner heliosphere

3.1 Introduction

In this chapter, the propagation and modulation of low-energy (3-30 MeV) electrons, particularly the Jovian electrons, in the inner heliosphere will be discussed. A brief discussion is given on the background of the sources of low-energy electrons with an overview of the development and improvement of the Jovian modulation model.

3.2 Sources of low-energy cosmic ray electrons in the heliosphere

The cosmic ray electron component is one of the rare species constituting only about one percent of the total cosmic particle radiation. In order to understand their propagation and modulation in the heliosphere, it is necessary to know their origin and investigate their propagation in the inner heliosphere. Between 1 and 10 AU, different sources contribute to the few-MeV electron intensities.

3.2.1 Astrophysical sources

It is believed that astrophysical phenomena such as supernova explosions are the main sources of cosmic ray electrons in our galaxy. This electron population is accelerated by supernova blast waves (e.g., Jones and Ellison, 1991; Koyama et al., 1995; Tanimori et al., 1998) and penetrates the heliosphere isotropically to be modulated by different physical processes in the heliosphere. At distances beyond 10 AU in the ecliptic, GCR electrons are the dominant population (Ferreira et al. 2001b). Ulysses observations of a few-MeV electrons in the inner heliosphere have been successfully modelled by Ferreira et al. (2001a) during the time period from launch in 1990 until 1998, during the declining and minimum phase of solar cycle 22. It is important to note that for low-energy ($E < 30$

MeV) electrons drift effects are of minor importance, so that the model is dominated by diffusion (Potgieter, 1985).

3.2.2 Solar flares and shocks

Solar flares are regarded as the main source of electrons with energies up to a few hundred MeV which can be observed on Earth for short periods only (e.g., Forbush, 1946; del Peral et al., 2003; Heber et al., 2001a). The increase of MeV electrons during solar particle events is accompanied by an increase in the several tens of MeV protons. Interplanetary electrons (e.g., Roelof et al., 1996; Keppler et al., 1996) showed that several-hundred keV electrons are accelerated by corotating shock waves. Although no increases in the MeV range have been reported, reacceleration of energetic electrons at travelling shocks should be possible (e.g., Classen et al. 1999).

3.2.3 Jovian magnetosphere

It became clear that Jupiter is a continuous source of MeV electrons in the inner solar system when Pioneer 10 came within 1 AU of the planet (e.g., Teegarden et al., 1974; Simpson 1974). Teegarden et al. (1974) further identified Jupiter as the source of quiet-time electron increases previously observed at 1 AU (McDonald et al., 1972; L'Heureux and Meyer, 1976). It was successfully proposed that electrons are continuously released from the Jovian magnetosphere and that their variability is mainly caused by varying heliospheric conditions. This was also indeed observed with the KET telescope during the whole in-ecliptic first part of the Ulysses trajectory (Ferrando et al. 1993a). The location of Jupiter with respect to the structure of the HMF is precisely determined and noncentral. This makes Jovian electrons very interesting and nonredundant with solar flare electrons for the modelling of interplanetary propagation. Jovian electron studies resulted in the first strong observational evidence for a diffusive transport of electrons perpendicular to the mean HMF (Chenette et al., 1974; Hamilton and Simpson, 1979).

3.3 Electron modulation models in 3D

Observations made along the unique Ulysses trajectory revealed the effects of the third dimension of the inner heliosphere and imposed a challenge to the modulation modellers to construct realistic models to account for the 3D heliospheric transport of Jovian and

galactic electrons. Fichtner et al. (2000b) developed a 3D steady-state, non-drift model and a more recent time dependent version (e.g., Fichtner et al., 2001b; Kissmann et al., 2004; Lange et al., 2005) based on the Parker (1965) transport equation and are most suitable to simulate the modulation of Jovian and galactic electrons in the inner heliosphere. The latter is still being further developed and will therefore not be applied in this study.

Besides the Fichtner et al. (2000b) model, Ferreira et al. (2001a, b) using a different numerical approach developed an advanced 3D steady-state Jovian electron modulation model based on the Parker transport equation including gradient, curvature, and current sheet drifts. The details of this numerical model will be discussed in the following Chapter. This model and the Fichtner et al. (2000b) model yield similar solutions when the same set of transport parameters is assumed. Figure (3.1) shows the features of the three-dimensional distribution of 7 MeV Jovian electrons within the first 10 AU of the heliosphere computed with this model. Here, the Jovian source is located at 5 AU in the equatorial plane. Using this 3D Jovian electron model, Ferreira et al. (2001a) studied the latitudinal transport of both 7 MeV Jovian and galactic electrons by illustrating how the electron intensities are affected at different latitudes by the enhancement of the perpendicular diffusion coefficient in the polar direction. In particular, the electron intensity-time profiles along the Ulysses trajectory were calculated for different assumptions for heliospheric polar diffusion and compared to the 3-10 MeV electron flux observed by Ulysses from launch up to the end of the first out-of-ecliptic orbit. Comparison of the model computations and observations gave an indication as to the magnitude of heliospheric polar diffusion. This has improved our understanding of the role the perpendicular diffusion plays in transporting low energy electrons to high latitudes. The relative contributions of the Jovian and galactic electrons to the total electron intensity were also successfully computed along the Ulysses trajectory.

Ferreira et al. (200lb) further studied the radial transport of 4 and 16 MeV Jovian and galactic electrons by comparing model computations with the electron intensities (e.g., Eraker, 1982; Lopate, 1991) observed by the University of Chicago experiment on board the Pioneer 10 spacecraft up to ~ 70 AU. It was shown that the computed electron intensities are sensitive to the radial dependence of the diffusion coefficients in the inner

heliosphere and that the compatibility between the model and observations gives an indication as to the radial dependence of the diffusion coefficients. The relative contributions of Jovian and galactic electrons to the total electron intensity were also computed along the Pioneer 10 trajectory. It was illustrated that the Jovian electrons dominate the total electron intensity in the inner equatorial regions only up to ~ 10 AU. From 15 AU outward, the Jovian contribution becomes insignificant, decreasing rapidly as a function of increasing distance.

Ferreira (2002) also produced model solutions compatible with the 3 - 10 MeV KET observations of Ulysses first out of ecliptic orbit (up to ~ 1998). These results indicated that no time-dependence changes in the transport parameters were required to compute realistic electron modulation during solar minimum conditions. But, when this model was applied to solar maximum conditions, the period after 1998 by assuming the same set of transport parameters as during solar minimum periods, the computed intensities were significantly lower than the observed 3 - 10 MeV electrons (Heber et al., 2003a, b; Ferreira et al., 2003a, b).

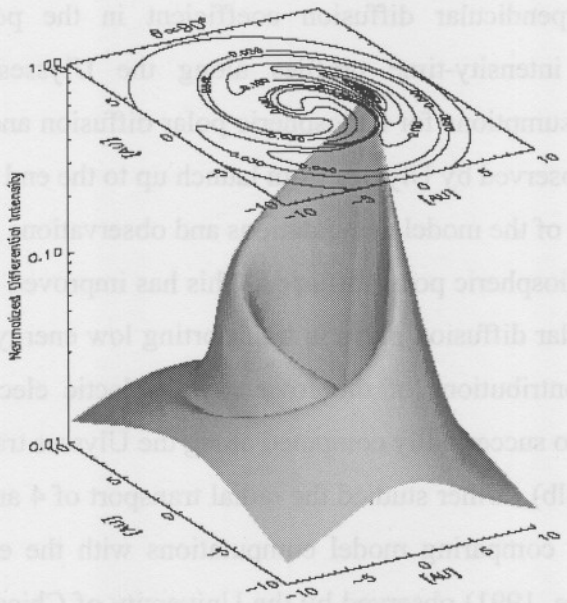

Figure (3.1): Computed distribution of 7 MeV Jovian electrons in the inner heliosphere in units of particles $m^{-2}\ s^{-1}\ sr^{-1}MeV^{-1}$. The source is at 5 AU (adapted from Ferreira et al., 2001a.).

These observed low-energy electron intensities stayed almost unchanged, in contrast to higher energies where observed intensities decreased as solar activity picked up. Heber (2002) argued that these low-energy observations could neither be explained by solar particles nor by locally accelerated electrons and should therefore be of galactic and Jovian origin. To improve modelling of the compatibility between the model computations and the 3 -10 MeV observations after 1998, a study of effects of changing only the solar wind speed in the model with changing heliospheric conditions and some of the results thereof were published by Ferreira et al., (2003a, b). An overview of Jovian electron modulation in general is given in the next section.

3.4 Modulation of Jovian electrons

Electron data collected close to Earth by IMP8 showed unexpected increases in the measured flux levels during quiet times (e.g., McDonald et al., 1972). The discovery of Jovian electrons by Pioneer 10 led to the recognition of this quiet time electron increase as being of Jovian origin (Teegarden et al., 1974; Mewaldt et al., 1976). Observations of these electrons at 1 AU showed a strong modulation with a period of 13 months (Mewaldt et al., 1976), which is associated with the Jovian synodic period. Every 13 months, the HMF lines connect more effectively between the Earth and Jupiter so that electrons transported along the field lines can easily reach the Earth. At other times, these electrons also have to diffuse across the field lines toward the Earth, and normal to heliospheric equatorial region to high latitude (e.g., Hamilton, 1979).

Moeketsi et al. (2005) modelled the changes in the solar wind speed in relation to perpendicular diffusion. By using different *d*-scenarios (*d* is the factor increase of perpendicular diffusion with polar angle; see also Chapter 4) they computed the latitude dependence of the solar wind related to the perpendicular diffusion of 7 MeV electron intensities along the Ulysses trajectory from the end of the first out-of-ecliptic orbit in 1998 to the end of 2003. Figure (3.2) shows the Ulysses trajectory and the computed 7 MeV Jovian and galactic electron intensities for each population as well as the combined Jovian and galactic electron intensities along the Ulysses trajectory.

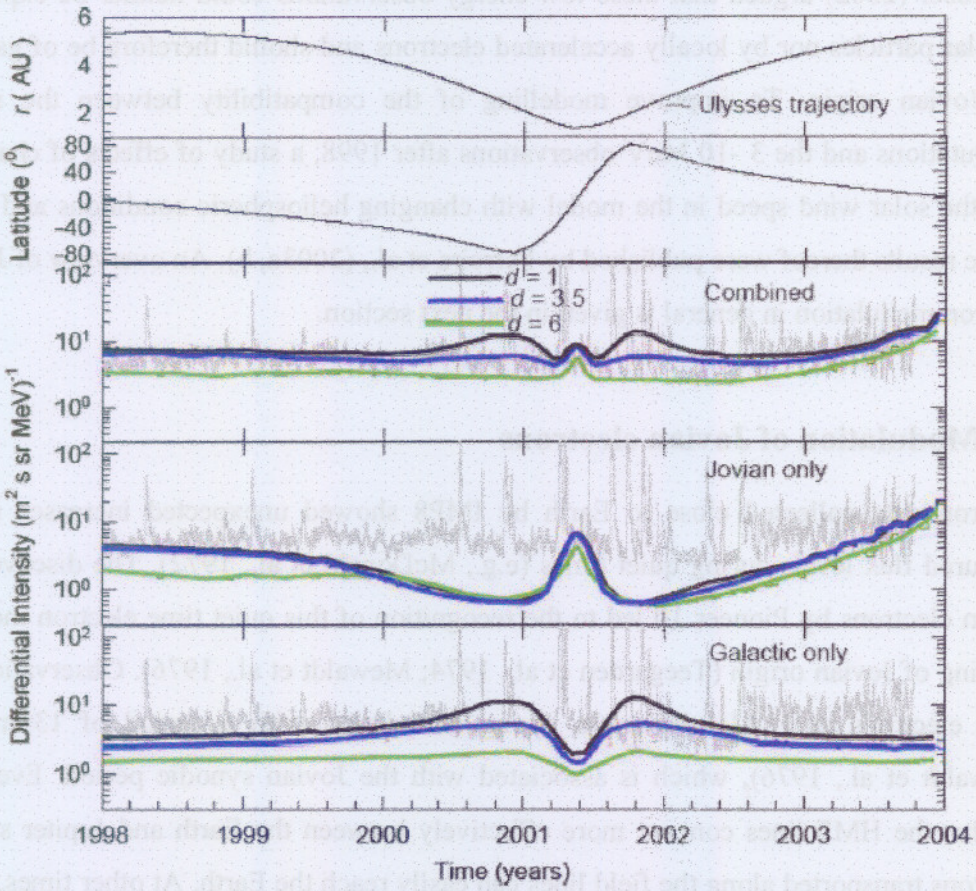

Figure (3.2): The top two panels show the Ulysses trajectory in radial and heliographic coordinates (data from http:/SWOOPS.lanl.gov/recentvu.html). In the third panel the computed 7 MeV combined Jovian and galactic electrons are shown; fourth panel: computed Jovian electron intensities; bottom panel: computed galactic electron intensities (Moeketsi et al., 2005).

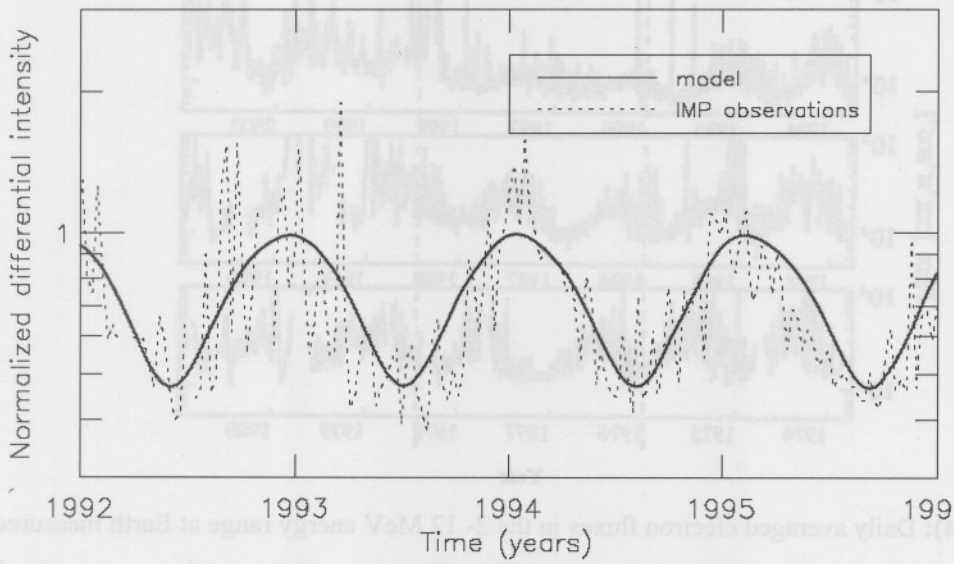

Figure (3.3): Normalized computed 7 MeV electron intensities at Earth in units of particles m^{-2} s^{-1} $sr^{-1}MeV^{-1}$ for the period 1992-1996 (dark solid line), in comparison with the average 2-12 MeV electron data from IMP (Heber et al. 2001a; Ferreira, 2002; Ferreira et al., 2003).

When Ulysses was within 1 AU of Jupiter during the first encounter, it observed short and sharp increases and decreases of low-energy electron fluxes which are called Jovian jets (bursts). These jets are characterised by a spectrum identical to the electron spectrum within the Jovian magnetosphere and a strong anisotropy (e.g., Chenette et al., 1974; Ferrando et al., 1993a). A similar feature has also recently been observed (Heber et al., 2004; McKibben et al., 2005). The causes of these short time variations in the Jovian electron flux are not yet well described and are a topic for future studies. By using the 3D Jovian electron modulation model and assuming the relative position of the Sun and Jupiter as the only time-varying factor, Ferreira (2002) could compute the 13-month periodicity of Jovian electrons observed at 1AU with the IMP satellite as shown in Figure (3.3). Jovian electrons observed at 1 AU also experience ~ 27 day modulation due to corotating interaction regions perturbing interplanetary propagations (e.g., Conlon and Simpson, 1977).

A different study of the effects of CIRs on the shorter-term modulation of low-energy electrons in the inner heliosphere has been done recently by Kissmann et al., (2004).

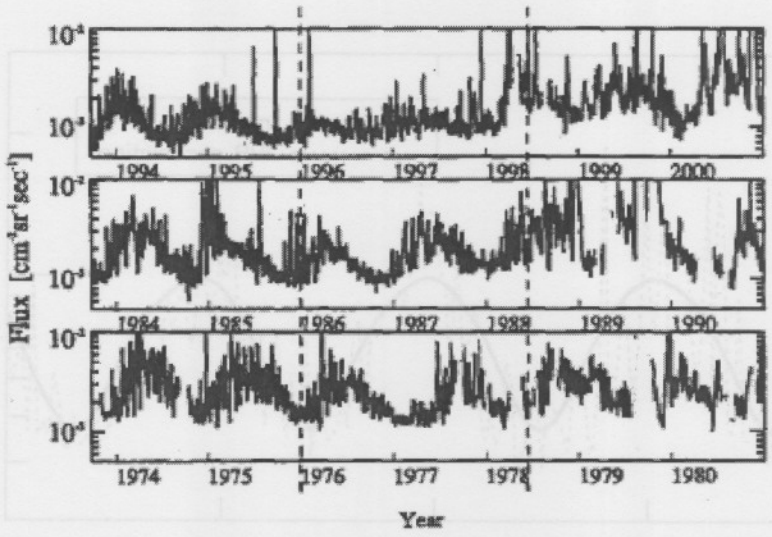

Figure (3.4): Daily averaged electron fluxes in the 2- 12 MeV energy range at Earth measured by the IMPB/CRIiC instrument (Kanekal et al., 2003). The top, middle and bottom panels show electron fluxes for years 1993 to 2001, 1984 to 1991 and 1974 to 1981 respectively. Dashed vertical lines denote a two year period around solar cycle minima. (From Kanekal et al., 2003).

These effects were not taken into account for this study. It was suggested by Morioka and Tsuchiya (1997) that Jovian electrons are also modulated by solar wind variations at Jupiter. By scrutinizing Pioneer 11 electron data collected during 1974, they found that the Jovian electron intensity was inversely correlated with solar wind dynamic pressure. Tsuchiya et al. (1999) also suggested that the polarity of the HMF at the vicinity of Jupiter may control the release rate of Jovian electrons into the interplanetary space. More recently, Kanekal et al. (2003), by analysis of electron data observed at Earth during the time period 1992 to 2002 with instruments on board SAMPEX and IMP8, discovered a puzzling non-transient decrease in Jovian fluxes near solar cycle minimum (from 1996-1998) as shown in the top panel of Figure (3.4). The Jovian electron flux diminished significantly from early 1996 to the end of 1997 then recovered subsequently and was observed until the end of 2001. In an attempt to explain these observations, they suggested either a change in the Jovian source function strength and/or a softening of the Jovian electron spectrum may account for these apparent anomalous observations. See also Moeketsi et al. (2005).

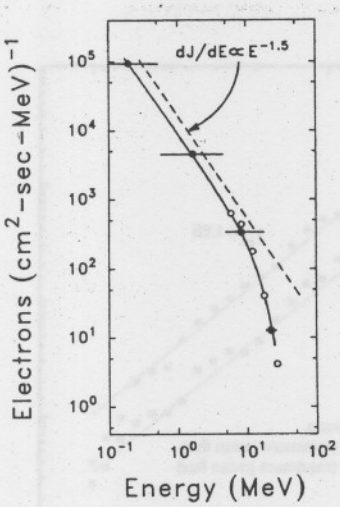

Figure (3.5): Comparison of the Pioneer 10 electron spectrum (filled circles) within the Jovian magnetosphere during the time of maximum flux (Baker and Van Allen, 1976) and ISEE 3 spectrum (open circles). The intensity normalization of the ISEE 3 data is arbitrary. (From Moses, 1987; see also Haasbroek, 1997, and Ferreira, 2002).

3.5 The Jovian electron source spectrum

Moses (1987) showed that the Jovian electron spectrum between 5 and 30 MeV, measured by the University of Chicago instrument on board ISEE 3, during a period of best magnetic connection between Jupiter and Earth, and Pioneer 10 electron spectrometer obtained within Jovian magnetosphere (e.g., Baker and Van Allen, 1976) as shown in Figure (3.5), can be fitted by a simple power-law

$$j \propto E^{-\gamma}, \tag{3.1}$$

with γ the spectral index and j the differential intensity. A power-law representation of the observed electron spectrum at 1 AU requires the spectral index to be a function of energy, which increases from $\gamma = \gamma_{jov} = 1.51$ at low energies to $\gamma < \sim 6$ at high energies. Moses (1987) also found agreement with electron spectra of other authors in overlapping regions of energy (e.g., Teegarden et al., 1974; Eraker, 1982; Eraker and Simpson, 1979). How the Jovian source function is constructed to simulate Jovian electron modulation will be discussed in the next Chapter.

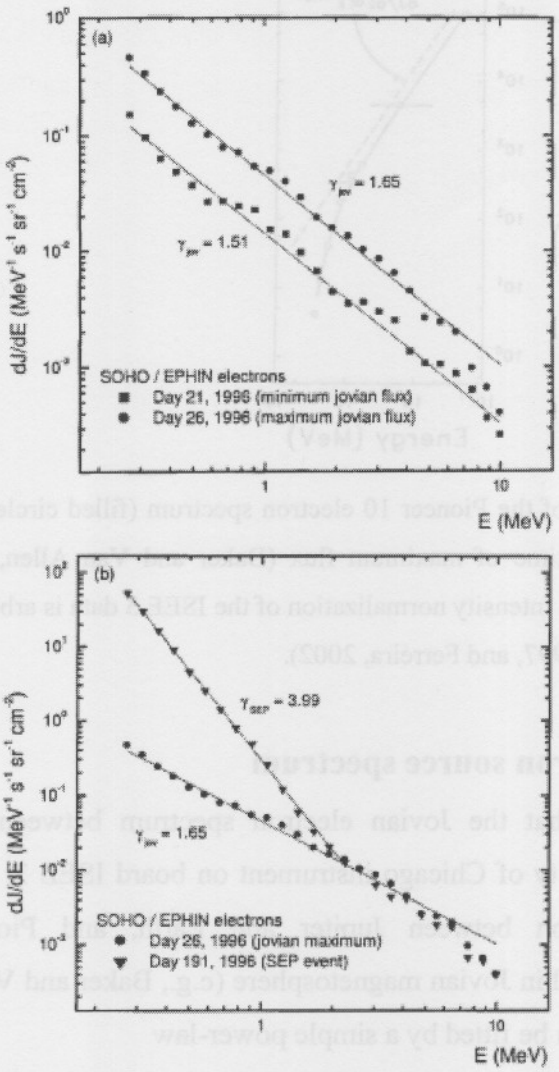

Figure (3.6): Panel (a) fits of the electron fluxes to an energy power-law during a day of minimum and a day of maximum Jovian flux observed by the SOHO/EPHIN sensor. Panel (b) shows a comparison between the Jovian electron flux and the electron flux of a solar energetic particle event. (From del Peral et al., 2003).

Most recently, del Peral et al. (2003) showed measurements of the Jovian electron spectra at 0.99 AU from the SOHO/EPHIN sensor observed during a day (day 21, 1996) of minimum flux and a day (day 26, 1996) of maximum flux fitted by Equation (3.1) with spectral index $\gamma = \gamma_{jov} = 1.51$ and $\gamma_{jov} = 1.65$ respectively as shown in Figure (3.6) panel (a). These values of the spectral indices are in good agreement with the values

expected from the Jovian magnetosphere. The other electron population observed shows a spectral index of $\gamma > 2$, shown in Figure (3.6) panel (b) as $\gamma_{SEP} = 3.99$, which indicates that it is of solar origin associated with a solar energetic particle (SEP) event.

3.6 Summary

In this Chapter a short overview of the propagation and modulation of low energy electrons (3- 10 MeV) in the inner heliosphere was given, with main emphasis on Jovian electrons. This discussion includes the sources contributing to the few MeV electron intensities in the inner heliosphere, a brief overview of 3D Jovian electron propagation and modulation models, and a brief discussion on the observed modulation and spectra of Jovian electrons. In Chapter 5, the 3D Jovian electron modulation model applied in this work will be discussed in more detail, including the Jovian source function.

Chapter 4

Aspects of the diffusion tensor in the heliosphere

4.1 Introduction

A theoretical background on aspects of the diffusion tensor will be given in this chapter. Cosmic rays propagate into the inner heliosphere due to random motions and diffuse, gyrating around the HMF lines and scattering at irregularities in the field. They also lose energy through adiabatic cooling and experience gradient, curvature and current sheet drifts and get convected back toward the heliospheric boundary by the solar wind. These processes were combined by Parker (1965) into a transport equation (TPE).

$$\frac{\partial f}{\partial t} = -\left(\mathbf{V} + \langle v_D \rangle\right)\cdot\nabla f + \nabla\cdot\left(\mathbf{K}\cdot\nabla f\right) + \frac{1}{3}(\nabla\cdot\mathbf{V})\frac{\partial f}{\partial \ln P} + Q, \tag{4.1}$$

where $f(\mathbf{r},P,t)$ is the omni-directional cosmic ray (CR) distribution function, dependent on position $\mathbf{r}$, rigidity P, and time t. The solar wind velocity is denoted by $\mathbf{V}$, see Equation (2.2), and $\mathbf{K}$ is the diffusion tensor discussed in the next section. The term Q on the right side describes the Jovian source function for the purpose of this work and will be discussed in detail in the next chapter. All forms of diffusive acceleration are neglected for this study (see e.g, Langner et al. 2006b). This transport equation in a spherical coordinate system rotating with the Sun (e.g. Kóta and Jokipii 1983), and for a steady-state with $\frac{\partial f}{\partial t} = 0$, is given by

$$
\overbrace{\left[\frac{1}{r^2}\frac{\partial}{\partial r}\left(r^2 K_{rr}\right)+\frac{1}{r\sin\theta}\frac{\partial K_{\phi r}}{\partial \phi}\right]\frac{\partial f}{\partial r}+\left[\frac{1}{r^2\sin\theta}\frac{\partial}{\partial \theta}\left(K_{\theta\theta}\sin\theta\right)\right]\frac{\partial f}{\partial \theta}}^{diffusion}
$$

$$
\overbrace{+\left[\frac{1}{r^2\sin\theta}\frac{\partial}{\partial r}\left(rK_{r\phi}\right)+\frac{1}{r^2\sin\theta}\frac{\partial K_{\phi\phi}}{\partial \phi}+\mathbf{\Omega}\right]\frac{\partial f}{\partial \phi}}^{diffusion}
$$

$$
\overbrace{+K_{rr}\frac{\partial^2 f}{\partial r^2}+\frac{K_{\theta\theta}}{r^2}\frac{\partial^2 f}{\partial \theta^2}+\frac{K_{\phi\phi}}{r^2\sin^2\theta}\frac{\partial^2 f}{\partial \phi^2}+\frac{2K_{r\phi}}{r^2\sin\theta}\frac{\partial^2 f}{\partial r\partial \phi}}^{diffusion}
$$

$$
\overbrace{+\left[-\left\langle \mathbf{v}_d\right\rangle_r\right]\frac{\partial f}{\partial r}+\left[-\frac{1}{r}\left\langle \mathbf{v}_d\right\rangle_\theta\right]\frac{\partial f}{\partial \theta}+\left[-\frac{1}{r\sin\theta}\left\langle \mathbf{v}_d\right\rangle_\phi\right]\frac{\partial f}{\partial \phi}}^{drift}
$$

$$
\overbrace{-V\frac{\partial f}{\partial r}}^{convection}
$$

$$
\overbrace{+\frac{1}{3r^2}\frac{\partial}{\partial r}\left(r^2 V\right)\frac{\partial f}{\partial \ln P}}^{adiabatic\ energy\ change}
$$

$$
\overbrace{=-Q}^{source}. \qquad (4.2)
$$

The three components of the drift velocity are:

$$
\left\langle \mathbf{v}_d\right\rangle_r=-\frac{sign(Bq)}{r\sin\theta}\frac{\partial}{\partial \theta}(K_{\theta r}),
$$

$$
\left\langle \mathbf{v}_d\right\rangle_\theta=-\frac{sign(Bq)}{r}\left[\frac{1}{\sin\theta}\frac{\partial}{\partial \phi}(K_{\phi\theta})+\frac{\partial}{\partial r}(rK_{r\theta})\right], \qquad (4.3)
$$

$$
\left\langle \mathbf{v}_d\right\rangle_\phi=-\frac{sign(Bq)}{r}\frac{\partial}{\partial \theta}(K_{\theta\phi}),
$$

or alternatively as given by Hattingh (1998), the drift velocity is:

$$
\begin{aligned}
\mathbf{v}_d &= \nabla\times K_A\mathbf{e}_B \\
&= \nabla\times(K_A\mathbf{e}_B)\left[1-2H(\theta-\theta')\right]+2\delta_D(\theta-\theta')(K_A\mathbf{e}_B)\times\nabla(\theta-\theta'),
\end{aligned} \qquad (4.4)
$$

with $\mathbf{e}_B = \mathbf{B}_m/B$, with $\mathbf{B}$ the modified HMF given by Equation (2.8), H is the Heaviside function Equation (2.13), K_A the 'drift' coefficient and δ_D the Dirac function. The first term in Equation (4.4) describes gradient and curvature drifts caused by the HMF, and the second term describes the drifts caused by the HCS. These drift aspects will be discussed in more detail later in this chapter.

The nine elements of the diffusion tensor in Equation (4.2) are discussed below. Understanding the indicated physical mechanisms in Equation (4.2) and their consequences for the modulation of cosmic rays, particularly galactic and Jovian electrons, is still one of the most important research areas in heliospheric modulation studies.

4.2 The diffusion tensor

The diffusion tensor in Equation (4.1) in terms of spherical coordinates is given by

$$\mathbf{K}=\begin{bmatrix} K_{rr} & K_{r\theta} & K_{r\phi} \\ K_{\theta r} & K_{\theta\theta} & K_{\theta\phi} \\ K_{\phi r} & K_{\phi\theta} & K_{\phi\phi} \end{bmatrix}=\begin{bmatrix} K_{\parallel}\cos^2\psi+K_{\perp r}\sin^2\psi & -K_A\sin\psi & \left(K_{\perp r}-K_{\parallel}\right)\cos\psi\sin\psi \\ K_A\sin\psi & K_{\perp\theta} & K_A\cos\psi \\ \left(K_{\perp r}-K_{\parallel}\right)\sin\psi\cos\psi & -K_A\cos\psi & K_{\perp r}\cos^2\psi+K_{\parallel}\sin^2\psi \end{bmatrix}, \tag{4.5}$$

where the diffusion coefficients of special interest for this study are

$$K_{rr}=K_{\parallel}\cos^2\psi+K_{\perp r}\sin^2\psi, \tag{4.6}$$

$$K_{\theta\theta}=K_{\perp\theta}, \tag{4.7}$$

$$K_{\phi\phi}=K_{\perp r}\cos^2\psi+K_{\parallel}\sin^2\psi, \tag{4.8}$$

$$K_{\phi r}=\left(K_{\perp r}-K_{\parallel}\right)\sin\psi\cos\psi=K_{r\phi}, \tag{4.9}$$

with $K_{\parallel}$ and $K_{\perp}$ the diffusion coefficients parallel and perpendicular to background HMF, respectively. $K_{\perp}$ can be subdivided into two independent coefficients, namely $K_{\perp r}$ and $K_{\perp\theta}$, the perpendicular diffusion coefficient in the radial/azimuthal direction and in the polar direction respectively. $K_{\phi\phi}$ describes the diffusion coefficient in the azimuthal direction and $K_{\phi r}$ is the diffusion coefficient in the ϕr direction and can be regarded as a correction term which marginally reduces the radial and azimuthal gradient of cosmic rays (see Moeketsi, 2004). The coefficients describing drifts, e.g., $K_{r\theta}$ in terms of K_A, can be neglected for Jovian electron studies (energies of up to 10-20 MeV) but not for the modulation of galactic cosmic rays (see also Potgieter, 1996; Ferreira, 2002; Moeketsi, 2004). The spiral angle ψ is the angle between the radial direction and the average HMF at certain position given by Equation (2.6).

Shown in Figure (4.1) are the terms, $\cos^2\psi$ (dash-dot-dash lines), $\sin^2\psi$ (dash lines) and $\sin\psi\cos\psi$ (dotted lines) in Equations (4.6) to (4.9), as a function of radial distance r for the heliospheric polar regions ($\theta = 10^0$) and equatorial plane ($\theta = 90^0$), respectively. It

is shown that $\cos^2\psi$ near the pole decreases with increasing radial distance, but more significantly in the equatorial plane, while $\sin^2\psi$ stays almost constant for most of the heliosphere, except for the inner heliosphere where it rapidly decrease for both polar and equatorial region. On the other hand, the product of $\sin\psi\cos\psi$ near the poles increases rapidly as a function of increasing radial distance in the inner heliosphere and then decreases.

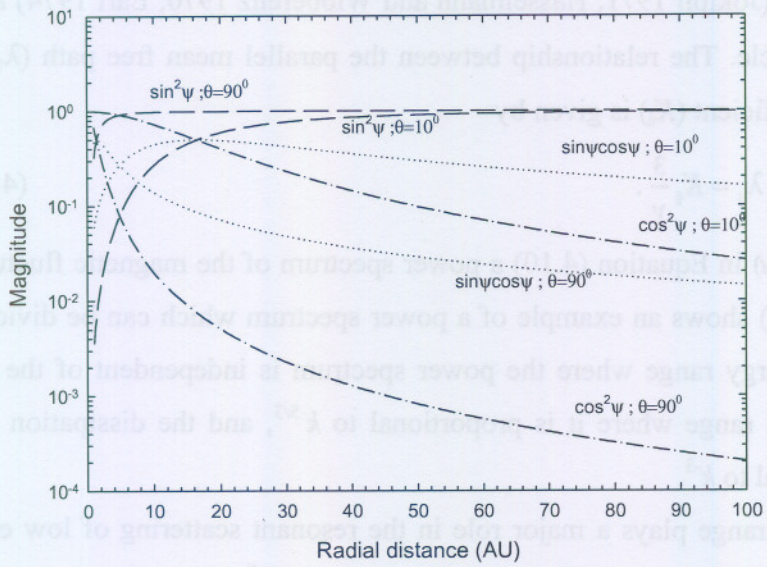

Figure (4.1): This figure shows $\cos^2\psi$ (dash-dot-dash lines), $\sin^2\psi$ (dash lines) and $\sin\psi\cos\psi$ (dotted lines) in Equations (4.6) to (4.9), as a function of radial distance r for the polar regions ($\theta = 10^0$) and the equatorial plane ($\theta = 90^0$) of the heliosphere.

4.3 The parallel diffusion coefficient

Transport of energetic particles through the heliosphere depends on diffusion (due to scattering by magnetic irregularities) both along and across the mean HMF lines. For recent reviews on diffusion coefficients, see Dröge (2003, 2005) and for an advanced treatment from a turbulence and diffusion theory point of view, see Stawicki (2003) and Minnie (2005).

In this section the focus is on the parallel diffusion coefficient ($K_{\parallel}$) which describes the transport of cosmic rays parallel to the HMF lines. The process can be described by the quasi-linear theory (QLT) (e.g., Jokipii 1966; Hasselmann and Wibberenz 1968), with the parallel mean free path ($\lambda_{\parallel}$) given by

$$\lambda_{\parallel} = \frac{3v}{2}\int_0^{\pi}\frac{(1-\mu^2)^2}{\Phi(\mu)}, \tag{4.10}$$

with μ the cosine of the particle pitch angle, $\Phi(\mu)$ the Fokker-Planck coefficient for the pitch angle scattering (Jokipii 1971; Hasselmann and Wibberenz 1970; Earl 1974) and v the speed of the particle. The relationship between the parallel mean free path ($\lambda_{\parallel}$) and parallel diffusion coefficient ($K_{\parallel}$) is given by

$$\lambda_{\parallel} = K_{\parallel}\frac{3}{v}. \tag{4.11}$$

To calculate $\Phi(\mu)$ in Equation (4.10) a power spectrum of the magnetic fluctuation is needed. Figure (4.2) shows an example of a power spectrum which can be divided in three ranges: The energy range where the power spectrum is independent of the wave number k, the inertial range where it is proportional to $k^{-5/3}$, and the dissipation range where it is proportional to k^{-3}.

The dissipation range plays a major role in the resonant scattering of low energy particles where the pitch angle of these particles approaches 90^0. In original derivation of $\lambda_{\parallel}$ the dissipation range was neglected (e.g., Jokipii 1966; Fisk et al., 1974). It became evident from magnetometer and plasma observations in the solar wind (e.g., Coroniti et al., 1982) that the magnetic fluctuation spectra typically exhibit a dissipation range. By neglecting the dissipation range, $\lambda_{\parallel}$ is too small at lower rigidities and has incorrect rigidity dependence (Bieber et al., 1994). This $\lambda_{\parallel}$ can be applied to high energy protons modulation in the heliosphere because protons experience large adiabatic energy changes below ~ 300 MeV and at these energies proton modulation in the inner heliosphere ($r <$ ~ 10 AU) is unaffected by changes in $\lambda_{\parallel}$ (e.g., Potgieter, 1984). For electron modulation the knowledge of $\lambda_{\parallel}$ is vital because CR electrons respond directly to changes in $\lambda_{\parallel}$ even for P < 100 MV (Potgieter, 1996).

Including the dissipation range, the original QLT predicts a $\lambda_{\parallel}$ which is infinite. This is because $\Phi(\mu)$ goes to zero more rapidly than without the dissipation range as the

pitch angle approaches 90^0. When $\Phi(\mu) \rightarrow 0$, from Equation (4.10) then follows that $\lambda_{\parallel} \rightarrow \infty$. A higher order theory is therefore needed. Several mechanisms have been proposed to overcome this problem. Examples are mirroring by the fluctuations of the magnetic field magnitude (see e.g. Goldstein et al. 1975), a variety of nonlinear extensions of the theory of pitch angle scattering (see e.g. Goldstein, 1976), wave propagation (Schlickeiser, 1988) and the effect of dynamic turbulence (Bieber and Matthaeus 1991; Bieber et al. 1994). The latter introduced two dynamical turbulence models, namely the damping model and the random sweeping model. The inclusion of dynamic turbulences causes $\Phi(\mu)$ not to decrease to zero for small μ which leads to a finite $\lambda_{\parallel}$ at lower energies (Hattingh, 1998). See also Bieber (2003).

Taking into account theoretical arguments by Burger et al., (2000), Ferreira (2002) constructed a parallel diffusion coefficient to compute realistic cosmic ray electron modulation inside the heliosphere. For cosmic ray ions, see Langner (2004).

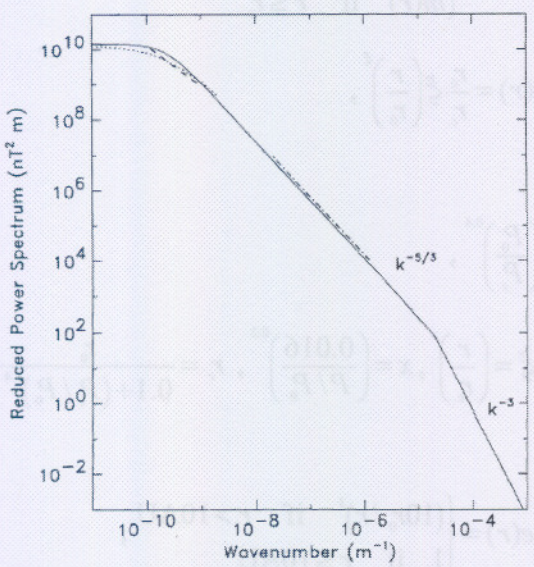

Figure 4.2: The power spectrum of the slab turbulence model (solid line) compared to observations (other lines). Note that the power spectrum can be divided into three ranges: The energy range where the power spectrum variation is independent of the wave number, k, the inertial range where it is proportional to $k^{-5/3}$, and the dissipation range where it is proportional to k^{-3} (from Bieber et al., 1994).

By comparing model results with cosmic ray electrons observations by Pioneer 10 and Ulysses, a diffusion tensor was constructed which included a $\lambda_{\parallel}$ similar to the damping model (Bieber et al. 1994) at low energies. Following the work of Burger et al. (2000), Ferreira (2002), and Moeketsi (2004), this coefficient is given by

$$K_{\parallel} = K_0 \beta f_1(r,P), \tag{4.12}$$

where

$$f_1(r,P) = 0.2 g(P) c(r) h(r,P), \tag{4.13}$$

with

$$h(r,P) = 0.02\left(\frac{P}{P_0}\right)^2\left(\frac{r}{r_0}\right)^{1.7} + 0.02\left(\frac{P}{P_0}\right)\left(\frac{r}{r_0}\right)^{2.2} + 0.02\left(\frac{P}{P_0}\right)^{1/3}\left(\frac{r}{r_0}\right) + 7.0e(r), \tag{4.14}$$

$$c(r) = \begin{cases} 1 & \text{if} \quad r > r_c \\ m(r) & \text{if} \quad r \le r_c \end{cases}, \tag{4.15}$$

$$m(r) = \frac{r_0}{r_c}\xi\left(\frac{r}{r_0}\right)^{\xi}, \tag{4.16}$$

and

$$g(P) = \left(\frac{P_0}{P_s}\right)^{0.4}, \tag{4.17}$$

where

$$\xi = \left(\frac{r}{r_c}\right)^{x}, x = \left(\frac{0.016}{P/P_0}\right)^{0.2}, r_c = \frac{r_0}{0.1 + (P_s/P_0)^{1.4}}$$

and

$$e(r) = \begin{cases} (10 r_0/r)^k & \text{if} \quad r > 10\text{AU} \\ 1 & \text{if} \quad r \le 10\text{AU} \end{cases}, \tag{4.18}$$

with $k = 125 \times 10^{-4} (r / r_0)^2$. Here β is the ratio of the speed v of a cosmic ray particle to the speed c of light, $K_0 = 4.5 \times 10^{22}$ cm^{2}s^{-1}, $P_0 = 1$ GV, $r_0 = 1$ AU and $P_s = P$ when $P < 1$ GV and $P_s = 1$ GV when $P \ge 1$ GV. This is based on the theoretical argument for higher rigidities of Burger et al. (2000) and is comparable to solar particle events at lower energies (Dröge, 2000).

For this work a new $\lambda_{\parallel}$ is used based on theoretical work by Teufel and Schlickeiser (2002) for $\lambda_{\parallel}$ at Earth, and constructed and implemented by Ndiitwani (2005) and Ndiitwani et al. (2005) for describing especially long-term modulation. The time dependent term was neglected for this work, because a steady-state model is used. This parallel mean free path $\lambda_{\parallel}$ is given by

$$\lambda_{\parallel} = \lambda_1(r,P)\lambda_2(r,P), \tag{4.19}$$

where

$$\lambda_1(r,P) = \frac{5}{3}\left(0.0106\left(P/P_0\right)^{1/3} + \frac{3.57}{\left(0.511^2 + (P/P_0)^2\right)^{1/4}} + (r/r_0)^{1.4} \mathrm{x}\, 10^{-9} (P/P_0)^2 \right), \tag{4.20}$$

$$\lambda_2(r,P) = \frac{c_1(P) + 0.08}{c_1(P)(r/r_0)^{-2.30} + 0.08(r/r_0)^{0.37}}, \tag{4.21}$$

with

$$c_1(P) = 83.0\left(\frac{0.02}{1000P}\right)^{0.75}, \tag{4.22}$$

thus parallel diffusion coefficient is assume as

$$K_{\parallel} = \frac{v}{3}\lambda_{\parallel}(r,P), \tag{4.23}$$

for lower rigidity $\lambda_{\parallel}$ has almost no rigidity dependence as needed to compute realistic electron modulation (Ferreira, 2002). The rigidity and spatial dependence of the parallel diffusion coefficient will be discussed in the next section.

4.3.1 The rigidity dependence

Shown in Figure (4.3) in panel (a) is the computed rigidity dependence of $K_{\parallel}$ (Ndiitwani et al., 2005) at 1 AU (dotted) and 5 AU (solid line) in the equatorial plane. It is evident from panel (a) that $K_{\parallel}$ at 1 AU is changing moderately for $P \leq 0.1$ GV but is increasing significantly for $P > 0.1$ GV, and especially at high rigidities ($P > \sim 5$ GV). At 5 AU, $K_{\parallel}$ is increasing steadily for $P \leq 1$ GV but at $P > 1$ GV there is a sharp increase. In previous

work (Moeketsi, 2004; see his Figure 5.4) an artificial kink occurred at 1 GV, which was insignificant for Jovian electron modulation (Ferreira, 2002) but cannot be ignored for

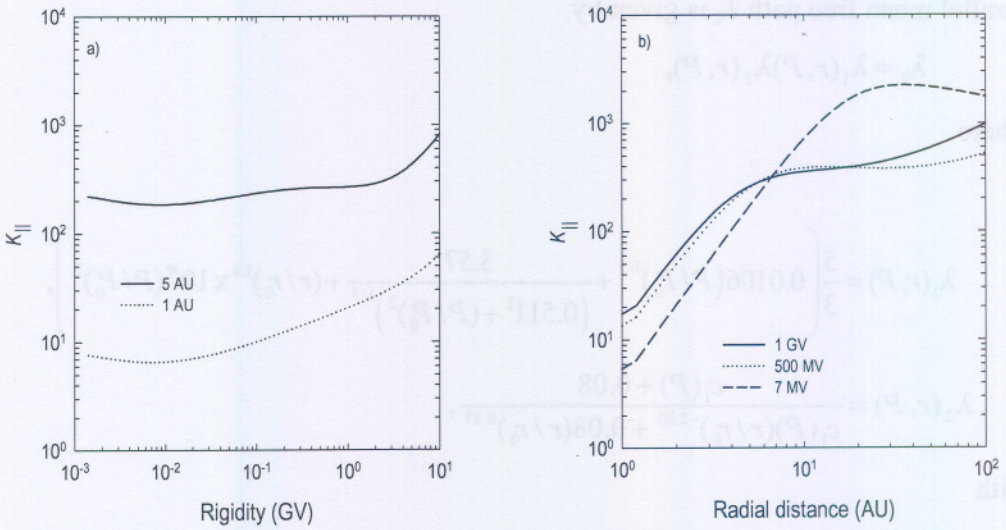

Figure (4.3): Panel (a) shows the rigidity dependence of $K_{||}$ for electrons at 1 AU and 5 AU in the equatorial plane. Panel (b) shows the radial dependence of $K_{||}$ in the equatorial plane at rigidities of 1 GV (solid line), 500 MV (dotted line) and 7 MV (dashed line) respectively. $K_{||}$ is in units of 6.0×10^{20} cm^{2}s^{-1}.

galactic electron modulation. The new parallel mean free path ($\lambda_{||}$) in Equation (4.19) solves this problem.

From Equation (4.11) follows that $\lambda_{||}$ has the same rigidity dependence as $K_{||}$ down to low energies (which is not the case for protons).

4.3.2 The spatial dependence

Panel (b) in Figure (4.3) shows $K_{||}$ as a function of radial distance in the equatorial plane for 7 MV (dash line), 500 MV (dotted line) and 1 GV (solid line) respectively. It follows that for low rigidity (7 MV), $K_{||}$ increases rapidly up to 10 AU and remains approximately constant throughout the rest of the heliosphere. For 500 MV and 1 GV, $K_{||}$ also increases rapidly up to ~ 10 AU, but then levels off in the outer heliosphere. Since $\lambda_{||}$ is assumed to

have no latitudinal dependence in Equation (4.19), it follows that $K_{\parallel}$ will also not have a latitudinal dependence as given in Equation (4.23).

4.4 The perpendicular diffusion coefficient

Perpendicular diffusion is caused by two fundamental processes: (1) the gyro-centres of particles are displaced transverse to the mean field because of scattering and (2) the random walk of magnetic field lines themselves (e.g., Giacalone and Jokipii, 1999; Kóta and Jokipii, 1999). As mentioned in the previous section, $K_{\perp}$ can be subdivided in two independent coefficients, $K_{\perp\theta}$ and $K_{\perp r}$, which give perpendicular diffusion in the polar and radial direction of the heliosphere respectively. $K_{\perp}$ is very important at lower energies (e.g. E < 300 MeV) for electron modulation where drifts and energy changes are not as important as for protons (e.g., Ferreira et al., 2000). Because of its complexity, it became a standard and convenient practice when using modulation models to spatially scale $K_{\perp}$ as $K_{\parallel}$ (e.g., Kóta and Jokipii, 1995; Potgieter, 1996; Ferreira et al., 2000; Ferreira et al., 2001a, b). It then follows that

$$K_{\perp r} = aK_{\parallel}, \tag{4.24}$$

and

$$K_{\perp\theta} = bK_{\parallel}, \tag{4.25}$$

where a and b are either constants or functions of rigidity (see e.g., Ferreira, 2002; Burger et al., 2000). In this chapter, a = 0.010 and b = 0.015 are assumed as in the studies by Ferreira et al. (2001a, b) and Moeketsi et al. (2005) to allow compatibility to the observations of low energy Jovian and galactic electrons in the equatorial plane during solar minimum conditions.

Concerning the latitude dependence of perpendicular diffusion, Ferreira et al. (2000) studied the effect of anisotropic perpendicular diffusion on cosmic ray electron modulation. They showed that increasing $K_{\perp\theta}$ results in reducing the latitudinal dependence of cosmic rays intensities in the inner heliosphere as required by Ulysses measurements for both polarity epochs at almost all energies. The radial dependence also increases in general, except for the innermost heliosphere. It was shown by Potgieter (1996) and Potgieter et al., (1997) that assuming anisotropic perpendicular diffusion and

increasing $K_{\perp\theta}$ relative to $K_{\parallel}$ led to a remarkable reduction in drifts as experience by cosmic ray protons. Ferreira et al. (2000) found similar results for galactic cosmic ray electrons. Therefore increasing $K_{\perp\theta}$ gradually, smears out the signature of drifts. In this work it is assumed that

$$K_{\perp\theta} = bK_{\parallel}F(\theta), \tag{4.26}$$

with

$$F(\theta) = A^{+} \pm A^{-} \tanh\left[\frac{1}{\Delta\theta}\left(\theta_A - 90^0 + \theta_F\right)\right], \tag{4.27}$$

where $A^{\pm}=1/2(d \pm 1)$, $\Delta\theta = 1/8$, $\theta_A = \theta$ and $\theta_F = 35^0$ for $\theta \leq 90^0$ while for $\theta > 90^0$, $\theta_A = 180 - \theta$ and $\theta_F = -35^0$. Panel (a) in Figure (4.4) shows $F(\theta)$ as a function of polar angle for ~ 7 MeV electrons with d = 2.5, 6 and 13 respectively. It is evident how $F(\theta)$ in Equation (4.27) can enhance $K_{\perp\theta}$ according to Equation (4.26) with respect to $K_{\parallel}$ by a factor d from the equatorial plane to the poles. The motivation for this enhancement can be found in Ferreira et al., (2001a) and Burger et al., (2000). They showed that to produce the correct magnitude and rigidity dependence of the latitudinal cosmic ray proton and electron gradients, as observed by Ulysses, enhanced latitudinal transport is required (see also Kóta and Jokipii, 1995; Potgieter et al., 1997).

Panel (b) in Figure (4.4) shows $K_{\perp\theta}$ as function of polar angle at 1 AU and 5 AU for 7 MeV electrons with $d = 6$. $K_{\perp\theta}$ is significantly more enhanced at 5 AU than at 1 AU. This implies that electrons produced by the source such as the Jovian magnetosphere located at 5 AU in the ecliptic plane, may be more effectively transported to high heliolatitude than at 1 AU. $K_{\perp\theta}$ and $K_{\perp r}$ has the same rigidity dependence (not shown) as $K_{\parallel}$ from Equations (4.24) and (4.25). The enhancement of $K_{\perp\theta}$ plays a major in modulation studies as is shown in later chapters.

4.5 The effective diffusion coefficient in the radial and azimuthal direction

The radial diffusion coefficient K_{rr} is expressed as a linear combination of $K_{\parallel}\cos^2\psi$ and $K_{\perp r}\sin^2\psi$ as given in Equation (4.6) and describes the effective radial inward diffusion of

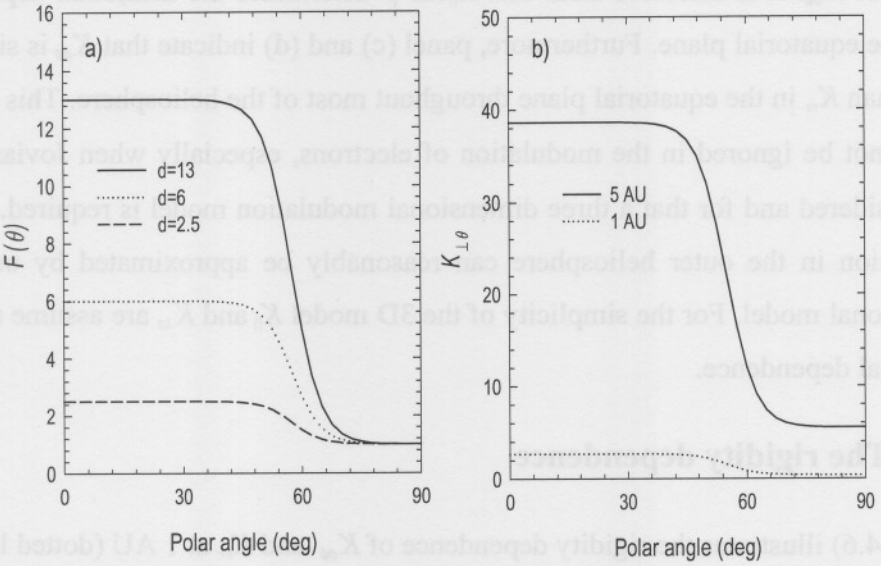

Figure (4.4): Panel (a) is an illustration of $F(\theta)$ in Equation (4.26) as a function of polar angle θ for scenarios with $d = 2.5$, 6 and 13 respectively. Panel (b) shows $K_{\perp\theta}$ as a function of polar angle at 1 AU and 5 AU for 7 MeV electrons for $d = 6$. Here $K_{\perp\theta}$ is in units of 6.0×10^{20} cm^{2}s^{-1}.

cosmic rays particles entering the heliosphere isotropically to become modulated due to turbulence in the HMF and the solar wind. The effective azimuthal diffusion coefficient $K_{\phi\phi}$ is also expressed as a linear combination of the terms $K_{\parallel}\sin^2\psi$ and $K_{\perp r}\cos^2\psi$ as given in Equation (4.8).

4.5.1 The spatial dependence

Figure (4.5) shows the radial dependence of K_{rr} and $K_{\phi\phi}$ in the equatorial plane for 7 MeV electrons. Shown in panels (a) and (b) are the values of $K_{\parallel}$ (dotted lines) and of $K_{\perp r}$ (dashed lines) in comparison to the radial dependence of K_{rr} and $K_{\phi\phi}$, respectively. Shown in panel (a) is that K_{rr} has the same radial dependence in the outer heliosphere than $K_{\perp r}$ and in panel (b) that $K_{\phi\phi}$ has the same radial dependence as $K_{\parallel}$ with $r > 10$ AU, but differs in the inner heliosphere. Shown in panels (c) and (d) are how $\sin^2\psi$ and $\cos^2\psi$ 'modify' the situation according to Equations (4.6) and (4.8). Panel (c) indicates that $K_{\parallel}\cos^2\psi$

dominates K_{rr} in the inner heliosphere where $r < 10$ AU, whereas $K_{\perp r} \sin^2\psi$ dominates in the outer heliosphere in the equatorial region. Panel (d) illustrates how $K_{||} \sin^2\psi$ totally dominates $K_{\phi\phi}$. It is therefore clear that $K_{||}\sin^2\psi$ determines the azimuthal dependence of $K_{\phi\phi}$ in the equatorial plane. Furthermore, panel (c) and (d) indicate that $K_{\phi\phi}$ is significantly larger than K_{rr} in the equatorial plane throughout most of the heliosphere. This means that $K_{\phi\phi}$ cannot be ignored in the modulation of electrons, especially when Jovian electrons are considered and for that a three dimensional modulation model is required. Studies of modulation in the outer heliosphere can reasonably be approximated by using a two dimensional model. For the simplicity of the 3D model $K_{||}$ and $K_{\perp r}$ are assume not to have azimuthal dependence.

4.5.2 The rigidity dependence

Figure (4.6) illustrates the rigidity dependence of $K_{\phi\phi}$ and K_{rr} at 1 AU (dotted lines) and 5 AU (solid lines) respectively in the equatorial plane. The rigidity dependence of $K_{\phi\phi}$ shown in panel (a) is essentially determined by the rigidity dependence of $K_{||}$ because $K_{||}\sin^2\psi$ dominates $K_{\phi\phi}$ throughout the heliosphere in the equatorial region as discussed in the previous section. The rigidity dependence of K_{rr}, shown in panel (b), is also determined by the rigidity dependence of $K_{||}$ because $K_{||}\cos^2\psi$ dominates K_{rr} in the inner heliosphere where $r < 10$ AU.

4.5.3 The latitudinal dependence

Shown in Figure (4.7), panels (a) and (b), are the latitudinal dependence of $K_{\phi\phi}$ and K_{rr} at 1 AU (dotted lines) and 5 AU (solid lines) for 7 MeV electrons. In panel (a) it is illustrated that $K_{\phi\phi}$ is large in the equatorial plane and decreases towards the poles because spiral angle at poles becomes zero thus from Equation (4.8) $K_{\phi\phi}$ is dominated by $K_{\perp r}$, whereas K_{rr}, shown in panel (b), becomes significantly larger towards the poles because in Equation (4.6) K_{rr} is dominated by $K_{||}$ at the pole. As discussed in section (4.5.1) that $K_{||}$ dominates $K_{\perp r}$ in the inner heliosphere thus K_{rr} increases towards the poles while $K_{\phi\phi}$ decreases towards the poles.

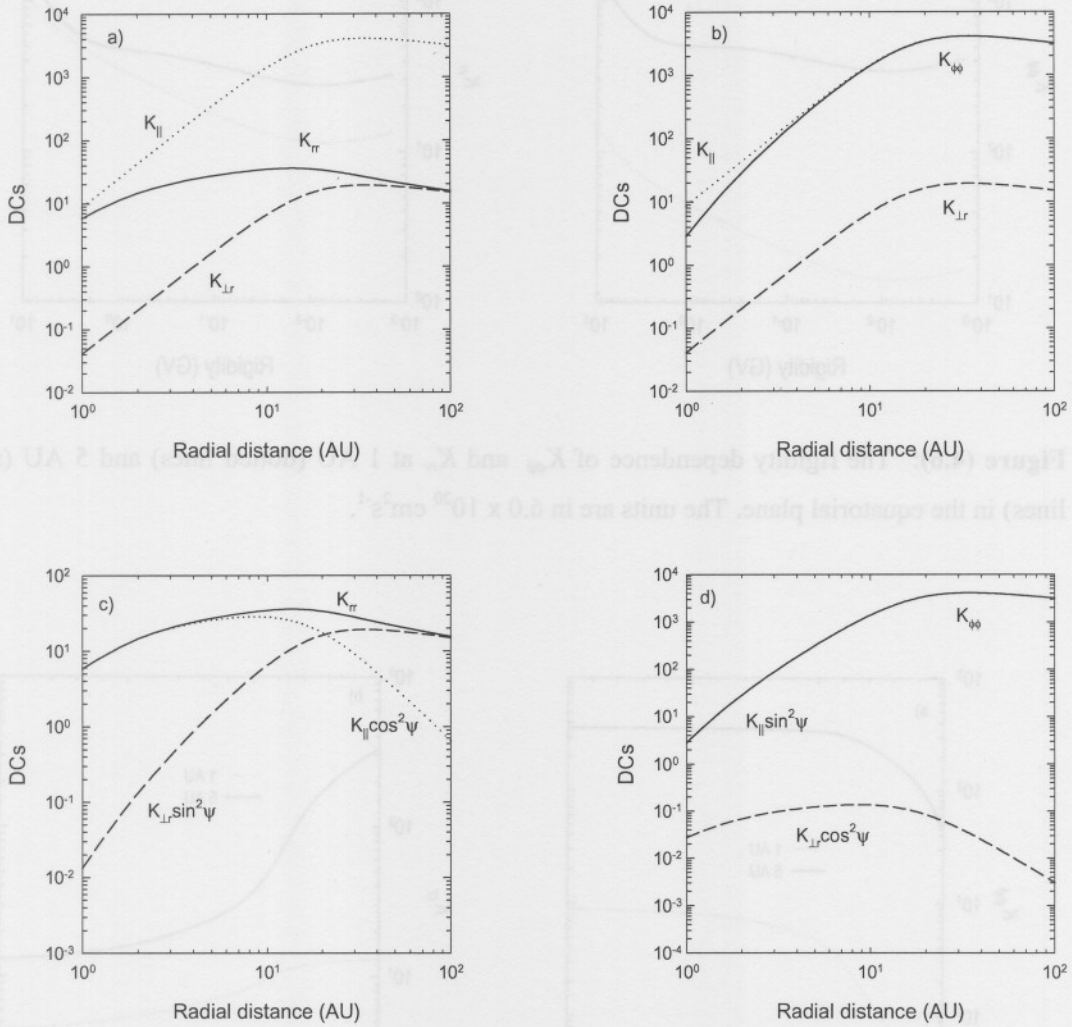

Figure (4.5): The radial dependence of the diffusion coefficients K_{rr} and $K_{\phi\phi}$ (indicated as DCs) shown in the equatorial plane for 7 MeV electrons (solid lines). Shown in (a) and (b) are the values of $K_{||}$ and $K_{\perp r}$ (dotted and dashed lines respectively) compared to K_{rr} and $K_{\phi\phi}$, respectively. The effects of $\cos^2\psi$ and $\sin^2\psi$ according to Equations (4.6) and (4.8) are shown in (c) and (d) respectively. The DCs are in units of 6.0×10^{20} cm^2s^{-1}.

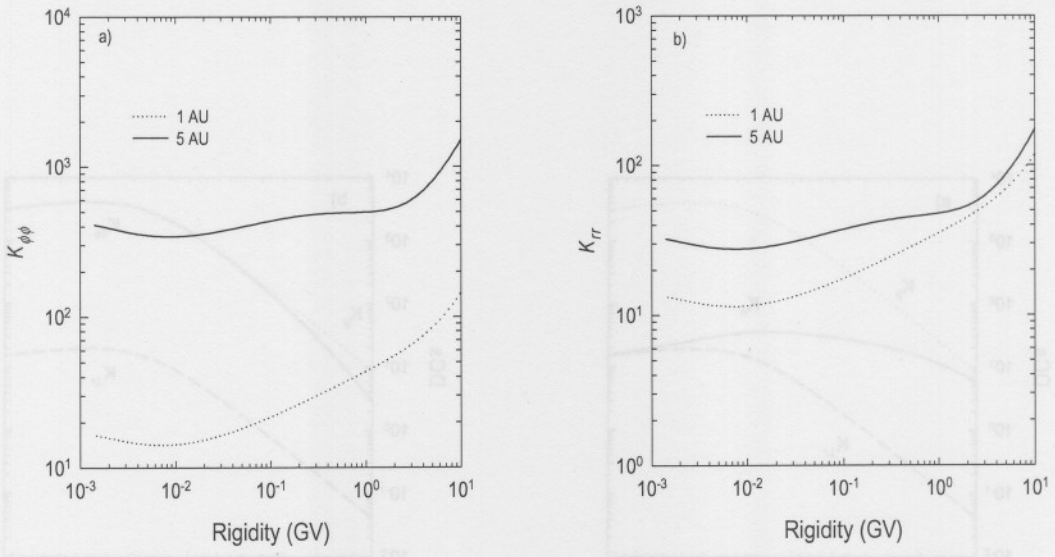

Figure (4.6): The rigidity dependence of $K_{\phi\phi}$ and K_{rr} at 1 AU (dotted lines) and 5 AU (solid lines) in the equatorial plane. The units are in 6.0 x 10^{20} cm^2s^{-1}.

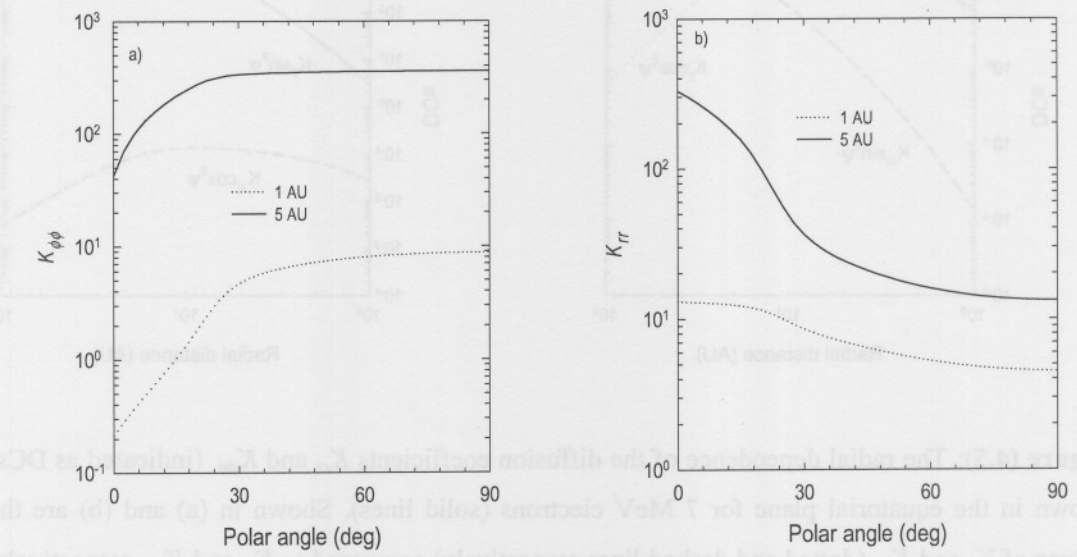

Figure (4.7): Panel (a) shows $K_{\phi\phi}$ and panel (b) shows K_{rr} as a function of polar angle at 1 AU (dotted lines) and 5 AU (solid lines) for 7 MeV electrons. The equatorial plane is at 90°. The units are in 6.0 x 10^{20} cm^2s^{-1}.

4.6 The 'drift' coefficient

The large scale HMF leads to gradient and curvature drifts of cosmic rays in the heliosphere. Drift effects were neglected until Jokipii et al. (1977) pointed out that particle drifts in the global HMF are an important mechanism of cosmic ray modulation. The inclusion of drifts into Equation (4.1) leads to important implications for CR modulation in the heliosphere (e.g., Jokipii and Thomas, 1981; Potgieter, 1984; Potgieter and Moraal, 1985; Burger, 1987; Hattingh, 1998; Ferreira and Potgieter, 2004a, b). Potgieter (1996) addressed the importance of drifts for electron modulation, see also Ferreira (2002), and Ndiitwani (2005) for details on the long-term implications over a 22-year modulation cycle, in particular the consequent charge-sign dependence.

The 'drift' coefficient under the assumption of weak scattering is given by

$$(K_A)_{standard} = (K_A)_0 \frac{\beta P}{3B_m}, \tag{4.28}$$

Here the constant $(K_A)_0$ is the dimensionless and may be chosen as 1.0, 0.5 and 0.0 which describe what Potgieter et al., (1999a) called 100% (full drifts), 50% (half drifts) and 0% (non drifts). The drift coefficient used by Burger et al., (2000) and Ferreira et al., (2002) differs slightly from the standard form and is given by

$$(K_A) = \frac{(K_A)_0 K_{drift}(P)}{3B_m}, \tag{4.29}$$

with B_m the modified HMF given by Equation (2.8), and $K_{drift}(P)$ is given by

$$K_{drift}(P) = \beta P \left(\frac{D_{fak} P^2}{D_{fak} P^2 + 1} \right), \tag{4.30}$$

with D_{fak}=10.0 and $(K_A)_0$ =1.0.

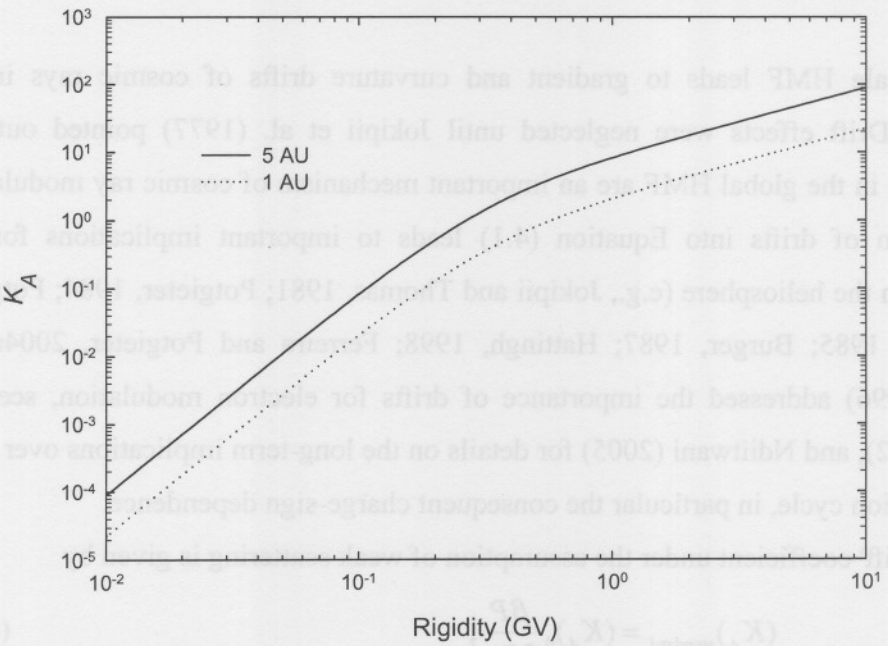

Figure (4.8): The rigidity dependence of K_A ('drift' coefficients) at 1 AU (dotted line) and 5 AU (solid line) according to Equation (4.29) in units of 6.0×10^{20} cm^{2}s^{-1}.

Equation (4.30) is shown in Figure (4.8) as a function of rigidity at 1 AU and 5 AU in the equatorial plane. It is evident that K_A decreases stronger as a function of decreasing rigidity than Equation (4.28). This illustration is consistent with the conclusions from Potgieter (1996), Potgieter and Ferreira (1999b), and Ferreira (2002) that drifts become less important with decreasing rigidity, especially with decreasing electron energy to have almost no effect on electron modulation below ~ 100 MeV, dependent of the diffusion parameters used, especially $K_{\perp\theta}$. From Equation (4.2) follows that drift effects depend on the product of the drift velocity and the spatial gradients; if the latter is small, drift effects will implicitly be diminished.

4.7 Summary

The distribution of cosmic rays in the inner heliosphere, especially between Earth and Jupiter, is a result of four modulation processes namely diffusion, convection, drifts and

adiabatic energy losses which can be combined into the transport equation derived by Parker (1965). In this chapter a brief background was given on the existing knowledge of the diffusion process, focusing mainly on the diffusion tensor applicable to electrons in the heliosphere. It was shown that in modulation models four diffusion coefficients are of special importance, namely $K_{||}$ and $K_{\perp}$, the diffusion coefficients parallel and perpendicular to the HMF, respectively, and that $K_{\perp}$ can be subdivided into two independent coefficients, $K_{\perp r}$ and $K_{\perp \theta}$ which are perpendicular diffusion in the radial/azimuthal direction and in the polar direction. The fourth element of the diffusion tensor is the 'drift' coefficient K_A that represents gradient, curvature and current sheet drift. The spatial and rigidity dependence of the four coefficients were reviewed. An advanced treatment of the diffusion coefficients as described by Stawicki (2003), Schlickeiser (2002), Bieber (2003), and Minnie (2005) is beyond the scope of this dissertation.

In modeling based on solving the transport equation in spherical coordinates, the elements have to be specified in this system, so that emphasis was placed on the radial, latitudinal and rigidity dependence of $K_{\phi\phi}$ the effective diffusion in the azimuthal direction and on K_{rr}, the effective diffusion in the radial direction, and on the diffusion coefficients in e.g. the $r\phi$ direction which were neglected in the previous studies using 2D modulation models. It was shown that K_{rr} is dominated by $K_{||}\cos^2\psi$ in the inner heliosphere but dominated by $K_{\perp r}\sin^2\psi$ in the outer heliosphere and that K_{rr} increases towards the poles, whereas $K_{\phi\phi}$ is dominated by $K_{||}\sin^2\psi$ and is significantly larger throughout the most of the heliosphere in the equatorial plane and decreases significantly towards the poles.

In the next chapter the 3D Jovian electron modulation model will be discussed in more detail, including the Jovian electron source.

Chapter 5

A three-dimensional modulation model including a Jovian electron source

5.1 Introduction

In this chapter the steady-state, three-dimensional (3D) modulation model of Ferreira (2002) for Jovian and galactic electrons is described. This model is based on the numerical solution of the Parker (1965) transport equation for three spatial dimensions and one energy 'dimension' as discussed in the previous Chapters.

In the first part of this chapter a brief overview of the history of three-dimensional modulation models is given. After this, a discussion follows on the 3D Jovian modulation model, including the Jovian electron source function, and the local interstellar spectrum (LIS) for electrons. The last part of the chapter illustrates the sensitivity of the model when changing the radial grid size and when the radial position of the heliospheric modulation boundary for Jovian electrons is changed to save on computer time.

5.2 Short history of three-dimensional numerical models

Three-dimensional, steady-state models were independently developed by Kóta and Jokipii (1983), Williams (1990), Hattingh (1998), and recently by Gil and Alania (2001). See also Hattingh and Burger (1995b). New generation 3D models were developed independently for electron modulation by Fichtner et al. (2000b) and Ferreira et al. (2001a) both of which included the Jovian magnetosphere as a source of low-energy electrons. The model by Fichtner et al. (2000b) is a 3D non-drift model whereas the model by Ferreira et al. (2001a) also includes gradient, curvature and current sheet drifts. A 3D time dependent version (Fichtner et al., 2001b; Kissmann et al., 2004; Lange, 2004) followed but averages over energy to estimate adiabatic cooling so that it can be applied only to low-energy electrons. All these models are suitable to simulate the three-

dimensional modulation of low-energy Jovian and galactic CR electrons in the heliosphere, especially in the inner heliosphere where azimuthal dependence become important. This cannot be done with 2D models. ,

The steady-state models can describe solar cycle effects only as a series of steady-state solutions with each solution containing a solar activity related change in the modulation parameters such as the solar wind, the various diffusion coefficients, and the Jovian electron source. These models obviously neglect the effect of the solar wind termination shock (TS). This was described by Ferreira et al. (2001a, b, c) using a 2D TS model. Recently Moeketsi (2004) and Moeketsi et al. (2005) used the steady-state model by Ferreira et al. (2001a) to study for example the contribution of galactic and Jovian electrons to the total modulation along the Ulysses trajectory. The model was found to be most successful during solar minimum conditions. For solar maximum conditions the modulation parameters had to be changed significantly (Ferreira et al., 2004). Lange (2004) and Lange et al. (2005) did a similar simulation used the time dependent model mentioned above so that the study could be expanded to include solar maximum conditions implicitly.

In this work the steady-state model of Ferreira (2002) and Ferreira et al. (2001a, b, c), also used by Moeketsi (2004), is used to compute three-dimensional Jovian and galactic anisotropies in the inner heliosphere, a study not done before for electrons.

5.3 The 3D Jovian electron modulation model

The steady-state, 3D Jovian electron modulation model is based on the transport equation (TPE) (see section 4.1) and describes the major physical mechanisms of the heliospheric transport of low energy (< 30 MeV) Jovian and galactic electrons. To solve Equation (4.1) numerically, it is rewritten in a coordinate system rotating with the Sun and the heliospheric current sheet is assumed to be wavy but in a steady-state. In spherical coordinates and assuming $\partial f/\partial t = 0$, the TPE takes the form given in Equation (4.2). Following Hattingh (1998) and Ferreira (2002), it is solved numerically using the following boundary conditions:

(1) The heliosphere is assumed to be spherical with an outer boundary at r_b = 120 AU where a LIS is specified as an input spectrum, discussed in a later section.

(2) The inner boundary is specified at $r_i = r_\odot$ and it is assumed that the radial gradient of the distribution function just outside the boundary is equal to the gradient just inside. This implies that no particles enter or leave the Sun:

$$\left.\frac{\partial f}{\partial r}\right|_{r=r_\odot} = 0. \tag{5.1}$$

Siluszyk and Alania (2001) showed that

$$\left.\frac{\partial f}{\partial r}\right|_{r=r_\odot} \neq 0, \tag{5.2}$$

could be a more appropriate boundary condition implying an absorbing Sun. However, this only affects cosmic rays well within 1 AU, and is therefore not used.

(3) At the heliospheric poles it is assumed that:

$$\left.\frac{\partial f}{\partial \theta}\right|_{\theta=180^0}^{\theta=0^0} = 0. \tag{5.3}$$

This means that the solutions are symmetrical with respect to polar axis.

Equation (4.2) is a parabolic differential equation and is solved using the Alternating Direction Implicit (ADI) method, which is a modification of the Crank-Nicholson finite difference method. Douglas (1962) had initially developed this method to solve parabolic differential equations in terms of two spatial coordinates and a time coordinate (see Potgieter, 1984). The TPE solution is computed using this numerical scheme in the following manner: A first solution, using the LIS as an initial condition, is determined at a third of the rigidity step forward by solving the TPE implicitly in the direction of the first spatial coordinate, in this case, the radial distance r (in AU). A second solution is determined at another third of the rigidity step forward, in terms of the first solution by solving the TPE implicitly in the direction of the second spatial coordinate, the polar angle θ. This whole process is then repeated for the last spatial coordinate, the azimuthal angle ϕ, to determine a solution at the last third of the rigidity

step forward in terms of the previous two solutions. The result is a system of linear equations which can be solved using the Thomas algorithm (e.g. Lapidus and Pinder, 1982). The numerical scheme for solving the TPE in the mentioned three spatial coordinates and for rigidity (or energy or momentum) was first done locally by Williams (1990) for a flat current sheet and later by Hattingh (1998) for a wavy current sheet. For the technical details of solving the TPE numerically, the reader is advised to see Potgieter (1984), Hattingh (1998) and Ferreira (2002).

5.4 The Jovian electron source function

Simulating the modulation of Jovian electrons using an analytical model, Ferrando et al. (1991) and Rastoin (1995) used a source function given by Equation (3.1) with $\gamma = 2.5$ at all energies measured by the University of Chicago instrument on ISEE 3 (ICE) (Moses, 1987) during the period of best magnetic connection between Earth and Jupiter as well as Pioneer 10 electron spectra (e.g., Eraker, 1982; Lopate, 1991) as shown in Figure (5.1). Haasbroek (1997) used a source function with a roll-over in the spectral index from $\gamma =$ 1.5 to $\gamma = 3.5$ at 5 MeV and is expressed in terms of the differential intensity as a function kinetic energy E as:

$$j_{source}(E) = C_c \left(\frac{E}{E_0}\right)^{-1.5} \left(1+\frac{E}{h_c}\right)^{-n_c}, \qquad (5.4)$$

with $C_c = 4.8 \times 10^8$ particles $m^{-2}\ s^{-1} sr^{-1} MeV^{-1}$, $n_c = 3.5$, $h_c = 5$ MeV and $E_0 = 1$ MeV. This source is shown in Figure (5.1a). Recently, Ferreira et al. (2002) indicated that the spectrum given by Equation (3.1) does fit the Pioneer 10 lowest energy electron data because it decreases as a function of increasing energy much faster than indicated by the data because the roll-over from $\gamma = 1.5$ to $\gamma = 3.5$ occurs at a very low energy. By simulating the spectra where $j(E) \propto E^{-1.5}$ (dotted line)and $j(E) \propto E^{-6.0}$ (dashed line) as shown in Figure (5.1b), Ferreira et al. (2001a) could produce compatibility with the observed roll-over for the Jovian spectrum from $\gamma = 1.5$ to $\gamma = 6.0$ at ~ 20 MeV.

To construct the Jovian source function Q in Equation (4.1), Ferreira et al. (2001a) invoked the superposition of the spectra $j(E) \propto E^{-1.5}$ and $j(E) \propto E^{-6.0}$ and obtained:

$$Q = j_{source}(E) = 1.5\left(\frac{c_k j_{1.5} d_k j_{6.0}}{c_k j_{1.5} + d_k j_{6.0}}\right), \tag{5.5}$$

with

$$j_{1.5} = 5.0\times10^{3}\left(\frac{E}{E_0}\right)^{-1.5},$$

$$j_{6.0} = 10^{9}\left(\frac{E}{E_0}\right)^{-6.0},$$

$$c_k = 6.0,$$

$$d_k = 5.0, \tag{5.6}$$

with j_{source} in the units of particles m^{-2} $s^{-1}sr^{-1}MeV^{-1}$. This function above is shown in Figure (5.1c) and has been used in modulation studies by Ferreira et al. (2001a, b), Ferreira and Potgieter (2002), Kissmann et al. (2004) and Moeketsi (2004) to describe the source spectrum of low-energy electrons at Jupiter. It is also used in this study.

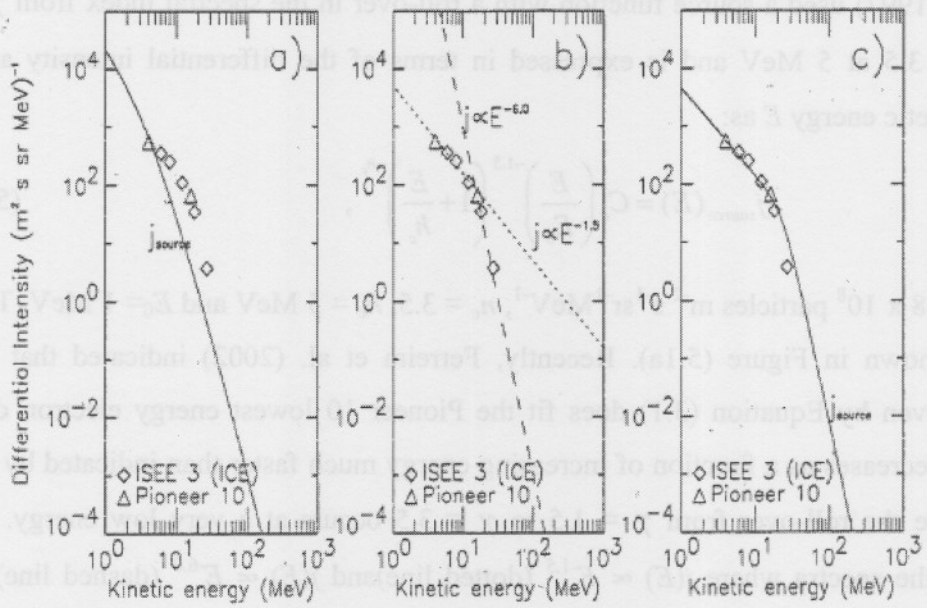

Figure (5.1): (a) The source function of Haasbroek (1997) given by Equation (5.4). Also shown are low-energy Jovian electron data from ISSE 3 ICE (Moses, 1987) and Pioneer 10 (Eraker, 1982; Lopate, 1991). (b) Spectra where $j(E) \propto E^{-1.5}$ (dotted line) and $j(E) \propto E^{-6.0}$ (dashed line). (c) A source function given by Equation (5.6) in comparison with observations. (From Ferreira, 2002).

5.5 The electron local interstellar spectrum

The LIS for electrons is defined as a spectrum of galactic origin that is not modulated before entering the heliosphere and is specified as an initial condition at the outer modulation boundary, typically the heliopause, and then modulated throughout the heliosphere according to the TPE. For implications of different LIS on the heliospheric modulation of CRs, see Langner (2000, 2004), Langner et al. (2001a, b, c) and Ferreira and Potgieter (2002).

In this study the electron LIS of Langner et al. (2001a, b, c) is used. The parameterisation of this LIS is given by:

if $P < 0.0026$ GV,

$$j_{LIS} = \frac{214.32 + 3.32\ln(P)}{1 + 0.26\ln(P) + 0.02(\ln(P))^2},$$

if $0.0026 \text{ GV} \le P < 0.1$ GV,

$$j_{LIS} = 1.7\left(\frac{52.55 + 23.01P}{1 + 148.62P}\right)^2,$$

if $0.1 \text{ GV} < P \le 10$ GV,

$$j_{LIS} = \frac{1555.89 + 17.36P - 3.4\times10^{-3}P^2 + 5.13\times10^{-7}P^3}{(1 - 11.22P + 7532.93P^2 + 2405.01P^3 + 103.87P^4)}, \quad (5.7)$$

if $P > 10$ GV,

$$j_{LIS} = 1.7\exp(-0.89 - 3.22\ln(P)),$$

with j_{LIS} the differential intensity in particles $m^{-2}s^{-1}sr^{-1}MeV^{-1}$, the rigidity is $P = pc/q$ in units of GV, where p is the momentum of the particle with charge q, and c the speed of light.

5.6 Sample solutions of the 3D Jovian model

In this section sample solutions of the 3D Jovian model are given to determine and illustrate the sensitivity of the model to the grid size in the radial direction. The model parameters that were discussed in the previous chapters are summarized briefly:

(1) The parallel diffusion coefficient $K_{\parallel}$ is given by Equation (4.32).

(2) The perpendicular diffusion $K_{\perp}$ scales as $K_{\parallel}$ with $K_{\perp r}$ given by Equation (4.24) with a = 0.010 and $K_{\perp\theta}$ with b = 0.015 as in Equation (4.26). The function $F(\theta)$ is given by Equation (4.27).

(3) The increase of $K_{\perp\theta}$ from its value in the equatorial plane towards the poles by a factor $d = 7$.

In the next subsections, an illustration is given of the effects of reducing the radial grid with grid number N = 300 over a heliosphere of 120 AU, typically used for galactic electrons (e.g., Ferreira, 2002; Moeketsi, 2004) to N = 150 over just 15 AU for Jovian electrons. This means that Δr = (120 AU)/300 = 0.4 AU per radial grid is changed to 0.1 AU per radial grid. For Jovian electrons the solution of the TPE is programmed to approach zero at 15 AU

5.6.1 The effect of the radial grid size on model computations

To study the effect of different radial grid sizes and modulation boundaries, the 7 MeV Jovian electron radial profiles are shown in Figures (5.2a, b, c) with polar angles $\theta = 30^0$, $\theta = 60^0$, $\theta = 80^0$ respectively, and in Figure (5.2d) for the equatorial plane where $\theta = 90^0$. Two solutions are shown, first for N = 150 and r_b = 15 AU (solid line) and second with N = 300 and r_b = 120 AU (dotted line), respectively. The polar and azimuthal grids are kept unchanged with the corresponding number of grid points M = 73 and S = 66, respectively. This leads to $\Delta\theta = 2.5°$ and $\Delta\phi = 5.5°$. For the sensitivity of the computations to the number of polar and azimuthal grid points, see Ferreira (2002).

Figure (5.2a), with $\theta = 30^0$ illustrates that changing the number of radial grid points results in a difference of factor of ~ 1.7 for $r < 5$ AU. Figures (5.2b, c, d) illustrate that the model solutions converge as polar angle increases from the poles to the equatorial plane at $r \leq 10$ AU. In this work the number of grid points and modulation boundary used is N = 150 (r_b = 15 AU) for Jovian electrons since the focus is in the inner heliosphere.

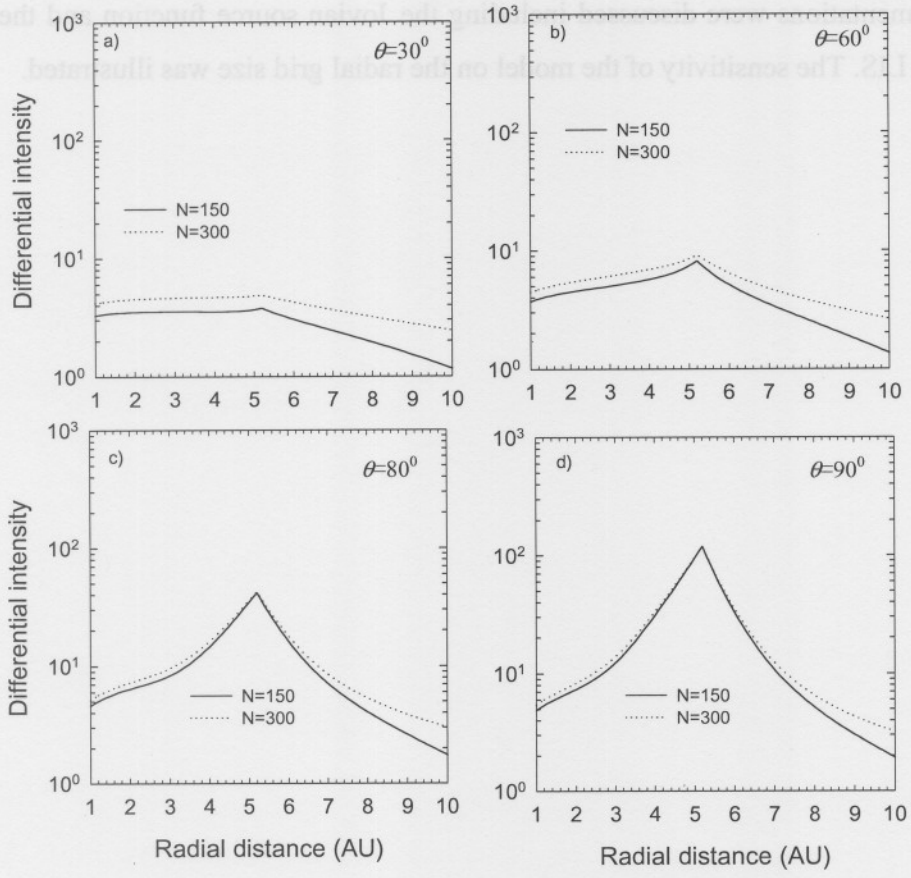

Figure (5.2): Computed radial profiles for 7 MeV electrons in units of particles $m^{-2}s^{-1}sr^{-1}MeV^{-1}$ for polar angles (a) $\theta = 30^0$, (b) $\theta = 60^0$, (c) $\theta = 80^0$ and (d) the equatorial plane at $\theta = 90^0$. Two solutions are shown for the radial grid number $N = 150$ ($r_b = 15$ AU) (solid line) and $N = 300$ ($r_b = 120$ AU) (dotted line) respectively, while keeping $\Delta\theta = 2.5^0$ and $\Delta\phi = 5.5^0$.

5.7 Summary

In this chapter the 3D Jovian electron modulation model of Ferreira (2002) and the numerical implementations were discussed including the Jovian source function and the galactic electron LIS. The sensitivity of the model on the radial grid size was illustrated.

Chapter 6

The role of perpendicular diffusion in the modulation of electron gradients

6.1 Introduction

Measurements of cosmic ray intensity with detectors on board various spacecraft have proven to be vital in understanding the modulation of cosmic rays in the heliosphere. One of these spacecraft is Ulysses, which has since its launch sampled the heliosphere between Earth and Jupiter in three dimensions. During this time the Jovian electron intensity measured by Ulysses has varied significantly because of the changing heliomagnetic distance to Jupiter and also with changing solar activity. In 1992 and 2004, Ulysses had an encounter with the Jovian magnetosphere, allowing the study of the propagation of electrons originating from this 'point' source in the inner heliosphere, from the viewpoint of global modulation. The closest approach to Jupiter was 0.003 AU in 1992 and 0.803 AU in 2004 (a distant close encounter). These observations are important in evaluating and testing numerical propagation and modulation models.

For the purpose of this chapter, the 3D steady-state electron modulation model described in the previous Chapter is used to calculate three-dimensional intensity gradients for galactic and Jovian electrons. Although early models of electron propagation in the inner heliosphere (Roelof et al., 1983) assumed that diffusion along the magnetic field was the dominant motion of the particles, measurement of latitudinal gradient of cosmic ray intensity by Ulysses spacecraft have indicated that diffusion perpendicular to the magnetic field is more important than expected (e.g., Potgieter, 1996; McKibben, 1998; Potgieter, 1998). In this chapter the emphasis is placed on the role that polar perpendicular diffusion plays in establishing electron intensity gradients in the inner heliosphere.

6.2 Three-dimensional gradients

The relationship between the differential intensity spectra, j, and omni-directional distribution, $f(r,\theta,\phi,P)$, for cosmic rays in the heliosphere as a function of the three spatial spherical coordinates and rigidity P, is given by

$$j \propto P^2 f, \tag{6.1}$$

where $P = pc/q$ with p the particle momentum, q the charge and c the speed of light. Since pc has the units of energy and q has the unit of charge, it can easily be shown that P has the unit of volts. For electrons with low energies ($E \leq 30$ MeV), $P \approx E$, where E is the kinetic energy of the particle.

The gradient in the intensity of cosmic rays in the heliosphere is defined as

$$G = \frac{1}{f}\frac{\partial f}{\partial r}\mathbf{e}_r + \frac{1}{rf}\frac{\partial f}{\partial \theta}\mathbf{e}_\theta + \frac{1}{r\sin\theta f}\frac{\partial f}{\partial \phi}\mathbf{e}_\phi. \tag{6.2}$$

The radial gradient is

$$G_r = \frac{1}{f}\frac{\partial f}{\partial r} = \frac{\partial \ln f}{\partial r}, \tag{6.3}$$

and latitudinal gradient G_λ is related to the polar gradient G_θ by

$$G_\lambda = rG_\theta = \frac{1}{f}\frac{\partial f}{\partial \theta} = \frac{\partial \ln f}{\partial \theta}, \tag{6.4}$$

and the azimuthal gradient G_χ is given by

$$G_\chi = rG_\phi = \frac{1}{f\sin\theta}\frac{\partial f}{\partial \phi} = \frac{1}{\sin\theta}\frac{\partial \ln f}{\partial \phi}. \tag{6.5}$$

In practice, generally only the difference between two intensities, measured at position (r_1, θ_1, ϕ_1) and (r_2, θ_2, ϕ_2) in the heliosphere is known. The average radial, latitudinal and azimuthal gradients are then be calculated using

$$\langle G_r \rangle = \frac{1}{f}\frac{\Delta f}{\Delta r} = \frac{\ln(f_2/f_1)}{r_2 - r_1}, \tag{6.6}$$

expressed in % per AU and

$$\langle G_\lambda \rangle = \frac{1}{f}\frac{\Delta f}{\Delta \theta} = \frac{\ln(f_2/f_1)}{\theta_2 - \theta_1}, \tag{6.7}$$

$$\langle G_\chi \rangle = \frac{1}{f \sin\theta} \frac{\Delta f}{\Delta \phi} = \frac{1}{\sin\theta} \frac{\ln(f_2 / f_1)}{\phi_2 - \phi_1}, \tag{6.8}$$

both are expressed in % per degree. Note that G_χ is undefined at the heliospheric poles. In this chapter the computed gradients are shown, calculated at 1 AU and 5 AU as a function of kinetic energy and position.

6.3 Modulation effects on electrons at all energies

6.3.1 Spectra

The latitude dependence of $K_{\perp\theta}$ is determined by the parameter $F(\theta)$ as discussed in Chapter 4, given by Equations (4.26) and (4.27) respectively. According to Equation (4.27), the extent of the latitude dependence of $F(\theta)$ can be changed by varying the parameter d. Moeketsi (2004) discussed the relation between the observed latitude dependence of the solar wind speed V, as modelled with the parameter φ, and by assuming a relation between φ and d, implicitly assuming a relation between the latitude dependence of V and $F(\theta)$. This is illustrated in Figure (6.1). It gives a simple relation between the latitude dependence of V and $K_{\perp\theta}$. The parameter $F(\theta)$ and V are shown as a function of polar angle. Simulations are done for a scenario with $\varphi = 20^0$ corresponding to $d = 6$, a scenario assumed for solar minimum, $\varphi = 55^0$ corresponding to $d = 3.5$, a scenario assumed for intermediate solar activity conditions, and then for $d = 1$, a scenario assumed for solar maximum conditions. The latitudinal dependence of V observed by the SWOOPS instrument (e.g., McComas et al., 2002b) for solar minimum (light data curve) and solar maximum conditions (dark data) is shown in the upper panel for comparison. The effects on the electron energy spectra of changing $K_{\perp\theta}$ using different d scenarios are illustrated next.

Shown in Figure (6.2) are electron spectra at 1 AU and in Figure (6.3) at 5 AU computed with $\theta = 10^0$, $\theta = 60^0$ and $\theta = 90^0$ respectively for the A > 0 magnetic polarity epoch. Panels (a), (c) and (e) show modulated galactic spectra with respect to the LIS of Langner et al. (2001), while (b), (d) and (f) show modulated Jovian electron spectra with respect to the electron source function given in Equation (5.7). The tilt angle α and drifts were changed in the model with increasing solar activity. It is well known that when solar

activity increases from solar minimum to solar maximum conditions, the tilt angle α increases from ~ 5° to 75° while the effects of drifts slowly diminishes (Ferreira and Potgieter, 2004). These features are included in the model, thus for solar minimum condition it is assumed that $\alpha = 5^0$ with constant $(K_A)_0 = 1.0$ (100% drifts) for the $d = 7$ scenario, $\alpha = 30^0$ for intermediate solar activity with $(K_A)_0 = 0.5$ (50% drifts) for the $d = 3.5$ scenario and $\alpha = 55^0$ for moderate solar maximum conditions with $(K_A)_0 = 0.2$ (20% drifts) for the $d = 1$ scenario respectively, where $(K_A)_0$ is given by Equation (4.29). The ratios $K_{\perp\theta}/K_{\parallel} = b = 0.015$ (in the equatorial plane) and $K_{\perp r}/K_{\parallel} = a = 0.010$ are kept constant for $d = 7$ for all polar angles. For $d = 1$, $b = 0.03$ at the equatorial plane but changes to $b = 0.025$ in the heliospheric polar regions, while $a = 0.001$ is kept constant for all polar angles. For $d = 3.5$, $b = 0.015$ and $a = 0.002$ for all polar angles.

It is evident for the galactic electron spectra both at 1 AU and 5 AU using the parameters specified that the intensity is similar in the lower energy region ($E < 100$ MeV) for all d scenarios. This means that the increasing enhancement of $K_{\perp\theta}$ towards the heliospheric poles gets progressively ineffective with decreasing galactic electron energies because it is related to drifts that are also getting negligible for low-energy electrons and with increasing solar activity (see also Potgieter, 1996; Ferreira et al., 2000). The "upturns" in the galactic spectra with increasing energy ($E > 50$ MeV) are a characteristic of the effect of drifts for this polarity epoch. At higher energies ($E \geq 1$ GeV), the galactic electron intensity computed with $d = 7$ is significantly larger than with $d = 1$. The largest differences between these two scenarios occur around ~ 50 MeV and ~ 500 MeV but with exactly the opposite trends. For Jovian electrons the effect of changing d is more noticeable in the low energy region ($E < 30$ MeV) of the spectra at all polar angles at 1 AU, while at 5 AU it is only noticeable at $\theta = 10^0$ and $\theta = 60^0$, as expected. The $d = 1$ scenario assumed to correspond to solar maximum conditions has higher intensities at all shown energies than for $d = 3.5$ which corresponds to intermediate solar activity and with $d = 7$ which corresponds to solar minimum. It is evident that Jovian electron intensities are modulated in the ecliptic plane. Also shown in Figures (6.2) and (6.3) is that galactic electrons increasingly dominate Jovian electrons towards the heliospheric polar regions, while Jovian electrons unmistakably dominate in

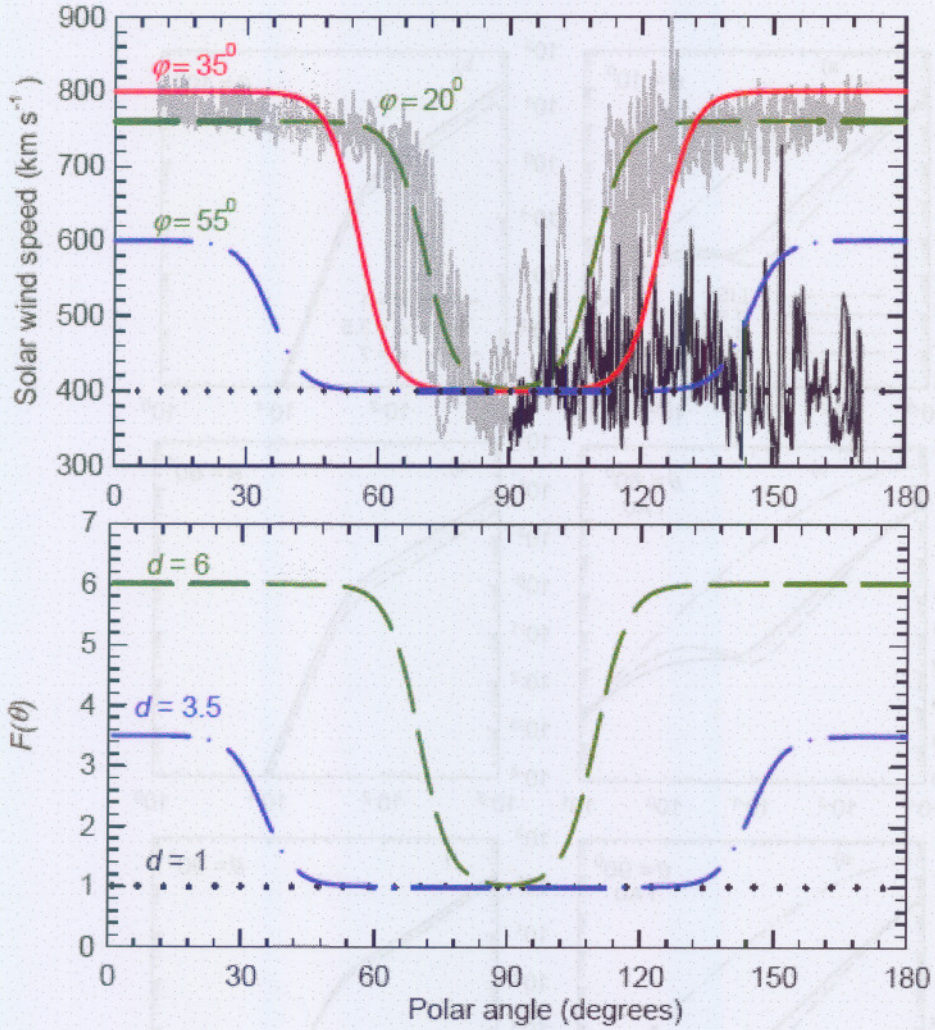

Figure (6.1): The solar wind speed V and function $F(\theta)$ according to Equation (4.24) are shown as a function of polar angle, θ. Simulations are done for a scenario with $\varphi = 20^0$ corresponding to $d = 6$, a scenario assumed for solar minimum; $\varphi = 55^0$ corresponding to $d = 3.5$, a scenario assumed for intermediate solar activity conditions; and for $d = 1$, a scenario assumed for solar maximum conditions. Latitudinal dependence of V observed by the SWOOPS instrument (e.g., McComas et al., 2002b) for solar minimum (light data curve) and solar maximum conditions (dark data) is shown in the upper panel for comparison. Adapted from Moeketsi (2004).

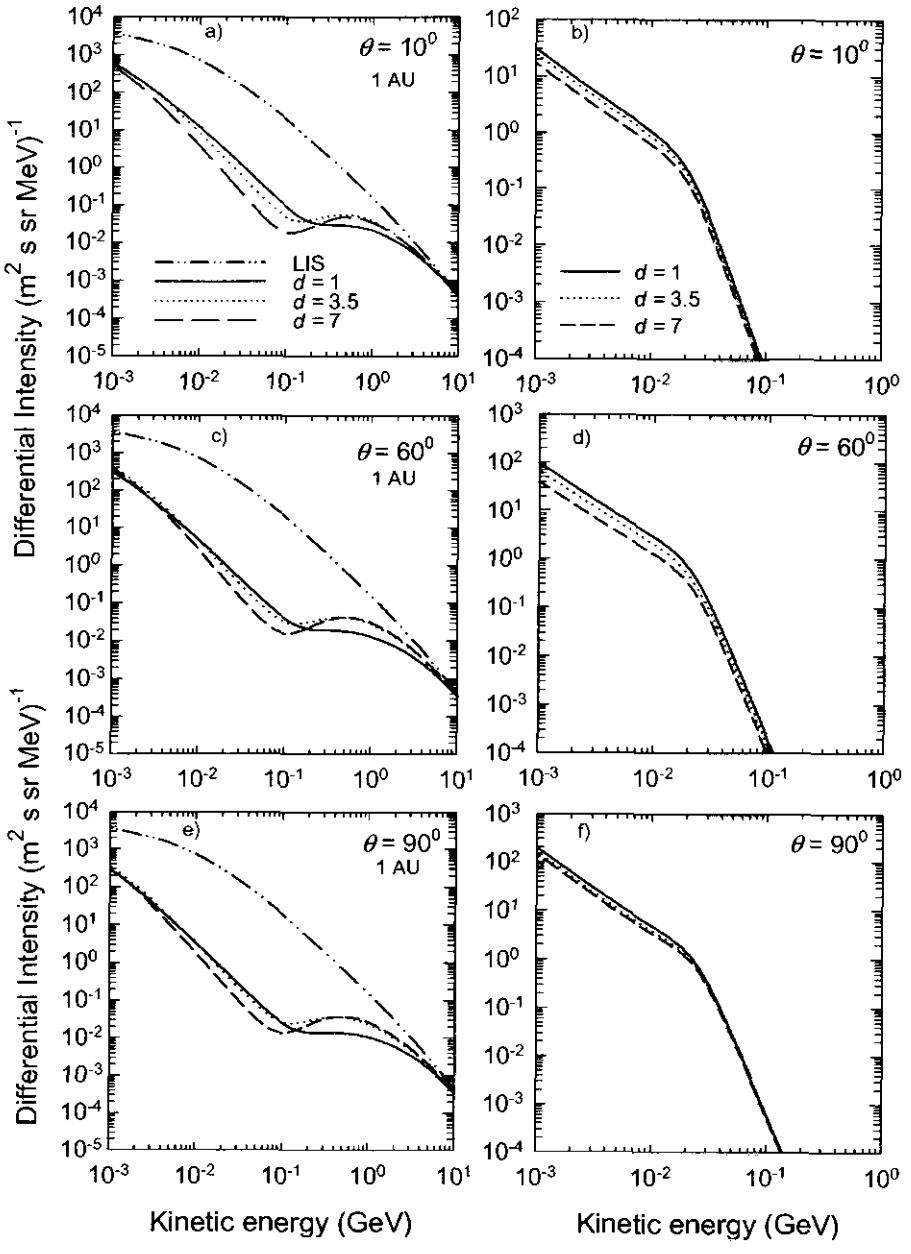

Figure (6.2): Computed galactic (left panels) and Jovian electron spectra (right panels) as a function of kinetic energy at 1 AU for three d scenarios during the A > 0 magnetic polarity epoch. Top panels: at $\theta = 10^0$ with $K_{\perp\theta}/K_{\parallel} = 0.025$ and $K_{\perp r}/K_{\parallel} = 0.001$; Middle panels: $\theta = 60^0$ $K_{\perp\theta}/K_{\parallel} = 0.02$ and $K_{\perp r}/K_{\parallel} = 0.001$; Bottom panels: $\theta = 90^0$ with $K_{\perp\theta}/K_{\parallel} = 0.03$ and $K_{\perp r}/K_{\parallel} = 0.001$ all for $d = 1$. Also for $d = 3.5$ and $d = 7$, for which $K_{\perp\theta}/K_{\parallel} = 0.015$ and $K_{\perp r}/K_{\parallel} = 0.010$, as given by Ferreira et al. (2002).

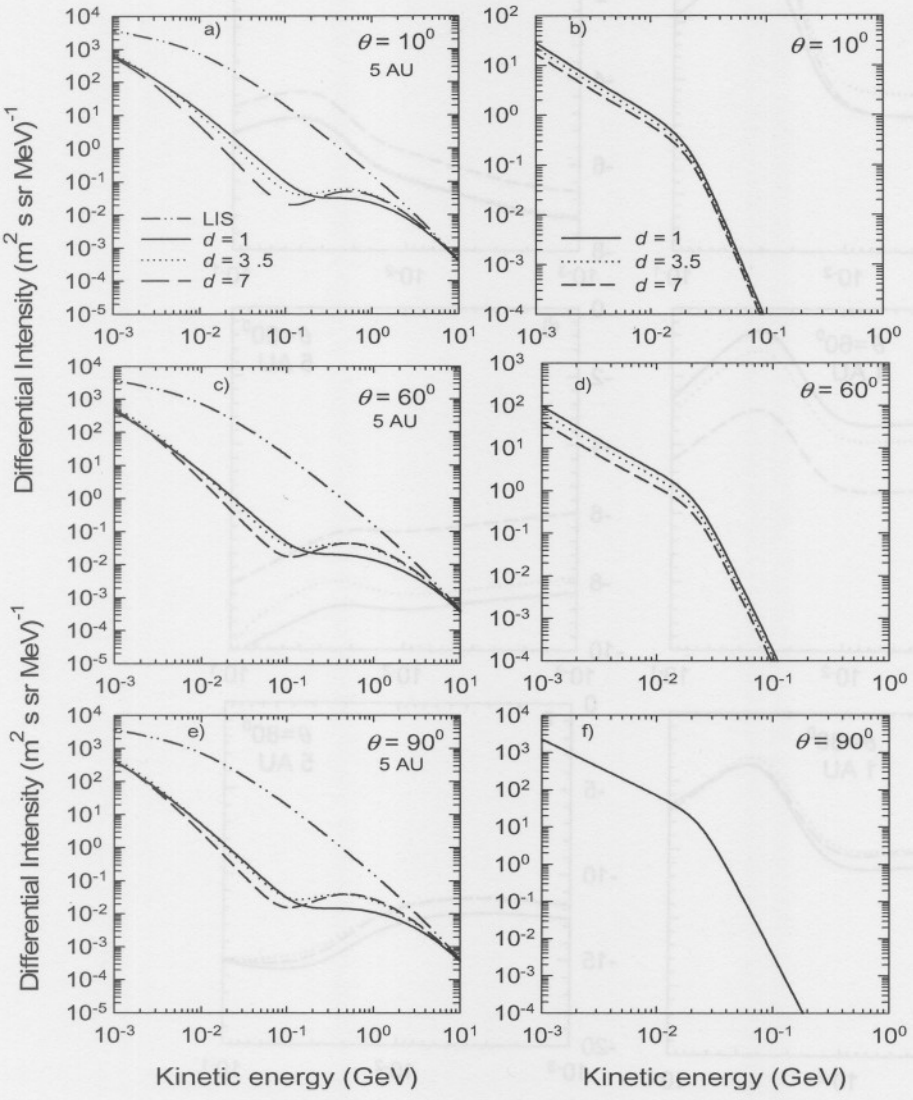

Figure (6.3): Similar to Figure (6.2), but with computed spectra at 5 AU.

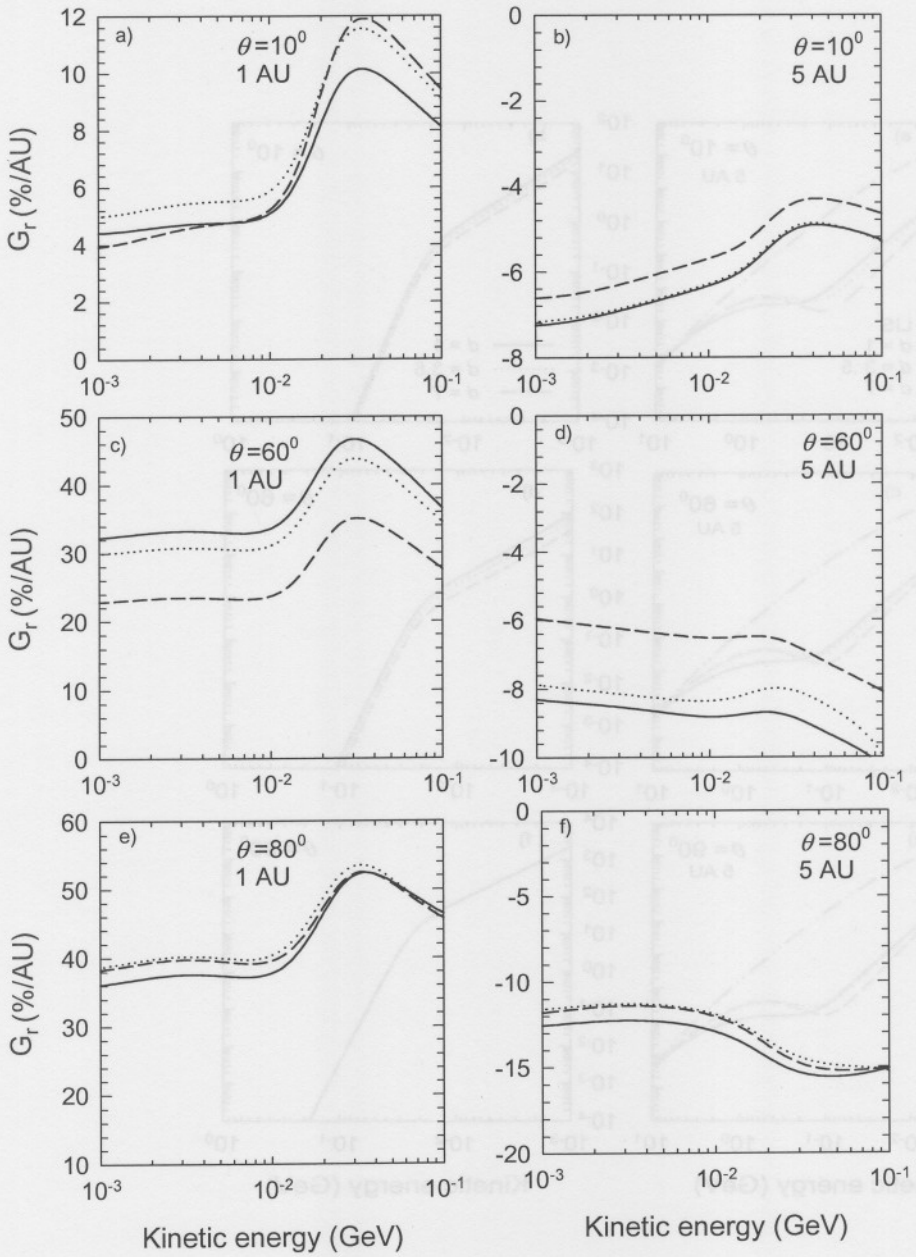

Figure (6.4): Computed Jovian electron radial gradient (G_r) at 1 AU and 5 AU as a function of kinetic energy, shown at $\theta = 10^0$ (upper panels), $\theta = 60^0$ (middle panels) and $\theta = 80^0$ (bottom panels) for the A > 0 magnetic polarity epoch. The computations are for the different d scenarios shown in Figure (6.1). The azimuthal angle is $\phi = 0^0$ and Jovian source at $r = 5.2$ AU.

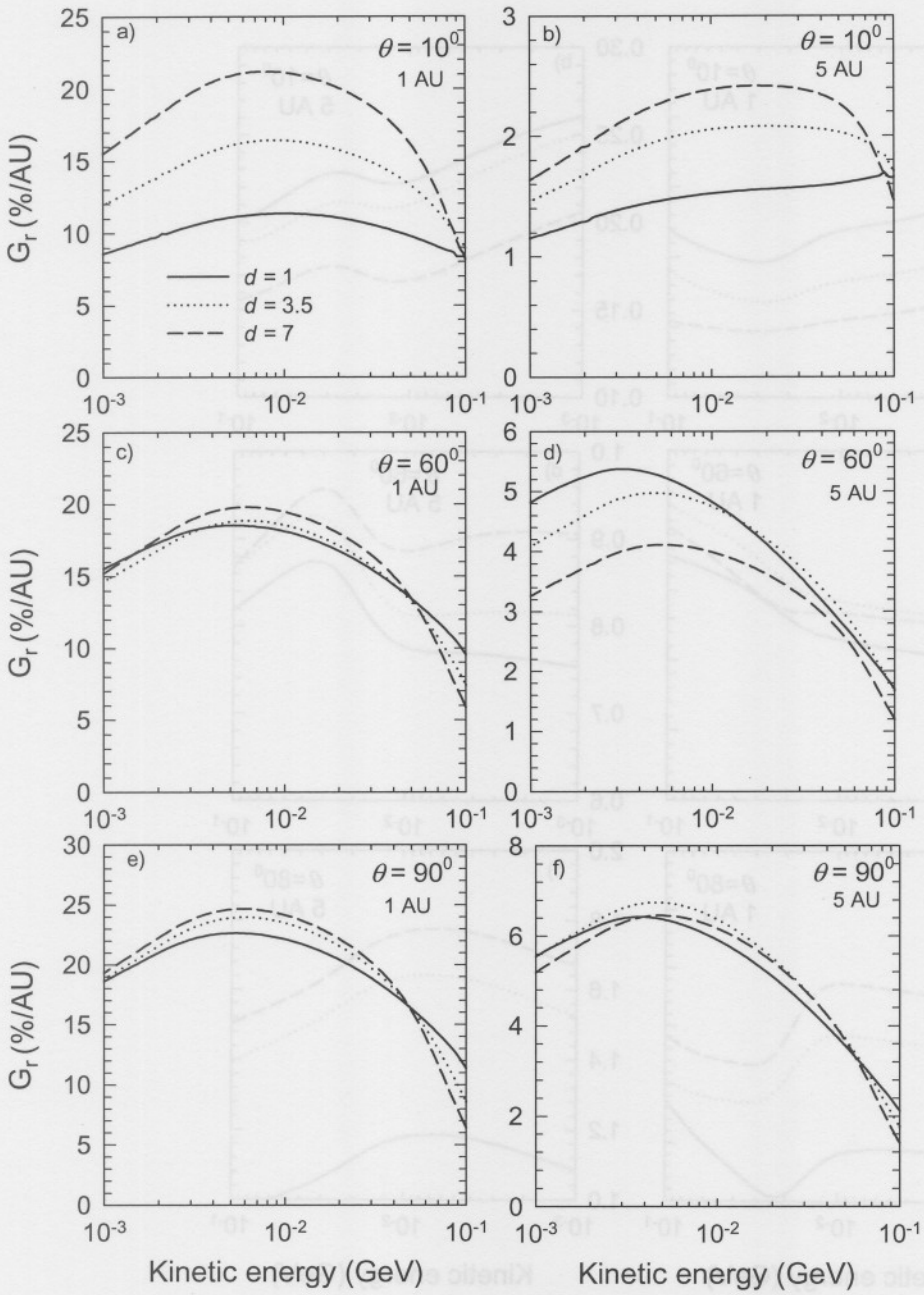

Figure (6.5): Computed galactic electron radial gradient (G_r) at 1 AU and 5 AU as a function of kinetic energy, shown at $\theta = 10^0$ (upper panels), $\theta = 60^0$ (middle panels) and $\theta = 90^0$ (bottom panels) for A > 0 magnetic polarity epoch. The computations are for the different d scenarios shown in Figure (6.1). The azimuthal angle is $\phi = 0^0$ and Jovian source at $r = 5.2$ AU.

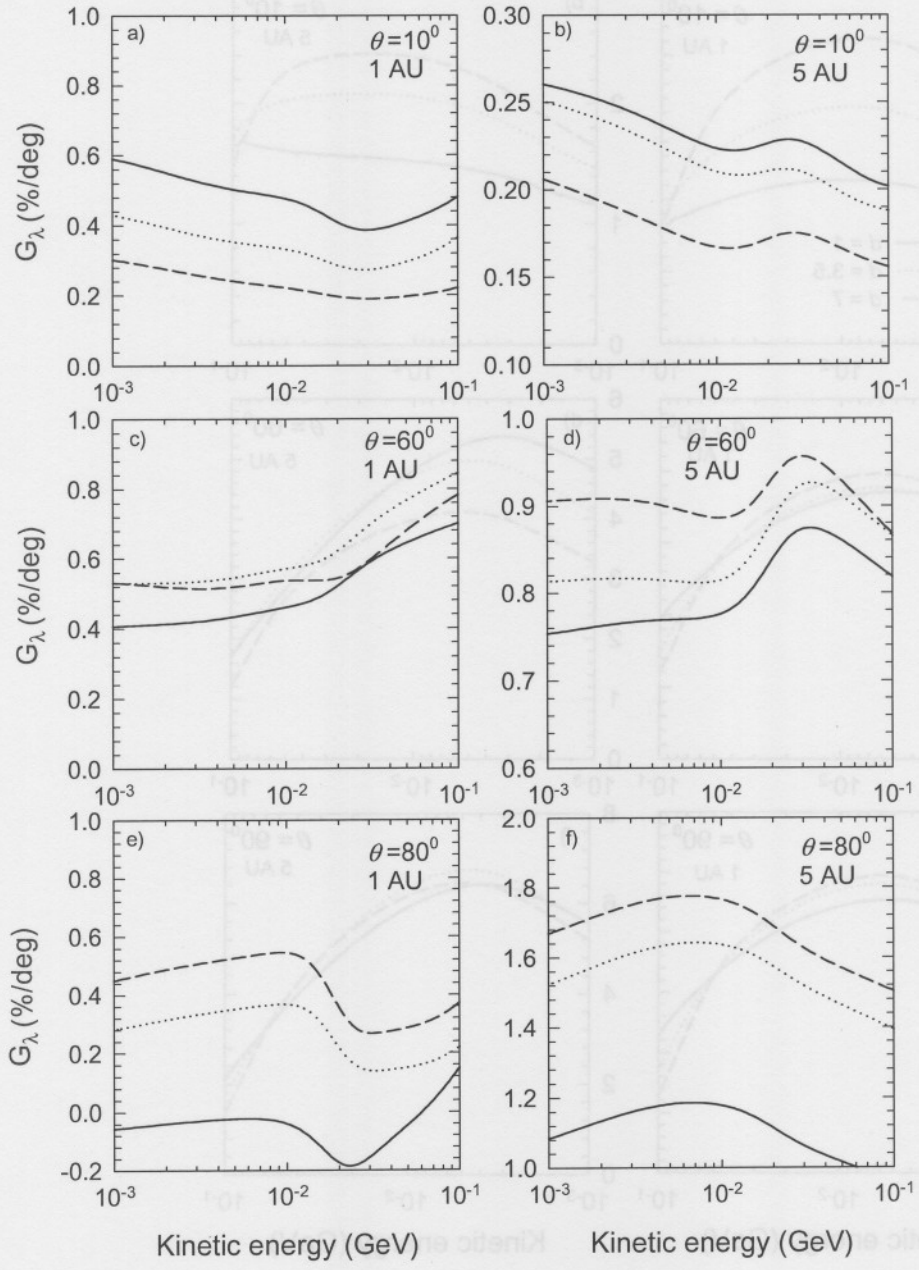

Figure (6.6): Computed Jovian electron latitudinal gradient (G_λ) at 1 AU and 5 AU as a function of kinetic energy, shown at $\theta = 10^0$ (upper panels), $\theta = 60^0$ (middle panels) and $\theta = 80^0$ (bottom panels) for the A > 0 magnetic polarity epoch. The computations are for the different *d* scenarios shown in Figure (6.1).

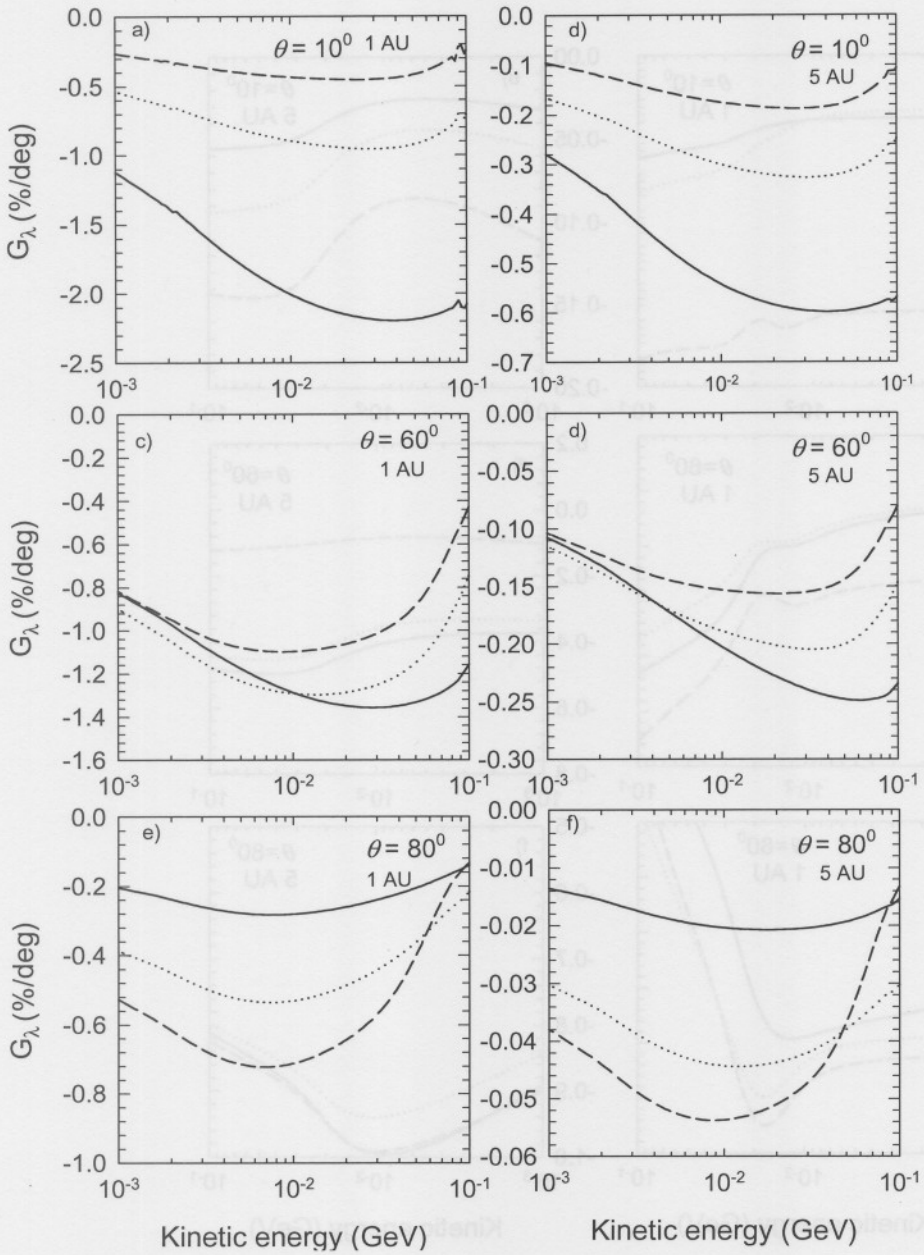

Figure (6.7): Similar to Figure (6.6), but for galactic latitudinal gradient (G_λ), again shown at 1 AU and 5AU.

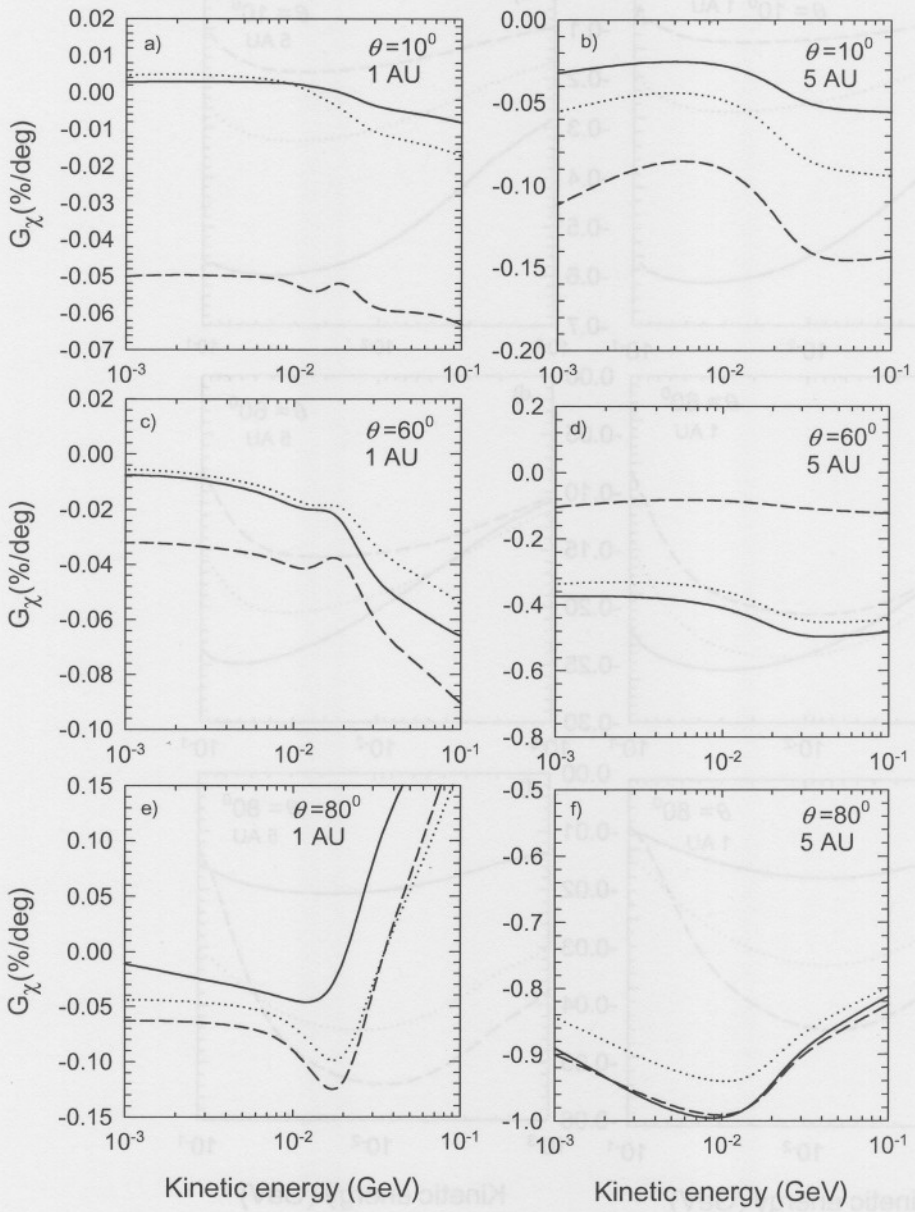

Figure (6.8): Similar to Figure (6.4), but now for the computed azimuthal gradient (G_χ) for Jovian electrons, shown at 1 AU and 5AU.

the equatorial region (see also Ferreira, 2002). At lower energies ($E < 30$ MeV) drifts have little effect on both Jovian and galactic electron modulation, which indicates that these low-energy electrons are indeed modulated primarily by diffusion and convection (Potgieter, 1996, Ferreira, 1998, 2002).

6.3.2 Three-dimensional gradients

Figure (6.4) shows the computed Jovian radial gradient as a function of energy at 1 AU and 5 AU, with $\theta = 10^0$, $\theta = 60^0$ and $\theta = 80^0$, respectively. The radial gradients were calculated using the numerical equivalent of Equation (6.6) for both 1 AU and 5 AU at the specified polar angles. The relative large positive radial gradients in panels (a), (c) and (e) have similar shapes with a peak at ~ 30 MeV. This energy dependence can be understood by inspection of the spectra at 1 and 5 AU. The Jovian electron intensity increases as one move from the poles to the equatorial plane, thus an increase in the radial gradient in the equatorial plane at 1 AU for lower energies ($E < 30$ MeV). The maximum gradient occurs at the energies where the spectra change slope. The negative radial gradients, because of the relative proximity to the source at 5 AU, in panels (b) and (d) have a similar trend but much less pronounced. Panel (f) differs from the latter because it is almost at the Jovian electron source. For Jovian electrons, the solution with $d = 3.5$ is not distinguishable from the solution with $d = 1$ at $\theta = 10^0$, while for $\theta = 80^0$ it is not distinguishable from the solution with $d = 7$. At both radial distances, the radial gradient increases in absolute value from the pole toward the equatorial plane; at 1 AU the radial gradient increases by almost a factor of 10 at low energies but only about a factor of 4 at 40-50 MeV, whereas at 5 AU the increase is significantly at energies ($E >$ 10 MeV) for the mid-heliolatitude towards the equatorial plane for all d scenarios.

Figure (6.5) shows galactic electron radial gradients as a function of energy at 1 AU, with azimuth angle $\phi = 0^0$ (where the Jovian electron source is located) and 5 AU, at $\theta = 10^0$, $\theta = 60^0$ and $\theta = 90^0$ respectively. For $\theta = 10^0$ at 1 AU and 5 AU, the radial gradients at lower energies ($E < 10$ MeV) remain almost constant for $d = 1$. For $d = 3.5$ and $d = 7$ the energy dependence starts with a low value to reach a maximum at ~ 10 MeV, decreasing at lower energies, with a clear difference between the three d scenarios below 100 MeV. For $\theta = 60^0$ and $\theta = 90^0$ the d scenarios differ much less. The radial gradients start from low values at higher energies (100 MeV) and rise to a maximum

value (at ~ 10 MeV) and then fall steadily at lower energies. This is expected since the radial gradients at high energies is approximately given by

$$G_r = \frac{CV}{K_{rr}}, \tag{6.9}$$

where C is the Compton-Getting factor,

$$C = -\frac{1}{3}\frac{\partial \ln f}{\partial \ln p}, \tag{6.10}$$

and V is the solar wind speed (e.g., Lemmer, 1982; Potgieter, 1984). The radial gradients are obviously larger at 1 AU than at 5 AU.

Figure (6.6) shows small but generally positive latitudinal gradients for Jovian electrons as a function of energy at 1 AU and 5 AU, with $\theta = 10^0$, $\theta = 60^0$ and $\theta = 80^0$ respectively. The latitudinal gradients were calculated using Equation (6.7). The energy dependence in all cases is relatively small. For $\theta = 60^0$ at 1 AU, the low energy latitudinal gradient shows almost no energy dependence. At $\theta = 80^0$ for 1 AU there is a peculiar stronger energy dependence between ~ 10 MeV and ~ 30 MeV, also seen at 5 AU for $\theta = 60^0$, even a negative gradient for the $d = 1$ case at $\theta = 80^0$ and 1 AU. At 5 AU for $\theta = 10^0$ there is an increasing trend with deceasing energy. In panel (f) it disappears at these low energies; the maximum latitudinal gradient occurs here just below 10 MeV. For low energies ($E < 10$ MeV) the latitudinal gradients at $\theta = 10^0$ and $\theta = 60^0$ increases steadily, while at $\theta = 80^0$ it decreases for both 1 AU and 5 AU. The latitudinal gradients are obviously larger at 5 AU than at 1 AU. The effect to have the largest gradients with $d = 1$ for $\theta = 10^0$ at 1 AU disappears at $\theta = 60^0$ to reverse at $\theta = 80^0$ so that $d = 7$ produces the largest gradient at this position. The trend is also evident at 5 AU.

In Figure (6.7) the relatively small and negative galactic electron latitudinal gradients are shown as a function of energy at 1 AU and 5 AU, with $\theta = 10^0$, $\theta = 60^0$ and $\theta = 80^0$ respectively. The basic energy dependence of the gradients is similar. At energies ($E <$ ~ 30 MeV) there is steady decrease, while at energies ($E >$ ~ 30 MeV) there is a relative sharp increase at $\theta = 60^0$ and $\theta = 80^0$. This is caused by the fact that $K_{\perp\theta}$ has the same rigidity dependence as $K_{\parallel}$ from Equations (4.25). The latitudinal gradients are larger at 1 AU than at 5 AU for all the specified polar angles. Close to the source (5 AU and $\theta = 80^0$), the latitudinal gradients are much smaller than elsewhere. At 1 AU and $\theta = 80^0$, the

gradient has the largest absolute value just below 10 MeV for the $d = 7$ case. The effect on the galactic latitudinal gradients of changing d is the opposite than for Jovian electrons at the poles and at the ecliptic. As for the Jovian electrons, the effect of changing d seems the smallest at mid-heliolatitudes, with different energy dependence than in the ecliptic, without changing the energy dependence of any of the diffusion coefficients. In the polar regions the galactic electrons respond significantly more to changing d (in other words the latitude dependence of $K_{\perp\theta}$) than the Jovian electrons, which is to be expected.

The azimuthal gradients for Jovian electrons are shown in Figure (6.8) as a function of energy again at 1 AU and 5 AU, with $\theta = 10^0$, $\theta = 60^0$ and $\theta = 80^0$ respectively. At 1 AU, for $\theta = 10^0$ and $\theta = 60^0$ it is noticeable that there is only a small difference between $d = 1$ and $d = 3.5$ at ($E < \sim 30$ MeV). The basic energy dependence of the gradients is similar at $\theta = 10^0$ and $\theta = 60^0$ for both 1 AU and 5 AU. However, at 1 AU there is sharp decrease from high to low energies, followed by a steady decrease at lower energies, while at 5 AU this trend is much less pronounced. Panel (e) depicts a trend that the azimuthal gradient close to Earth changes from a positive value to a negative value below ~ 20 MeV. Whereas at 5 AU for $\theta = 80^0$, next to the source, the azimuthal gradients are relative large negative at all energies, again reaching the largest absolute value just below 10 MeV. The azimuthal gradient increases clearly from the poles to the equatorial plane at 5 AU.

6.4 Modulation of 7 MeV electrons in the inner heliosphere

6.4.1 The polar dependence

In Figure (6.9) the differential intensity (particles.m^{-2}.s^{-1}.sr^{-1}.MeV^{-1}) as a function of polar angle for different d scenarios are shown for separately computed 7 MeV Jovian and galactic electrons. Panels (a) and (b) show the computed Jovian electron intensities at 1 AU and 5 AU respectively, similarly for panels (c) and (d) but for galactic electrons. The three solutions, $d = 1$, $d = 3.5$ and $d = 7$ correspond to different solar condition as was discussed with Figure (6.1); the diffusion coefficients used are the ones discussed in Chapter 4. In this study the focus is on low-energy (~ 7 MeV) electrons which respond directly to the energy dependence of the diffusion coefficients at low energies because

drifts become negligible. For higher energies ($E > \sim 30$ MeV) solar cycle related changes due to drifts are important (e.g., Potgieter, 1996, Ferreira, 2002).

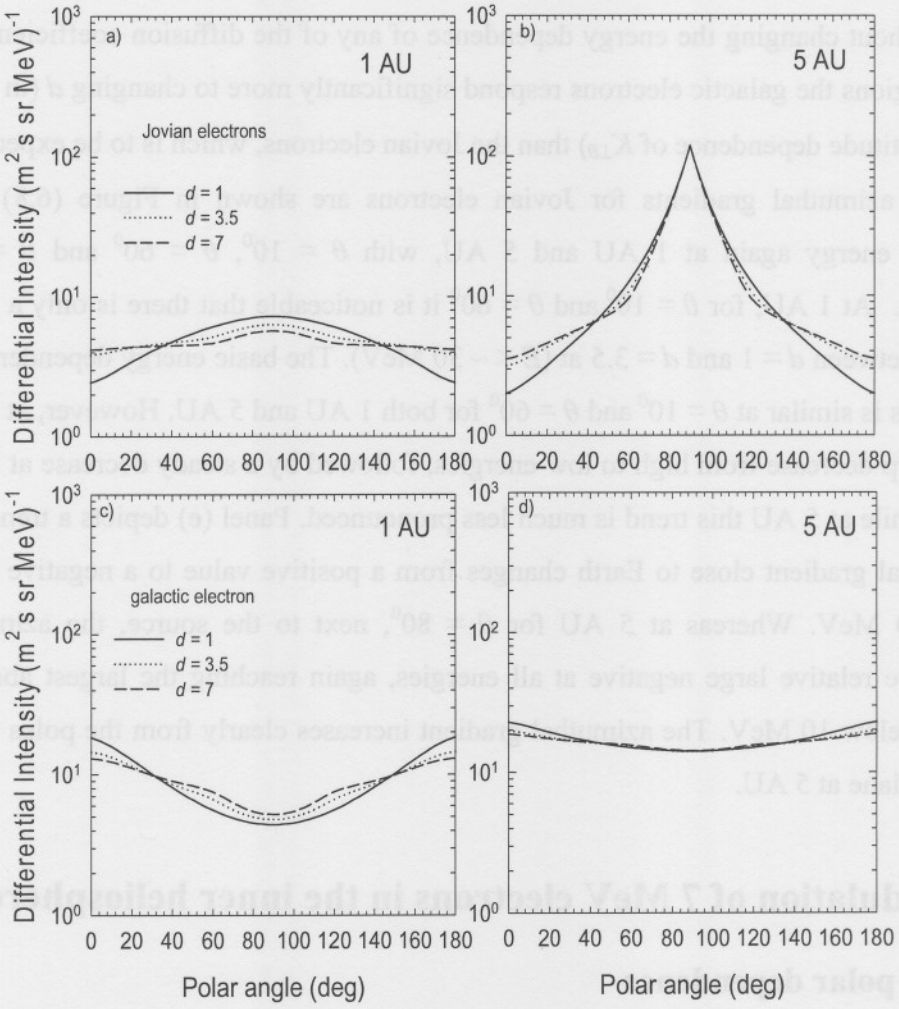

Figure (6.9): Computed 7 MeV electron intensities at 1 AU and 5 AU as a function of polar angle for the three different assumptions for d in Figure (6.1). Panels (a) and (b) show Jovian electron intensities only; panels (c) and (d) show galactic electron intensities only. The Jovian electron source is in the equatorial plane at $\theta = 90^0$, with $\phi = 0^0$.

In panel (a), the solution of Jovian electrons intensities at 1 AU with $d = 7$ differs very modestly from a solution with $d = 1$ for $140^0 \geq \theta \geq 40^0$, that is, towards the equatorial regions, but they differ by factor of ~ 2.5 towards the poles. The difference between the $d = 3.5$ and $d = 7$ solutions is a factor of ~ 0.5 towards the equatorial plane, that disappears towards the poles. Panel (b) shows strong latitude dependence because of the location of the Jovian electron source. The intensity increases for polar angles $\theta \leq 60^0$ and $\theta \geq 110^0$ as d is increased, and thus causing a reduction in the latitudinal dependence of the Jovian electron intensity in the polar regions. For $\theta \geq 70^0$ and $\theta \leq 110^0$ an increase in d shows little difference in the computed Jovian intensities and converges in the source.

For the galactic electron intensities, in panel (c), the solution for $d = 7$ differs modestly from that for $d = 1$ in the equatorial regions, but differs more significantly towards the poles. At 5 AU, panel (d), the differences are negligible.

6.4.1.1 Latitudinal gradients

Figure (6.10) shows computed 7 MeV Jovian and galactic electron latitudinal gradients at 1 AU and 5 AU as a function of polar angle for the three d scenarios. Panels (a) and (b) depict Jovian electrons and panels (c) and (d) galactic electrons. According to panel (a) the latitudinal gradients for $d = 7$ and $d = 3.5$ have basically the same polar angle dependence, whereas for $d = 1$ it increases almost linearly to about $\theta \sim 15^0$ and $\theta \sim 165^0$ before it drops abruptly caused by the boundary condition given by Equation (5.3). From Figure (6.9), panel (a), the intensity profiles for $d = 3.5$ and $d = 7$ show that the polar gradient should increase towards the equatorial plane. Panel (b) shows that for $d = 1$ the latitudinal gradient increases steadily from the poles towards the ecliptic plane where the source is located where it abruptly changes sign, as expected. According to panels (c) and (d), the polar dependence of the galactic electron latitudinal gradients are similar at 1 AU and 5 AU but the absolute values are much larger at 1 AU. The sign is negative between $\theta = 0^0$ and $\theta = 90^0$ which is consistent with what Potgieter et al. (1997) found and in

according with what is shown in Figure (6.9). The largest polar dependence occurs with $d = 1$, that is for solar maximum modulation conditions.

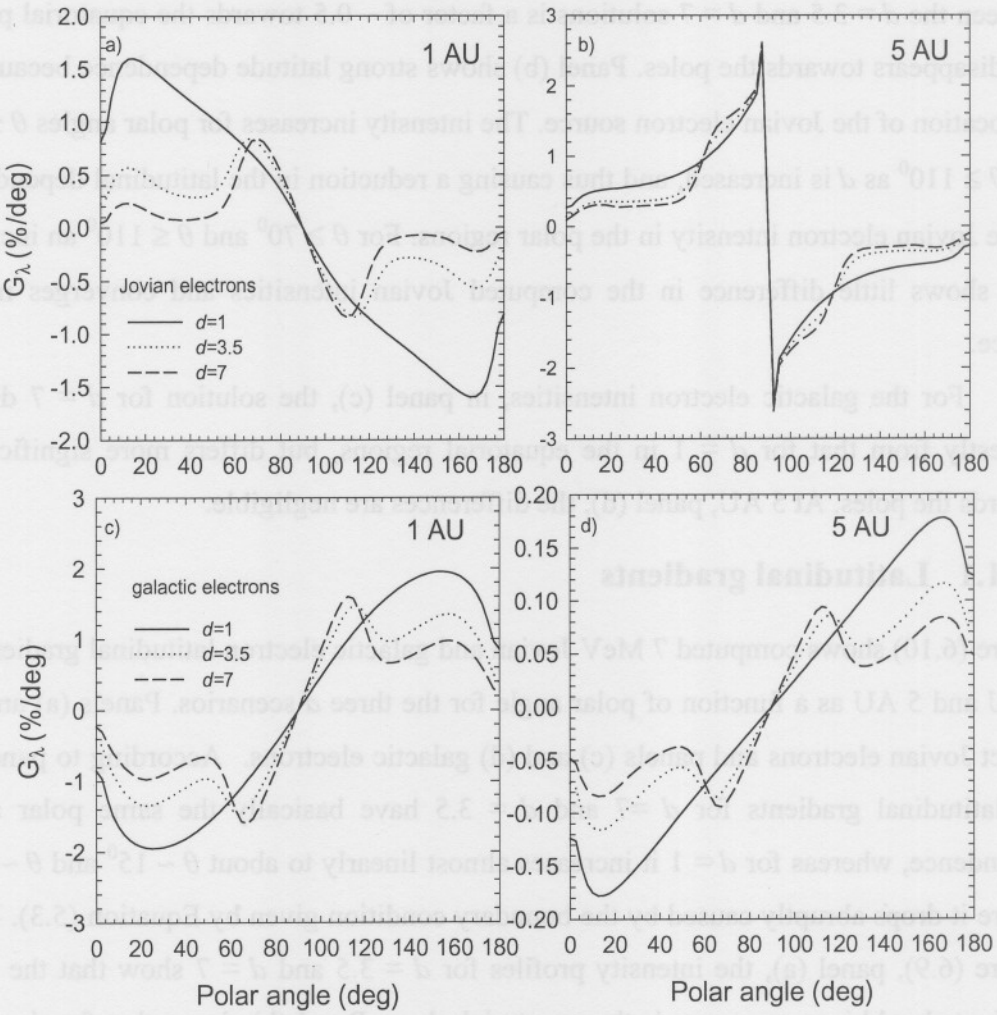

Figure (6.10): Computed 7 MeV latitudinal gradients at 1 AU and 5 AU as a function of polar angle for the assumed d scenarios shown in Figure (6.1). Panels (a) and (b) show Jovian electrons only, panels (c) and (d) show galactic electrons only.

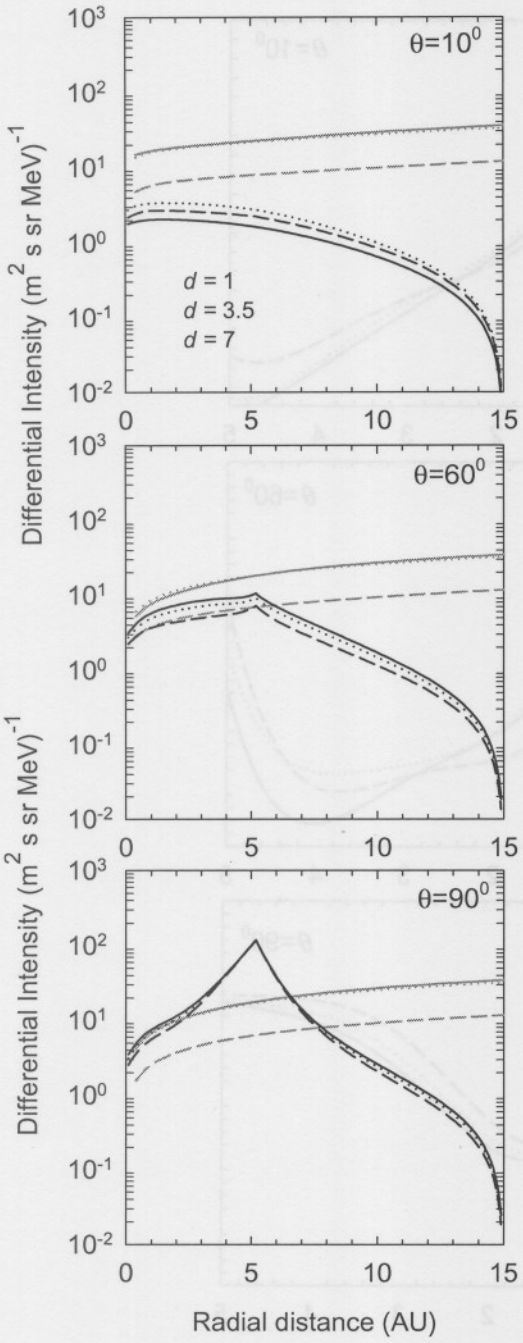

Figure (6.11): Computed differential intensities of 7 MeV Jovian (black darker lines) and galactic (grey lines) electrons as a function of radial distance for $r < 15$ AU. The solutions correspond to the three different d scenarios and computations are shown at $\theta = 10^0$, $\theta = 60^0$ and $\theta = 90^0$ respectively, with $\phi = 0^0$.

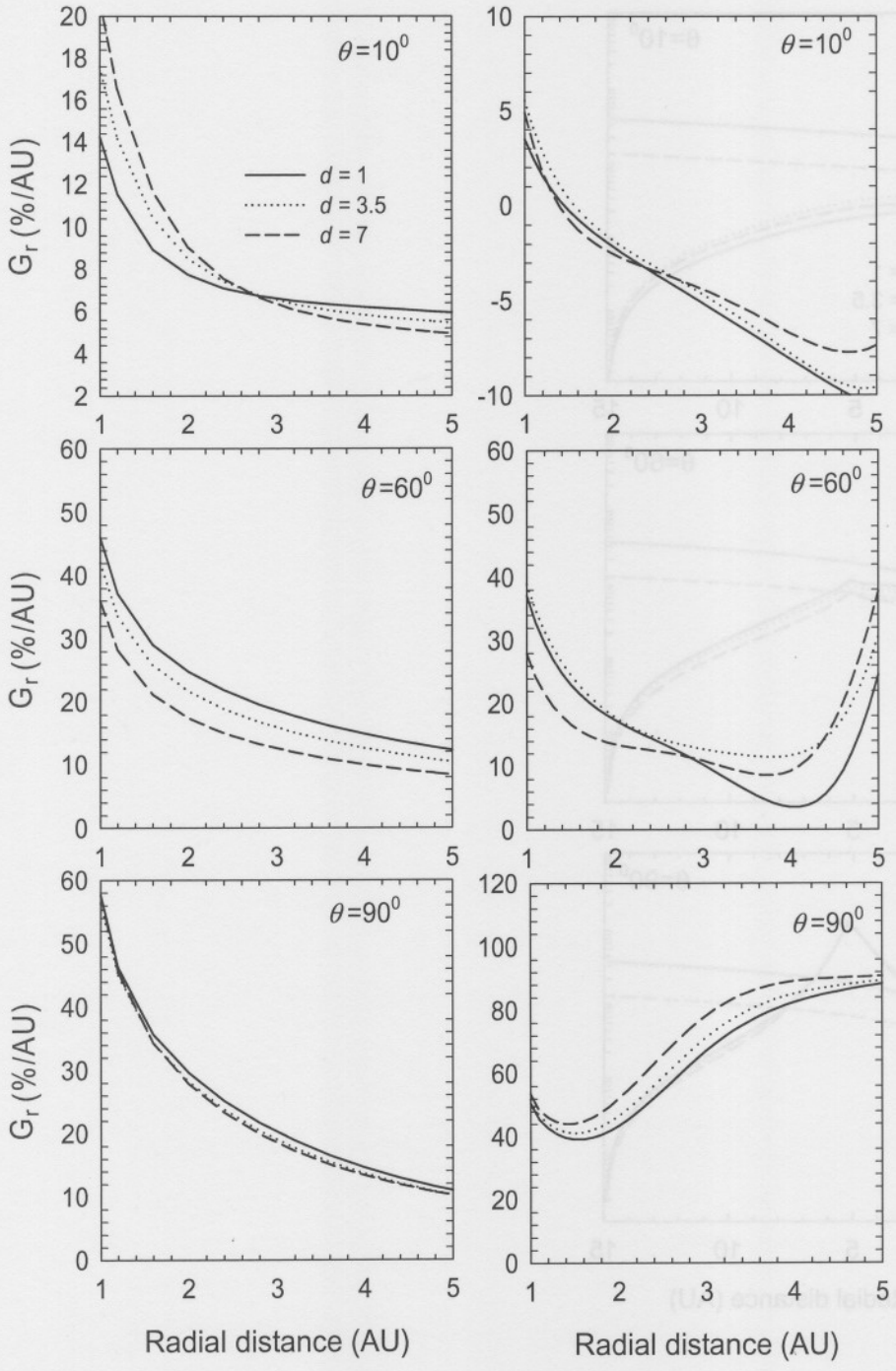

Figure (6.12): Computed radial gradients of 7 MeV Jovian (right panels) and galactic (left panels) electrons as a function of radial distance for $r < 5$ AU. The solutions correspond to the three different d scenarios, shown at $\theta = 10^0$, $\theta = 60^0$ and $\theta = 90^0$ respectively.

6.4.2 The radial dependence

Figure (6.11) shows the computed differential intensities of 7 MeV Jovian and galactic electrons as a function of radial distance up to $r = 15$ AU for the assumed d scenarios as discussed previously. It is assumed that the Jovian electron intensity goes to zero at 15 AU for all practical purposes. The exercise was primarily aimed to save on computation time when Jovian electrons alone were considered. This however causes the intensities to drop faster beyond ~ 10 AU than what Ferreira et al. (2001) computed. The diffusion coefficients are the same as used before. For $\theta = 10^0$ the galactic electron intensities clearly dominate with increasing radial distance and the effects of the three d scenarios are more pronounced than for Jovian electron intensities. At $\theta = 60^0$, the Jovian electron intensities show a stronger radial dependence as the effect of the source becomes visible. However, there are almost no differences in the radial dependence of galactic electrons for all the d scenarios. In the equatorial plane at $\theta = 90^0$, the Jovian electron intensities show general dominance for all d scenarios compared to the galactic electron d scenarios.

6.4.2.1 Radial gradients

In Figure (6.12) the computed radial gradients of 7 MeV Jovian (right panels) and galactic (left panels) electrons are shown as a function of radial distance for $r < 5$ AU. The solutions correspond to the three d scenarios. Computations are shown at $\theta = 10^0$, $\theta = 60^0$ and $\theta = 90^0$ respectively. For galactic electrons the radial gradients show the same trends in their radial dependence but the Jovian radial gradients change their radial dependence significantly from the polar to the ecliptic regions. As discussed above, the increase in d works differently for Jovian electrons than for galactic electrons. At mid-heliolatitude ($\theta = 60^0$), the galactic electron gradients are more or less similar close to 3 AU but the Jovian electrons dominate the gradients for $r > 4$ AU. In the inner heliospheric equatorial plane ($\theta = 90^0$), Jovian electron gradient dominates mostly, except close to 1 AU.

6.4.3 The azimuthal dependence

In Figure (6.13) the computed differential intensities of 7 MeV Jovian electrons are shown as a function of azimuthal angle at 5 AU for the assumed d scenarios as

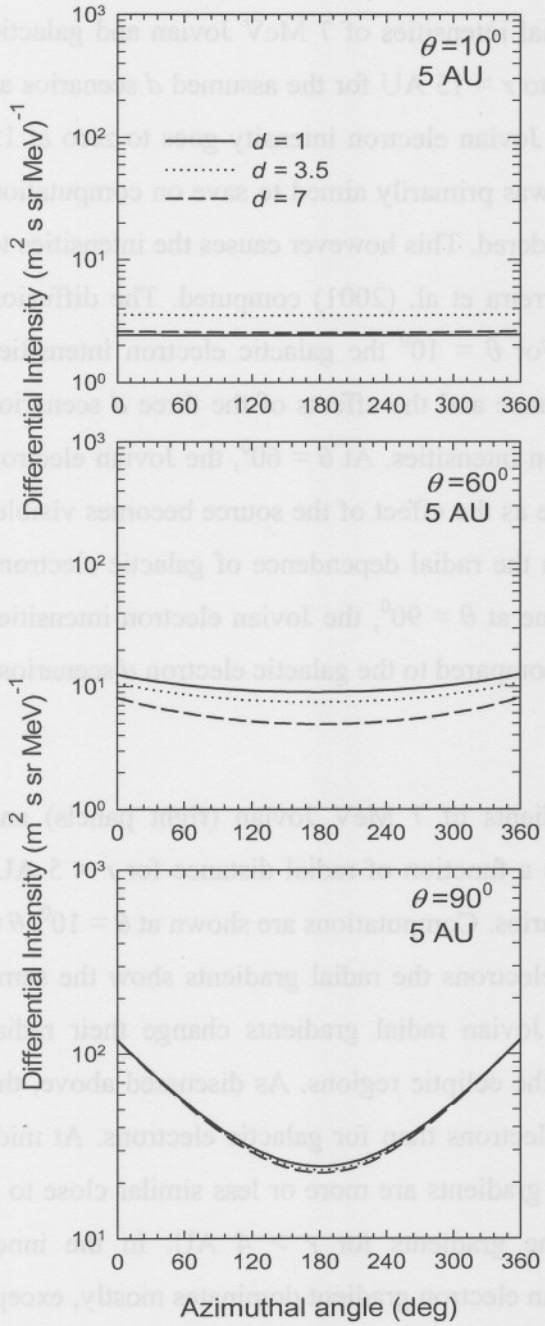

Figure (6.13): Computed differential intensities of 7 MeV Jovian electrons as a function of azimuthal angle at 5 AU and with $\theta = 10^0$, $\theta = 60^0$ and $\theta = 90^0$, respectively. The solutions correspond to the three d scenarios as discussed with Figure (6.1).

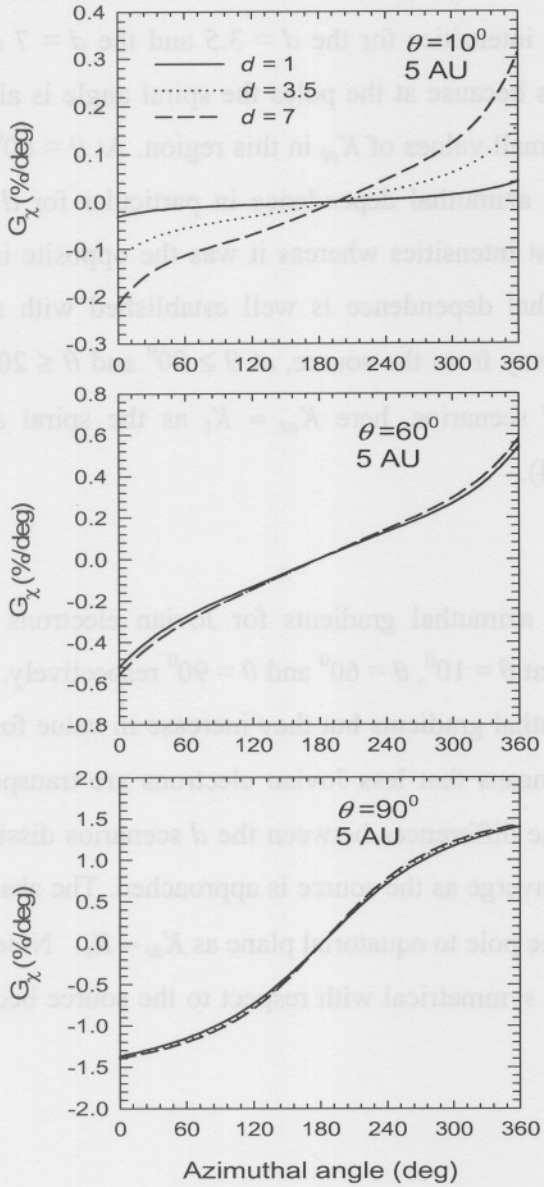

Figure (6.14): The corresponding computed 7 MeV azimuthal gradients for Jovian electrons as a function of azimuthal angle at 5 AU and at $\theta = 10^0$, $\theta = 60^0$ and $\theta = 90^0$ respectively.

discussed previously. The diffusion coefficients are the same as the ones discussed before. For $\theta = 10^0$, the Jovian electron intensities for the $d = 3.5$ and the $d = 7$ cases show no significant differences. . This is because at the poles the spiral angle is almost zero and thus $K_{\phi\phi} = K_{\perp r}$ which result in small values of $K_{\phi\phi}$ in this region. At $\theta = 60^0$, the Jovian electron intensities show modest azimuthal dependence in particular for $d = 7$. Here, the $d = 7$ case produces the lowest intensities whereas it was the opposite in the polar regions. For $\theta = 90^0$, the azimuthal dependence is well established with small differences between the d scenarios. Away from the source, at $\theta \geq 80^0$ and $\theta \leq 200^0$, a small difference occurs between the d scenarios, here $K_{\phi\phi} \approx K_{\parallel}$ as the spiral angle approaches 90^0. (See also Moeketsi, 2004).

6.4.3.1 Azimuthal gradients

Figure (6.14) shows the corresponding azimuthal gradients for Jovian electrons as a function of azimuthal angle at 5 AU and at $\theta = 10^0$, $\theta = 60^0$ and $\theta = 90^0$ respectively. At $\theta = 10^0$, for $d = 1$ there is almost no azimuthal gradients but they increase in value for $d = 3.5$ and $d = 7$. Here, $K_{\phi\phi} \approx K_{\perp r}$ which means that less Jovian electrons are transported along the HMF. At other polar angles the differences between the d scenarios dissipate. The values of the azimuthal gradients converge as the source is approached. The absolute values of these gradients increase from the pole to equatorial plane as $K_{\phi\phi} \approx K_{\parallel}$. Note that the computed intensity in azimuth is not symmetrical with respect to the source because the spiral angle changes.

6.5 Summary

In this chapter the latitudinal dependence of solar wind speed V, which describes the transition from solar minimum to solar maximum modulation conditions, was used to investigate the latitude dependence of the polar (perpendicular) diffusion coefficient, following up on the work of Moeketsi (2004).

The 3D electron modulation model of Ferreira (2002) was used to study the effects on low-energy electron intensities of making the perpendicular diffusion coefficients latitude and solar cycle dependent using a parameter d, described in section

(6.3.1). Three scenarios for d, corresponding to solar minimum, intermediate and maximum activity, were used as illustrated in Figure (6.1). These changes were applied to the modulation of Jovian and galactic electrons at 1 AU and 5 AU, and at different polar angles. The 3D radial, latitudinal and azimuthal gradients were studied as a function of kinetic energy. For Jovian and galactic electrons, it was found that the computed radial gradients are larger at 1 AU than at 5 AU and that they increase from the poles to the equatorial plane. For the Jovian electron latitudinal gradients it was found that at higher latitudes the low-energy electrons increase steadily unlike near the equatorial region where there is a decrease. For galactic electrons, the low-energy latitudinal gradients show a steady decrease. At 1 AU the gradients are larger than at 5 AU. For the azimuthal gradients, at higher latitudes and for $E < 30$ MeV, it was found that they decrease until they reach minimum value 0.03% at 5 AU, while at 1AU there is a sharp decrease, followed by a steady decrease.

The effects of the three different d scenarios were also illustrated on low energy electron modulation at 1 AU and 5 AU, respectively, as function of polar angle. It was found that for galactic electrons the effects of the three d scenarios are more significant in the polar regions, being insignificant in the equatorial plane. For Jovian electrons the effects produce a factor of ~ 2.5 at the poles, between the $d = 7$ and $d = 1$ scenarios at 1 AU. At 5 AU, the effect of the d scenarios diminishes in the equatorial plane for both the Jovian and galactic electrons.

The effects of the three d scenarios were illustrated on the latitudinal gradients and it was found that for the galactic electrons the values are negative between $\theta = 0^0$ and $\theta = 90^0$ whereas for the Jovian electrons they are positive at both radial distances. The galactic electron latitudinal gradients are larger at 1 AU than at 5 AU.

The effects of the d scenarios were illustrated on the 7 MeV Jovian electron modulation at 5 AU as a function of azimuthal angle at different latitudes. It was found that at the poles the effects are insignificant between the $d = 1$ and $d = 7$ cases. The electron intensities increase from the poles to the equatorial plane. The effect of changing d diminishes at the source. At the poles there is almost no azimuthal gradient for $d = 1$ and the three solutions converge as the Jovian electron source is approached.

Lastly, the effects of the three *d* scenarios were illustrated on the 7 MeV electron modulation as a function of radial distance in the inner heliosphere for different latitudes, for both galactic and Jovian. The galactic electron intensities were found to be dominant in the polar regions whereas the Jovian electron intensities dominate the equatorial regions in accordance with the results by Ferreira (2002) and Moeketsi (2004). The galactic electron radial gradients dominate in the polar regions, while the Jovian electron radial gradients dominate in the equatorial plane.

Chapter 7

Modulation of Jovian and galactic electron anisotropies in the inner heliosphere

7.1 Introduction

Since its launch in October 1990, Ulysses has sampled continuously the heliosphere between Earth and Jupiter in all three dimensions. Apart from electron flux observations at different energies, the Ulysses observations have also indicated the presence of low-energy electron 'jets' with extraordinary anisotropies off the equatorial plane as far as 2.2 AU from Jupiter during the recent encounter in 2004 (Kunow et al., 2005). These Jovian electron 'jets' were also observed during the first encounter with Jupiter in 1992 (Ferrando et al., 1993). They were observed during both encounters in the 3-10 MeV range as events with sharp increases and decreases, a strong field-aligned anisotropy, and the durations of up to a few hours. These and other Ulysses observations are very interesting features of the Jovian electron intensity-time profiles and are important in evaluating and testing the modulation models.

The purpose of this chapter is to use the basic modulation theory of how the different modulation mechanisms and processes contribute to the full three-dimensional anisotropy vector, from a global modulation point of view in order to establish to what extent these well-known mechanisms contribute to the extra-ordinary anisotropies mentioned above. It is recognized that these observed anisotropies are too large to be fully caused by these usual processes. Modelling these global anisotropies in 3D has not been reported before. The emphasis is placed on the role that the polar perpendicular diffusion plays in establishing these relatively large electron anisotropy in the inner heliosphere.

7.2 The anisotropy vector

The physical meaning of the anisotropy vector, ξ, can be expressed generally as

$$\xi(\mathbf{x},p,t)=\frac{\boldsymbol{J}_{p\max}-\boldsymbol{J}_{p\min}}{\boldsymbol{J}_{p\max}+\boldsymbol{J}_{p\min}}, \tag{7.1}$$

were $\boldsymbol{J}_{p\max}(\mathbf{x}, p, t)$ and $\boldsymbol{J}_{p\min}(\mathbf{x}, p, t)$ are maximum and minimum differential intensities at position $\mathbf{x}$ and time t in the momentum interval $(p, p + dp)$. The maximum intensity is assumed to come in the direction of $\mathbf{e}_0$. Consider now the case when the intensity is symmetric around the direction of $\mathbf{e}_0$ and only has a first harmonic, namely,

$$\boldsymbol{J}_p = j_p\left[1+\varepsilon(p)\cos(\theta-\theta_0)\right]\mathbf{e}_0, \tag{7.2}$$

Using Equation (7.2) and Equation (7.1) gives

$$\boldsymbol{\xi}=\varepsilon(p)\mathbf{e}_0. \tag{7.3}$$

The differential streaming density $\mathbf{S}_p(\mathbf{x}, p, t)$ can, in terms of the distribution function $f(\mathbf{x}, p, t)$, be written as

$$\mathbf{S}_p(\mathbf{x},p,t)=\int_\Omega \mathbf{v}f(\mathbf{x},p,t)p^2d\Omega. \tag{7.4}$$

The component of $\mathbf{S}_p$ in the direction $\mathbf{e}_0$ is

$$\begin{aligned}\mathbf{S}_p(\mathbf{x},p,t).\mathbf{e}_0 &= \int_\Omega \mathbf{v}.\mathbf{e}_0 fp^2d\Omega\\ &= \int_\Omega v\cos(\theta-\theta_0)fp^2d\Omega\\ &= \int_\Omega \boldsymbol{J}_p\cos(\theta-\theta_0)d\Omega\\ &= j_p\left[\frac{4\pi}{3}\varepsilon(p)\right],\end{aligned} \tag{7.5}$$

if Equation (7.2) is used.

The streaming density is thus

$$\begin{aligned}\mathbf{S}_p &= \left(\mathbf{S}_p.\mathbf{e}_0\right)\mathbf{e}_0\\ &= \frac{4\pi}{3}\varepsilon(p)j_p\mathbf{e}_0.\end{aligned} \tag{7.6}$$

Using Equation (7.6) and Equation (7.3) gives a useful expression for the anisotropy vector

$$\xi(\mathbf{x},p,t)=\varepsilon(p)\mathbf{e}_0$$

$$= \frac{3}{v}\frac{\mathbf{S}_p}{U_p}. \tag{7.7}$$

The relation between the differential intensity j, the differential density U and the omni-directional distribution function f, with respect to momentum p, kinetic energy E and rigidity P, is given by

$$4\pi p^2 f(p) = U_p = \left(\frac{4\pi}{A_p}\right) j_E = \left(\frac{4\pi}{c}\right)\frac{j_p}{\beta} = \left(\frac{c}{A_p}\right)\beta U_E,$$

$$4\pi P^2 f(p) = U_p = \left(\frac{4\pi Ze}{cA_p}\right) j_E = \left(\frac{4\pi}{c}\right)\frac{j_p}{\beta} = \left(\frac{Ze}{A_p}\right)\beta U_E, \tag{7.8}$$

with $\beta = v/c$, the particle speed v is in units of the speed of light c, A_p is the particle's mass number and Ze its charge. Notice that the intensity j_E with respect to kinetic energy is of the same form as the number density U_p with respect to momentum, while both differ with a factor p^2 from f. Therefore the relationship

$$j_E \propto U_p \propto p^2 f, \tag{7.9}$$

is convenient to use.

The solutions are done in heliocentric polar coordinates (r, θ, ϕ) for this work so that the differential streaming vector in terms of f is given by

$$\mathbf{S} = 4\pi p^2 \left(C\mathbf{V}f - \mathbf{K}.\nabla f\right), \tag{7.10}$$

with

$$C = -\frac{1}{3}\frac{\partial \ln f}{\partial \ln p}, \tag{7.11}$$

the Compton-Getting factor, $\mathbf{K}$ is the diffusion tensor given in Equation (4.5) and $\mathbf{V}$ is solar wind velocity with radial and polar dependence given in Equation (2.2) and Equation (2.3) respectively. See also Lemmer (1982) and Potgieter (1984).

In spherical coordinates (r, θ, ϕ), $\mathbf{S}$ has the following three components:

$$\mathbf{S}_r = -4\pi p^2\left[\left(K_\parallel \cos^2\psi + K_{\perp r}\sin^2\psi\right)\frac{\partial f}{\partial r} - \frac{K_A \sin\psi}{r}\frac{\partial f}{\partial \theta} + \frac{\left(K_{\perp r} - K_\parallel\right)\cos\psi\sin\psi}{r\sin\theta}\frac{\partial f}{\partial \phi} + \frac{V}{3}\frac{\partial f}{\partial \ln p}\right], \tag{7.12}$$

$$\mathbf{S}_\theta = -4\pi p^2 \left[\frac{K_A \sin\psi}{r} \frac{\partial f}{\partial r} + \frac{K_{\perp\theta}}{r} \frac{\partial f}{\partial \theta} + \frac{K_A \cos\psi}{r \sin\theta} \frac{\partial f}{\partial \phi} \right], \tag{7.13}$$

$$\mathbf{S}_\phi = -4\pi p^2 \left[\left(K_{\perp r} - K_\parallel \right) \cos\psi \sin\psi \frac{\partial f}{\partial r} - \frac{K_A \cos\psi}{r} \frac{\partial f}{\partial \theta} + \frac{K_{\perp r} \cos^2\psi + K_\parallel \sin^2\psi}{r \sin\theta} \frac{\partial f}{\partial \phi} \right]. \tag{7.14}$$

From these components, the three anisotropy vector components, ξ_θ, ξ_ϕ and ξ_r, that is, the latitudinal, azimuthal and radial anisotropies, can be easily calculated. It is assumed that for Jovian and low-energy galactic electrons drifts become negligible (Potgieter, 1986), i.e. $K_A \rightarrow 0$. This gives significantly reduced expressions (Potgieter et al., 2005):

$$\xi_r = -\frac{3}{v}\left[G_r K_{rr} - G_\phi K_{r\phi} - CV \right], \tag{7.15}$$

$$\xi_\theta = -\frac{3}{v}\left[G_\theta K_{\perp\theta} \right], \tag{7.16}$$

$$\xi_\phi = -\frac{3}{v}\left[G_r K_{\phi r} - G_\phi K_{\phi\phi} \right]. \tag{7.17}$$

The total anisotropy magnitude per definition is given by

$$|\xi| = \sqrt{\xi_r^{\,2} + \xi_\theta^{\,2} + \xi_\phi^{\,2}}, \tag{7.18}$$

with G_r, G_θ and G_ϕ the radial, polar and azimuthal gradients as given by Equations (6.3), (6.4) and (6.5) respectively and where ψ is the spiral angle, the angle between the radial direction and the average HMF direction.

7.3 Effects of polar perpendicular diffusion on the modulated electron anisotropy components

7.3.1 Radial anisotropy

Figure (7.1) shows the computed galactic electron radial anisotropy ξ_r as a function of kinetic energy ($E \leq 10$ MeV) at $\theta = 10^0$ (upper panels), $\theta = 60^0$ (middle panels) and $\theta = 80^0$ (bottom panels) for the A > 0 magnetic polarity epoch at 1 AU and 5 AU. The latitude dependence of $K_{\perp\theta}$ described by the parameter d (see Equation (4.27)) was kept unchanged with $d = 7$, while varying only the value of b, where $b = K_{\perp\theta}/K_\parallel$. In all cases, the increase from $b = 0.015$ to $b = 0.020$ is insignificant for all energies, but there is a

significantly larger difference between $b = 0.015$ and $b = 0.020$. For both 1 AU and 5 AU, ξ_r decreases from $\theta = 60^0$ towards the equatorial plane regions. At 1 AU and with $\theta = 10^0$, ξ_r is negative. Decreasing b from 0.015 to 0.005 changes ξ_r from negative to positive values, illustrating the role of an over-all larger $K_{\perp\theta}$. At 5 AU, ξ_r becomes less negative but not positive under this scenario. The effect of decreasing b reverses at larger polar angles, that is $b = 0.005$ produces the smallest ξ_r at larger polar angles. In all cases the energy dependence over this range is rather modest, being insignificant in the polar regions. At 5 AU, ξ_r is significantly larger than at 1 AU. For galactic electrons ξ_r is dominated by K_{rr} and G_r in Equation (7.15); increasing $K_{\perp\theta}$ does change G_r in the polar regions.

Figure (7.2) shows the computed Jovian electron ξ_r as a function of kinetic energy ($E \leq 10$ MeV) at $\theta = 10^0$ (upper panels), $\theta = 60^0$ (middle panels) and $\theta = 80^0$ (bottom panels) f at 1 AU and 5 AU. Again $d = 7$, while varying the value of b. As for galactic electrons, the effect of decreasing b reverses at larger polar angles. At 1 AU for $\theta = 10^0$ the increase from $b = 0.005$ to $b = 0.020$ is insignificant, with the largest differences at 1 AU and $\theta = 80^0$. In all cases, a modest energy dependence is found. For the Jovian electrons the energy dependence of ξ_r is clearly different because there is a stronger contribution of $K_{r\phi}$ and on the large azimuthal gradients in Equation (7.15).

7.3.2 Latitudinal anisotropy

Figure (7.3) shows the computed galactic electron latitudinal anisotropy ξ_θ as a function of kinetic energy, shown at $\theta = 10^0$ (upper panels), $\theta = 60^0$ (middle panels) and $\theta = 80^0$ (bottom panels) for the A > 0 magnetic polarity epoch at 1 AU and 5 AU. The solutions shown are obtained similarly to the radial anisotropy with only b varied. As it follows from Equation (7.16), ξ_θ is primarily determined by the product of the latitudinal (polar) gradient G_θ and $K_{\perp\theta}$ so that the negative values obtained for ξ_r is not seen here and that the trend of a decreasing b is the same at all polar angles. At 1 AU and 5 AU, ξ_θ increases from near the equatorial plane to the poles, due to the increase in G_θ. The latitudinal anisotropies are significantly larger at 1 AU than 5 AU, except for the polar regions. At 1 AU and 5AU, the energy dependence has similar shapes, which shows an

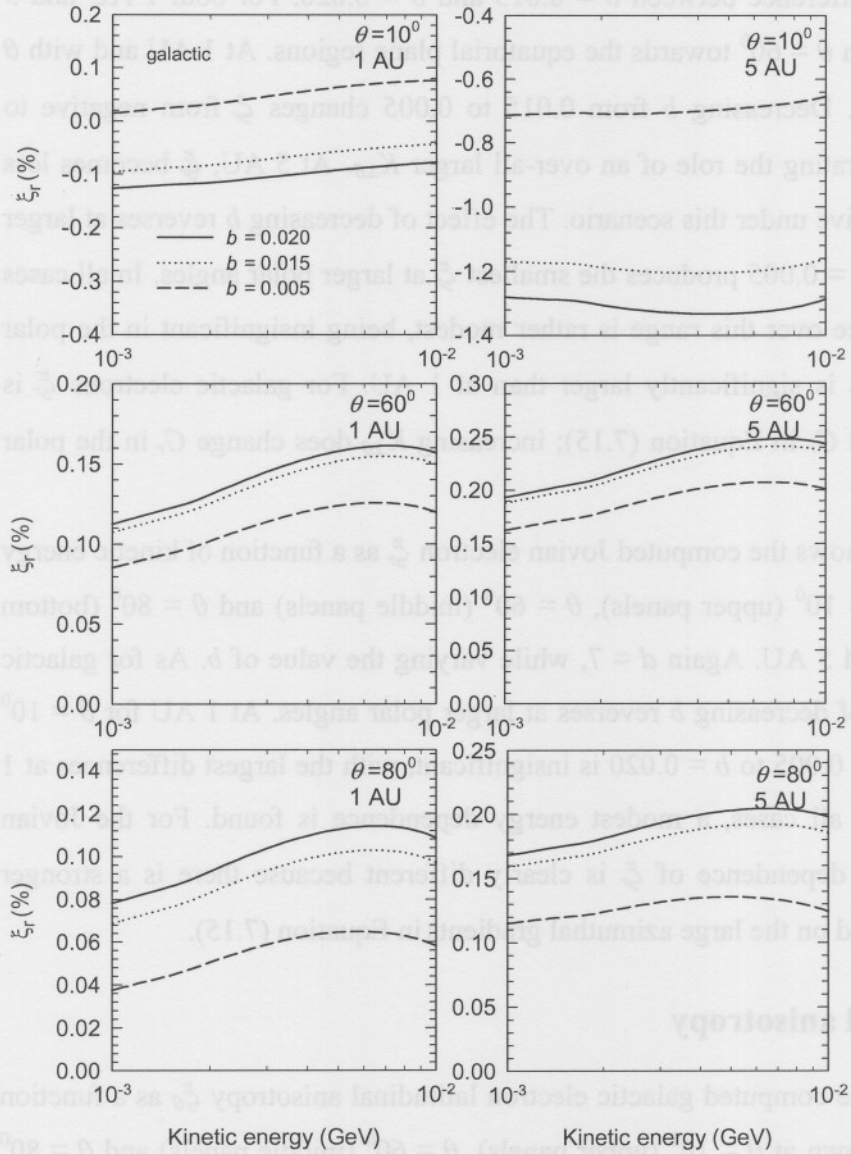

Figure (7.1): Computed galactic electron radial anisotropy ξ_r as a function of kinetic energy, shown at $\theta = 10^0$ (upper panels), $\theta = 60^0$ (middle panels) and $\theta = 80^0$ (bottom panels) for the A > 0 magnetic polarity epoch at 1 AU (left panels) and 5 AU (right panels) for three values of b, where $b = K_{\perp\theta}/K_{\parallel}$; the solid line corresponds to $b = 0.020$, dotted line to $b = 0.015$ and the dashed line to $b = 0.005$.

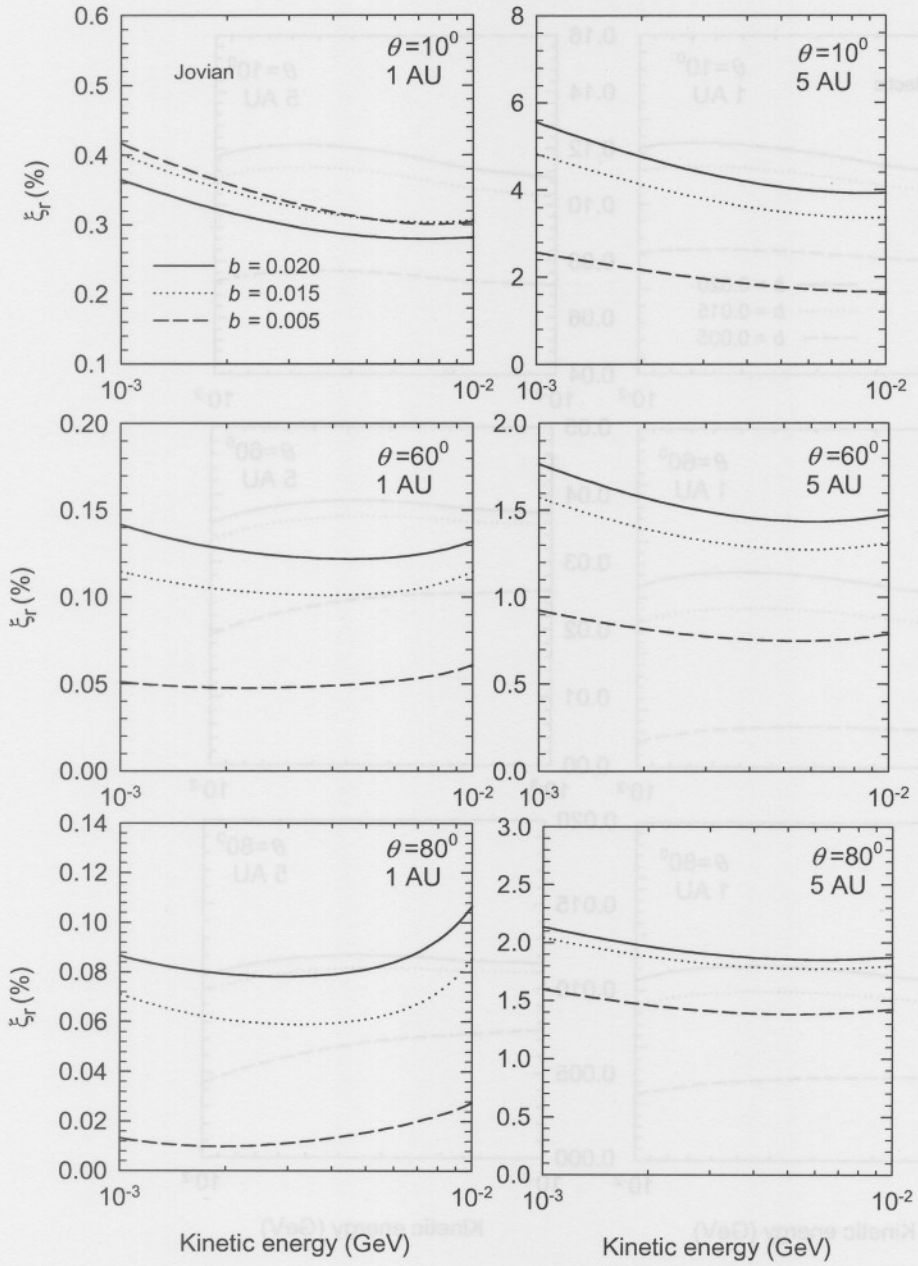

Figure (7.2): Similar to Figure (7.1), but for Jovian electrons.

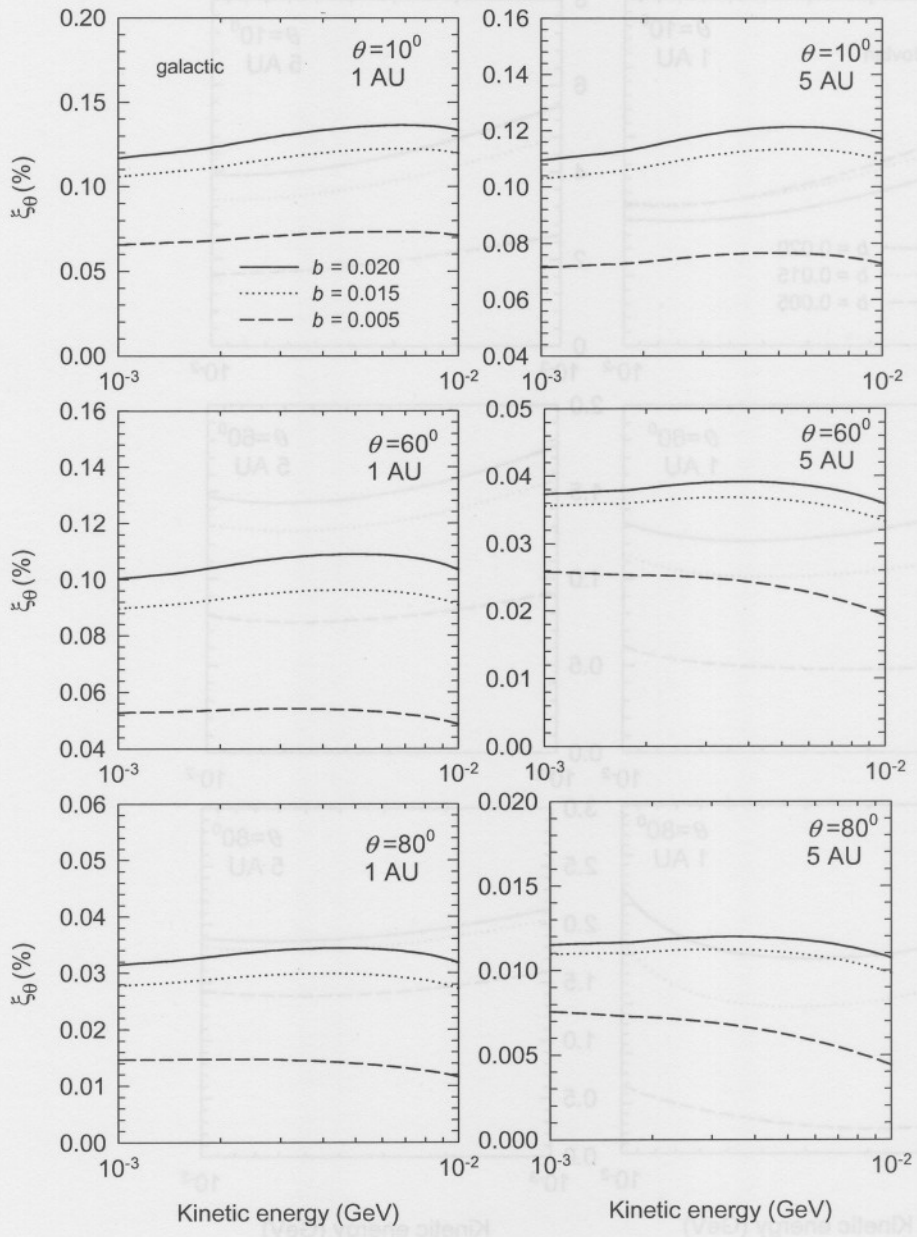

Figure (7.3): Computed galactic electron latitudinal anisotropy ξ_θ as a function of kinetic energy, shown at $\theta = 10^0$ (upper panels), $\theta = 60^0$ (middle panels) and $\theta = 80^0$ (bottom panels) for the A > 0 magnetic polarity epoch at 1 AU (left panels) and 5 AU. The rest is similar to Figure (7.1).

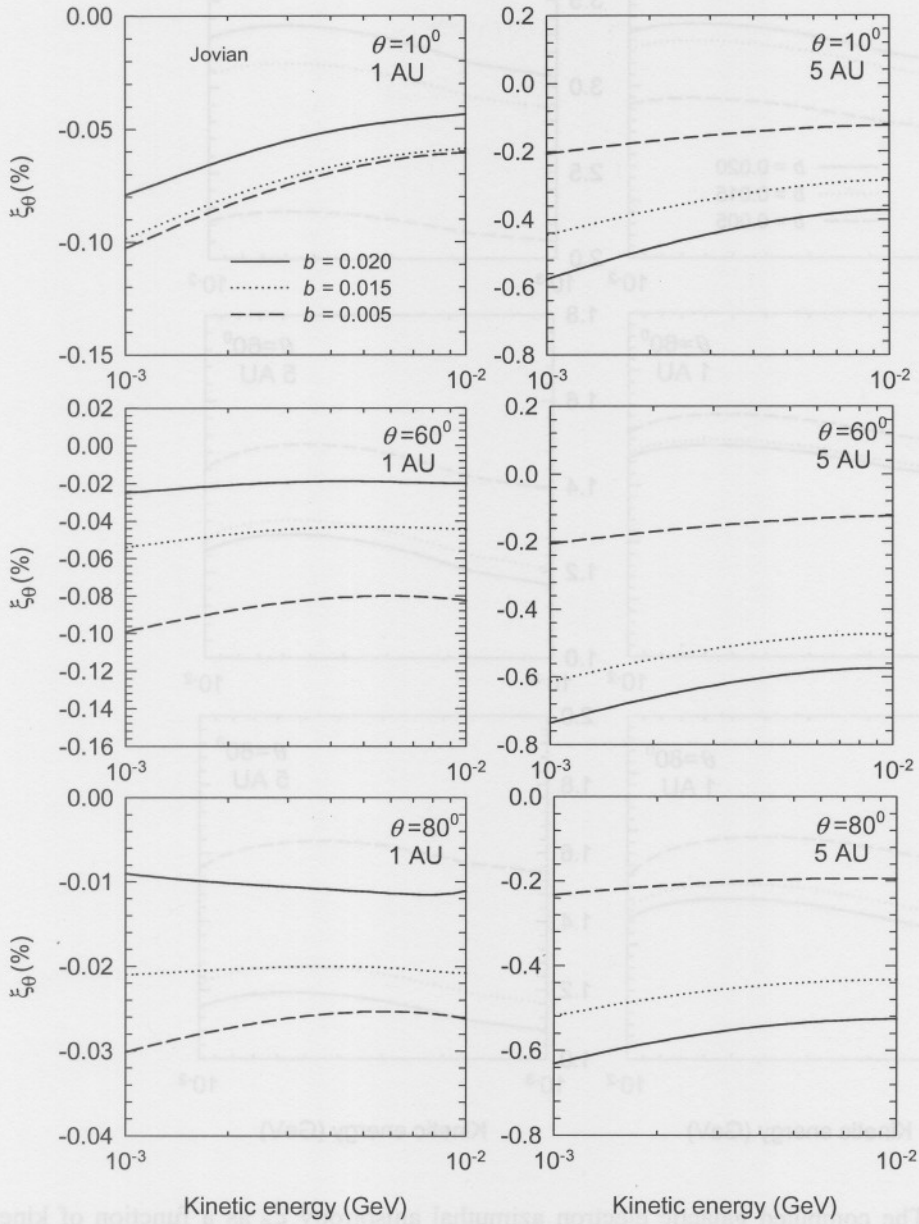

Figure (7.4): Similarly to Figure (7.3), but for Jovian electrons.

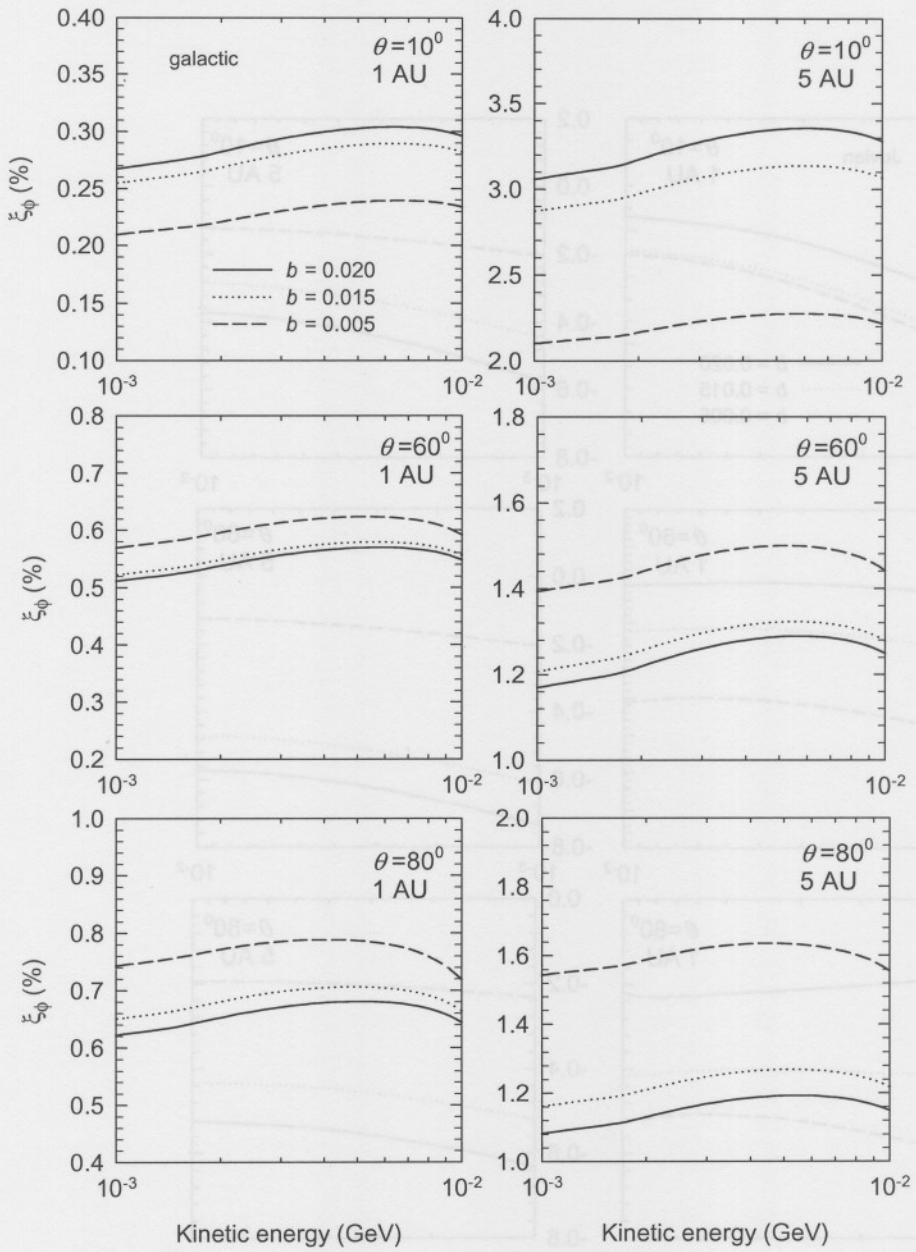

Figure (7.5): The computed galactic electron azimuthal anisotropy ξ_ϕ as a function of kinetic energy similar to Figures (7.1) to (7.4).

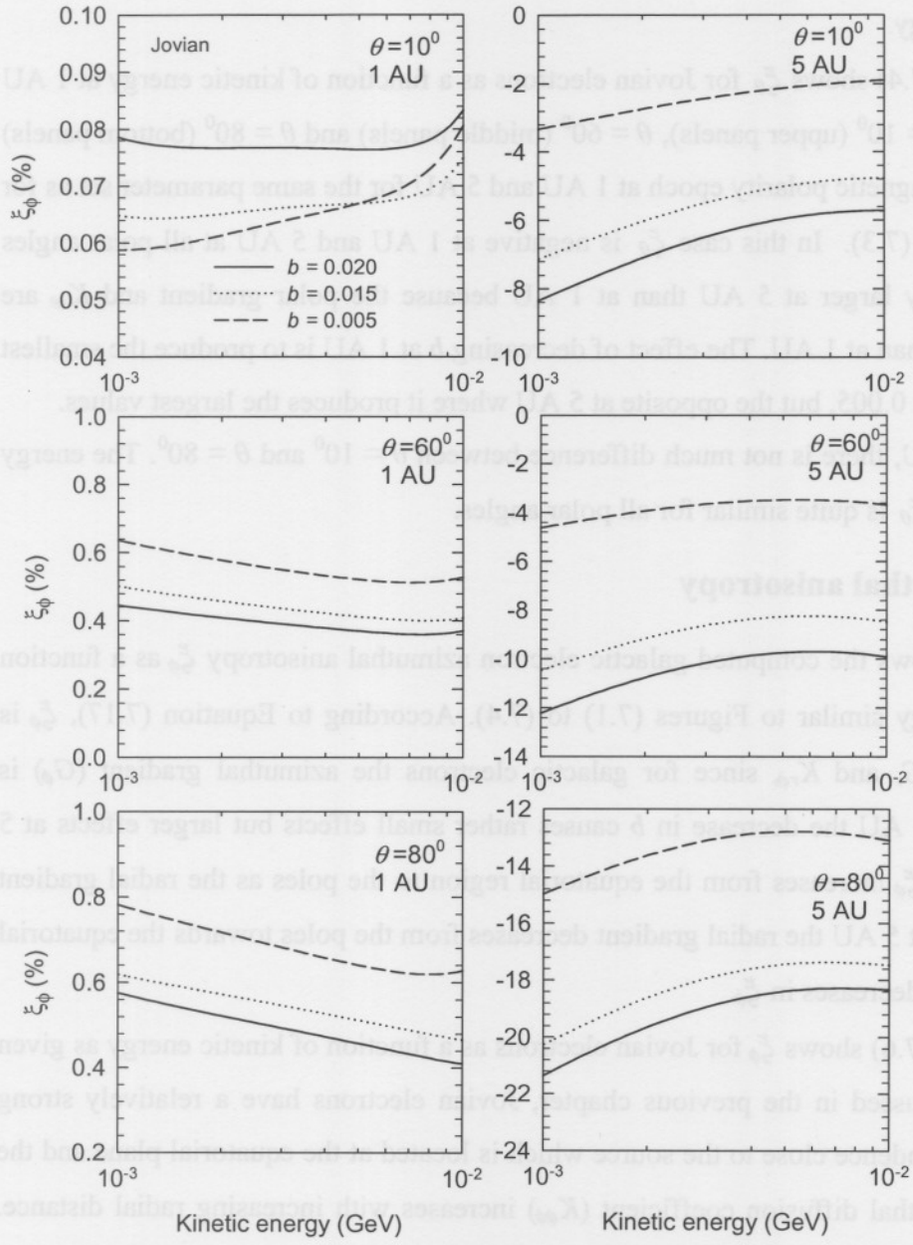

Figure (7.6): Similar to Figure (7.5), but for Jovian electrons.

increase from 10 MeV up to ~ 7 MeV, followed by a small drop and then flattens with decreasing energy.

Figure (7.4) shows ξ_θ for Jovian electrons as a function of kinetic energy at 1 AU and 5 AU, at $\theta = 10^0$ (upper panels), $\theta = 60^0$ (middle panels) and $\theta = 80^0$ (bottom panels) for the A > 0 magnetic polarity epoch at 1 AU and 5 AU for the same parameter set as for Figures (7.1) to (7.3). In this case ξ_θ is negative at 1 AU and 5 AU at all polar angles and significantly larger at 5 AU than at 1 AU because the polar gradient and $K_{\perp\theta}$ are larger at 5 AU than at 1 AU. The effect of decreasing b at 1 AU is to produce the smallest values when $b = 0.005$, but the opposite at 5 AU where it produces the largest values.

For 5 AU, there is not much difference between $\theta = 10^0$ and $\theta = 80^0$. The energy dependence of ξ_θ is quite similar for all polar angles.

7.3.3 Azimuthal anisotropy

Figure (7.5) shows the computed galactic electron azimuthal anisotropy ξ_ϕ as a function of kinetic energy similar to Figures (7.1) to (7.4). According to Equation (7.17), ξ_ϕ is dominated by G_r and $K_{r\phi}$, since for galactic electrons the azimuthal gradient (G_ϕ) is negligible. At 1 AU the decrease in b causes rather small effects but larger effects at 5 AU. At 1 AU, ξ_ϕ increases from the equatorial region to the poles as the radial gradient increases, and at 5 AU the radial gradient decreases from the poles towards the equatorial region thus the decreases in ξ_ϕ.

Figure (7.6) shows ξ_ϕ for Jovian electrons as a function of kinetic energy as given above. As discussed in the previous chapter, Jovian electrons have a relatively strong azimuthal dependence close to the source which is located at the equatorial plane and the effective azimuthal diffusion coefficient ($K_{\phi\phi}$) increases with increasing radial distance. For Jovian electrons ξ_ϕ will always be more dominate at 5 AU than at 1 AU and it also increases from the pole towards the equatorial plane, especially between $\theta = 60^0$ and $\theta = 10^0$. This is the only anisotropy component that has a different energy dependence in the polar regions at 1 AU for the three b-cases. The energy dependence is also different at 1 AU than at 5 AU.

7.4 The spatial dependence of the 7 MeV electron anisotropy components

7.4.1 Radial dependence

Figure (7.7) shows ξ_r for 7 MeV galactic electrons (left panels) and Jovian electrons (right panels) as a function of radial distance at $\theta = 10^0$ (upper panels), $\theta = 60^0$ (middle panels) and $\theta = 90^0$ (bottom panels). Three different solutions are shown, corresponding to the three different d scenarios discussed before - see Chapter 6. It follows that the galactic ξ_r is significantly larger for increasing d-values, and increases with radial distance at $\theta = 60^0$ and $\theta = 90^0$. At $\theta = 10^0$ the increase of d causes large negative values with a very strong radial dependence. The radial dependence of the Jovian electron ξ_r is much more complex, with an increased d causing a varying effect with increasing radial distance, having significant latitude dependence. Since the azimuthal dependence of galactic electrons is negligible, the galactic ξ_r is determined by the spatial dependence of G_r and the effective radial diffusion coefficient (K_{rr}). The galactic ξ_r shows the tendency to increase with radial distance in the inner heliosphere because it is dominated by K_{rr} which also increases in the inner heliosphere as a function of radial distance. The Jovian electrons have a complex azimuthal dependence so that the role of G_ϕ and $K_{r\varphi}$ becomes more important according to Equation (7.15).

It was discussed in Chapter 4 that K_{rr} dominates in the inner heliosphere due to the term $K_{\|}\cos^2\psi$ as particles tend to follow the HMF. From the shape of the Jovian electron anisotropy graphs, it is noticeable for $\theta = 60^0$ and $\theta = 90^0$ that K_{rr} dominates from 1 AU to ~ 2.8 AU and the effect of large G_ϕ is noticeable at ~ 3 AU to 5 AU. At $\theta = 60^0$, K_{rr} dominates G_ϕ from 1 AU to 3.8 AU.

7.4.2 Latitudinal dependence

Figure (7.8) illustrates separately the computed latitudinal anisotropy ξ_θ of 7 MeV galactic and Jovian electrons in the inner heliosphere as a function of polar angle. The profiles are shown at a radial distance of 1 AU and 5 AU with the Jovian source at $\theta = 90^0$ and azimuthal angle at 0^0. The solid line corresponds to solutions produce when $d = 1$

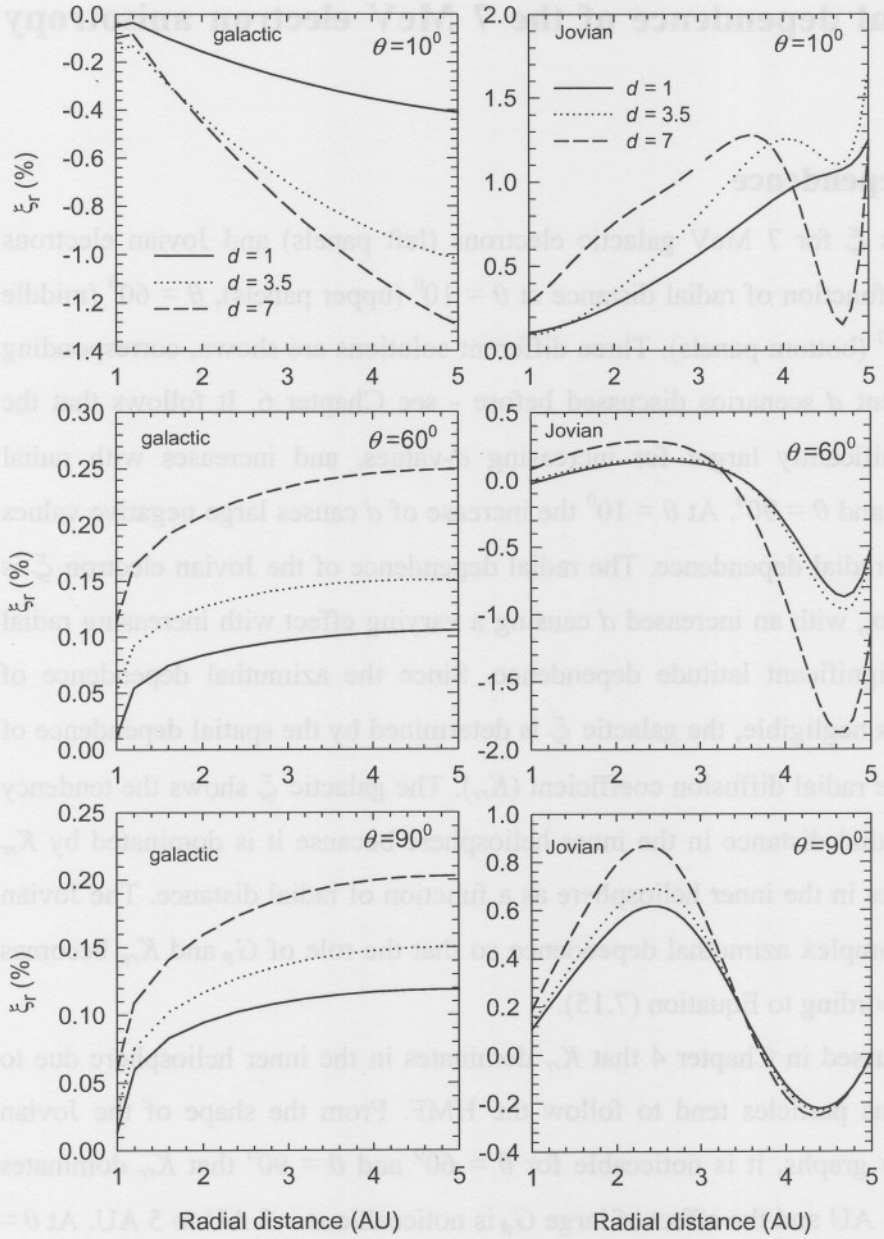

Figure (7.7): Computed ξ_r for 7 MeV galactic electrons (left panels) and Jovian electrons (right panels) as a function of radial distance at $\theta = 10^0$ (upper panels), $\theta = 60^0$ (middle panels) and $\theta = 90^0$ (bottom panels). Three different solutions are shown, corresponding to three different d scenarios. The solid line corresponds to solutions produced when $d = 1$, the dotted line corresponds to $d = 3.5$ and the dashed line corresponds to $d = 7$. In this case $b = 0.020$ in Equation (4.6) and $a = 0.006$ in Equation (4.24).

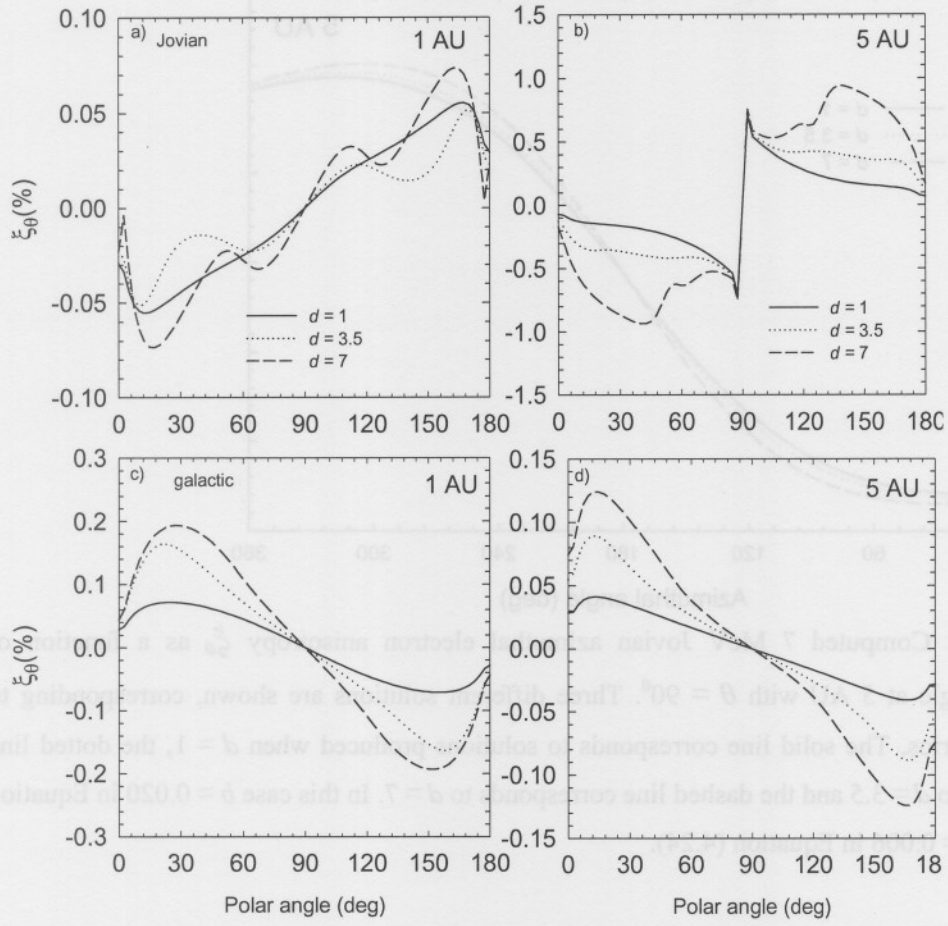

Figure (7.8): Computed ξ_θ for 7 MeV galactic and Jovian electrons as a function of polar angle at 1 AU and 5 AU. Panels (a) and (b) show it for Jovian electrons and panels (c) and (d) for galactic electrons. The rest is the same as in Figure (7.7).

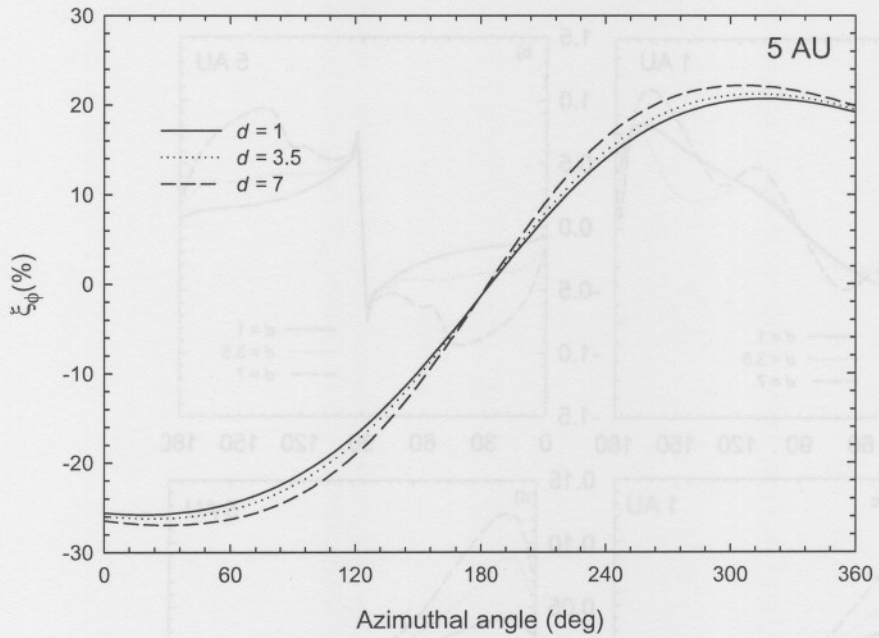

Figure (7.9): Computed 7 MeV Jovian azimuthal electron anisotropy ξ_ϕ as a function of azimuthal angle at 5 AU with $\theta = 90^0$. Three different solutions are shown, corresponding to three d scenarios. The solid line corresponds to solutions produced when $d = 1$, the dotted line corresponds to $d = 3.5$ and the dashed line corresponds to $d = 7$. In this case $b = 0.020$ in Equation (4.26) and $a = 0.006$ in Equation (4.24).

, the dotted line corresponds to $d = 3.5$ and the dashed line corresponds to $d = 7$. For panels (a) and (b) at 1 AU and 5 AU, there is no enhancement of $K_{\perp\theta}$ because $d = 1$. In panel (a) for $d = 3.5$ and $d = 7$, ξ_θ has similar shapes as the latitudinal gradient shown in Chapter 6, which shows that ξ_θ is dominated by the latitudinal gradient. In panel (b) for $d = 3.5$ and $d = 7$, the effect is noticeable for $\theta \leq 60^0$ and at $\theta \geq 120^0$. Thus, at 5 AU the absolute values of ξ_θ are larger than at 1 AU.

In Figure (7.8), panels (c) and (d) show the galactic electron ξ_θ at 1 AU and 5 AU, respectively. It decreases in absolute values from 1 AU to 5 AU. The polar angle dependence is similar for all the d scenarios.

7.4.3 Azimuthal dependence

Figure (7.9) shows ξ_ϕ for 7 MeV Jovian electrons as a function of azimuthal angle at 5 AU with $\theta = 90^0$. The Jovian electron source is at an azimuth angle of 0^0. Three different solutions are shown, corresponding to three different d scenarios. The solid line corresponds to solutions produced when $d = 1$, the dotted line corresponds to $d = 3.5$ and the dashed line corresponds to $d = 7$. The values of ξ_ϕ are large positive when $\phi > 240^0$ and large negative when $\phi < 120^0$. As discussed in Chapter 4, $K_{\parallel}$ and $K_{\perp r}$ are assumed not to have an azimuthal dependence for simplicity, but K_{rr} does because of the HMF spiral field. Thus the Jovian electron ξ_ϕ at the source will depend on the azimuthal gradient. Increasing d has insignificant effects on ξ_ϕ.

7.5 Modulation of the 7 MeV Jovian electron anisotropy along the Ulysses trajectory

In Figure (7.10) the modulation for the computed magnitude of the total anisotropy vector for 7 MeV Jovian electrons is shown for three assumptions for d along the Ulysses trajectory, with $b = 0.020$ and $a = 0.006$. This time sequence is simply a series of steady-state solutions which displays the effect of the spatial movement of Ulysses (see also Ferreira, 2002 and Moeketsi, 2004). After Ulysses' launch in 1990, it moved directly towards Jupiter in the equatorial plane so that there was an increase in the total anisotropy to ~ 20% in 1991.5, which could have been caused by a good magnetic link to the electron source, or an increase in solar activity or even interplanetary shock waves since they are also a source of 0.25 – 25 MeV electrons. In 1992 there was an abrupt increase up to ~ 38% during the first direct encounter with Jupiter, with the closest approach of 0.003 AU. After the 1992 encounter, Ulysses moved south of the planet which in Figure (7.10) is shown as the rapid decrease in the anisotropy as the spacecraft moved away from the source, but not as sharp as when Ulysses approached the planet in the equatorial plane. The next sharp increase was in 1998 but at that time Jupiter was on the other side of the Sun, thus the increase in the anisotropy is only up to ~ 20% which could again have been caused by a favourable magnetic connection to the source.

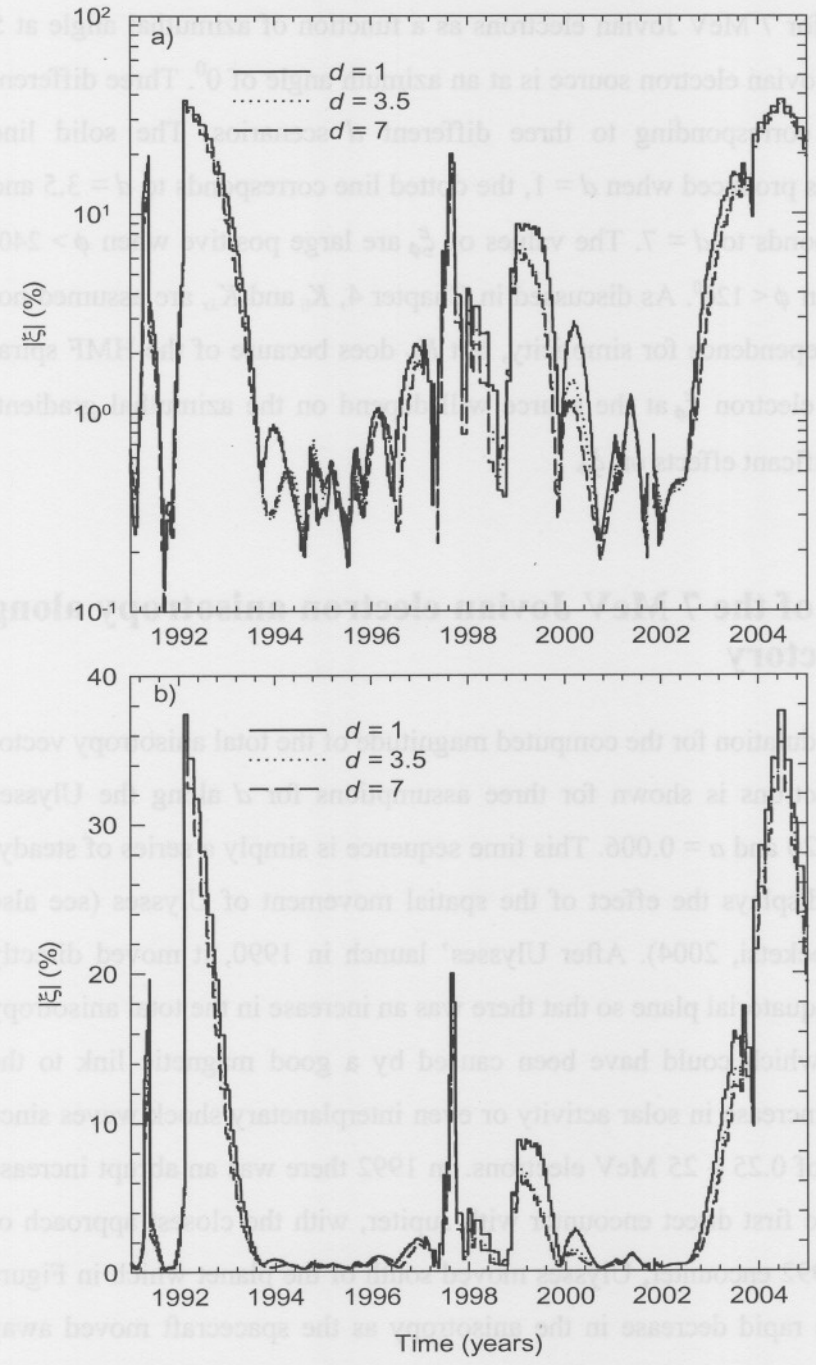

Figure (7.10): Computed magnitude of the total anisotropy for 7 MeV Jovian electrons for different assumptions of d along the Ulysses trajectory with $b = 0.020$ in Equation (4.6) and $a = 0.006$ in Equation (4.24). In the top panel a log-scale is used whereas in the bottom panels a linear scale is shown.

The recent distant close encounter was in 2004 when Ulysses approached Jupiter up to 0.804 AU from a northern heliolatitude, thus causing the difference in the shape of the peaks for 1992 and 2004, with the latter significantly wider. The maximum value of the anisotropy in 2004 was ~ 38% which is the same as in 1992, as such a remarkable result. This means that a maximum anisotropy can be obtained even if only a close encounter of the planet is made but that an equatorial approach produces a much sharper peak, a result of the global features of the modulation of 7 MeV electrons in the inner heliosphere. The broader peak in the total anisotropy is indicative of the role of perpendicular diffusion in the latitudinal direction. The Jovian source of electrons is perfectly suited to study in detail the role of perpendicular diffusion and the predicted enhancement of perpendicular diffusion in the polar direction.

7.6 Summary

In this chapter the three anisotropy vector components were computed, ignoring drifts as the focus was on low-energy electrons. The 3D electron modulation model of Ferreira (2002) was used to study the effect of increasing the polar perpendicular diffusion on the modulation of electrons at 1 AU and 5 AU. The anisotropy vector components where studied as a function of energy ($E \geq 10$ MeV). For the radial anisotropy component, it was found that for Jovian electrons, it is larger at 5 AU than at 1 AU; at 1 AU the radial anisotropy increases from near the equatorial region towards the poles. Whereas for galactic electrons the radial anisotropy increases from near the equatorial plane towards the poles at both 1 AU and 5 AU.

For the latitudinal anisotropy component as a function of kinetic energy it was found that it follows the behaviour of the latitudinal gradient because the latitudinal anisotropy depends primarily on the polar gradient (G_θ) and the polar diffusion coefficient ($K_{\perp\theta}$); the polar gradient at 1 AU and 5 AU increases from the equatorial plane to the polar regions for galactic electrons. It follows that the latitudinal anisotropy increases from the equatorial region to the poles and it is larger at 1 AU than 5 AU. Whereas for Jovian electrons at 1 AU the polar gradient increases from the equatorial regions to the poles, thus being an increase in the latitudinal gradient. At 5 AU for Jovian

electrons, the polar gradient decreases from the equatorial plane to the poles but have a very large $K_{\perp 0}$ next to the source which leads to small variation in the latitudinal anisotropy.

The galactic azimuthal anisotropy as a function of kinetic energy depends on the radial gradient (G_r) and $K_{r\phi}$ so that it decreases from the equatorial plane to the poles at 1 AU, while at 5 AU it increases from the equatorial plane to the poles due to the dependence on the radial gradient. For Jovian electrons, it increases for both 1 AU and 5 AU from the poles to the equatorial plane, because for Jovian electrons the azimuthal gradient plays a major role, especially close to the electron source.

The modulation effect of the different d scenario was illustrated for the spatial dependence of the anisotropy vector components. It was found that the $d = 7$ scenario dominates all three anisotropy components.

Lastly the effects of the assumed three d scenarios were illustrated on the magnitude of the 7 MeV total anisotropy along the Ulysses trajectory. A large increase in the anisotropy during the first direct encounter with Jupiter in 1992 is computed that has the same value (38%) as for the distant close encounter in 2004. This means that a maximum anisotropy can be obtained even if only a close encounter of the planet is made but that an equatorial approach produces a much sharper peak, that is, the anisotropy changes rapidly as the spacecraft approaches the source, a result of the global features of the modulation of 7 MeV electrons in the inner heliosphere. The broader peak in the total anisotropy found for 2004 is indicative of the role of perpendicular diffusion in the latitudinal direction. The Jovian source of electrons is perfectly suited to study in detail the role of perpendicular diffusion and the predicted enhancement of perpendicular diffusion in the polar direction. The peaks in the anisotropy-time profile in 1991.5 and 1998 need further investigation.

Chapter 8

Summary and conclusions

In **Chapter 1** the reader was introduced to the study of modelling galactic and Jovian electrons in the heliosphere. A brief overview of the concept used in the heliospheric modulation of cosmic rays was given in **Chapter 2**, which includes topics on the origin of cosmic rays, the Sun, the heliosphere, the heliospheric magnetic field and current sheet and its tilt angle, and solar cycle variations. The Ulysses mission was discussed in relation to the KET telescope which has provided the electron observational data.

An overview of the propagation and modulation of low-energy electrons (3-10 MeV) in the inner heliosphere was given in **Chapter 3**, with the main emphasis on the Jovian electrons, including the Jovian source function that contributes significantly to the few-MeV electron intensities in the inner heliosphere. An overview of 3D Jovian electron propagation and modulation models was given, followed by a brief discussion on the observed modulation and spectra of Jovian electrons. It is beyond the scope of this dissertation to use the model to reproduce observations but modulation parameters and diffusion coefficients from previous studies by Ferreira (2002) and Moeketsi (2004) were used that resulted in realistic electron modulation.

The transport mechanisms described in the Parker transport equation namely diffusion, convection, drifts and energy changes were discussed in **Chapter 4**. A brief background was given on the existing knowledge of the diffusion process, focusing mainly on the diffusion tensor applicable to low-energy electrons in the heliosphere and on investigating the spatial and rigidity dependence (Ferreira, 2002). It was shown that in the modulation model several diffusion coefficients are of special importance, namely $K_{\parallel}$ the diffusion coefficients parallel to the HMF, $K_{\perp r}$ and $K_{\perp \theta}$ which are the perpendicular diffusion coefficients in the radial/azimuthal direction and in the polar direction, respectively. Some emphasis was placed on the radial, latitudinal and rigidity dependence of $K_{\phi\phi}$, the effective diffusion coefficient in the azimuthal direction and on K_{rr}, the effective diffusion coefficient in the radial direction. It was shown that:

- K_{rr} is dominated by the term $K_{\parallel}\cos^2\psi$ in the inner heliosphere but dominated by $K_{\perp r}\sin^2\psi$ in the outer heliosphere; K_{rr} increases towards the poles because of the dependence on the HMF spiral angel ψ.
- $K_{\phi\phi}$ is dominated by $K_{\parallel}\sin^2\psi$ and is significantly larger throughout most of the heliosphere in the equatorial plane and decreases significantly towards the poles of the heliosphere.

In **Chapter 5,** the 3D Jovian electron modulation model and the numerical implementation thereof were discussed including the Jovian source function and the galactic electron LIS. The sensitivity of the model to the radial grid size and the modulation boundary was illustrated. The latitudinal dependence of the solar wind speed V, which describes the transition from solar minimum to solar maximum modulation conditions, was used in **Chapter 6.** It correspondingly describes the latitude dependence of the polar (perpendicular) diffusion coefficient, following up on the work of Ferreira (2002) and Moeketsi (2004). Three scenarios for the parameter d that determines the latitude dependence of $K_{\perp 0}$, and corresponding to solar minimum, intermediate and maximum activity, were used to illustrate the 3D radial, latitudinal and azimuthal gradients as a function of kinetic energy at 1 AU and 5 AU, and at different polar angles. It was found that:

- For both Jovian and galactic electrons, the radial gradients are larger at 1 AU than at 5 AU and they increase from the poles to the equatorial plane.
- At higher heliolatitudes, the Jovian electron latitudinal gradients increase steadily unlike near the equatorial region where there is a decrease. For galactic electrons, the low-energy latitudinal gradients show a steady decrease. At 1 AU the gradients are larger than at 5 AU.
- The azimuthal gradients, at higher heliolatitudes and for $E < 30$ MeV, decrease until they reach a minimum value 0.03% at 5 AU, while at 1AU there is a sharp decrease, followed by a steady decrease.

The effects on low-energy electrons of the chosen three d scenarios were also illustrated on their modulation at 1 AU and 5 AU, respectively, as function of polar angle. It was found that:

- For galactic electrons, the effects of the three d scenarios are more significant in the polar regions, being insignificant in the equatorial plane.
- For Jovian electrons, a factor of ~ 2.5 at 1 AU and at the poles was found when changing $d = 7$ to d = 1. At 5 AU, the effect diminishes in the equatorial plane for both the Jovian and galactic electrons.
- For galactic electrons, the latitudinal gradients are negative between $\theta = 0^0$ and $\theta = 90^0$, whereas for Jovian electrons they are positive at both mentioned radial distances. The galactic electron latitudinal gradients are larger at 1 AU than at 5 AU.

The effects of the three d scenarios were also illustrated on the 7 MeV Jovian electron modulation at 5 AU as a function of azimuthal angle at different heliolatitude. It was found that:

- At the poles the effects are insignificant between the two extreme cases, $d = 1$ and $d = 7$. The electron intensities increase from the poles to the equatorial plane and the effect of the d scenarios diminishes at the Jovian electron source.
- At the poles there is almost no azimuthal gradient for $d = 1$ and the three solutions converge as the Jovian electron source is approach.

And lastly the effects of the three d scenarios were illustrated on 7 MeV electron modulation as a function of radial distance in the inner heliosphere at three different latitude positions, $\theta = 10^0$, $\theta = 60^0$ and $\theta = 90^0$, respectively, for both galactic and Jovian electrons. It was found that:

- The galactic electron intensities were dominant the distribution of electrons in the polar regions whereas the Jovian electron intensities dominate the equatorial regions.
- The galactic electron radial gradients have the largest values in the polar regions, while the Jovian electron radial gradients dominate in the equatorial plane.

In **Chapter 7** the three anisotropy components were computed for the first time, ignoring drifts as the focus was on low-energy electrons. The effect of increasing polar perpendicular diffusion on the modulation of electrons at 1 AU and 5 AU was studied. The anisotropy components where computed as a function of energy only for the range 1 MeV $\leq E \leq$ 10 MeV. It was found that:

- The radial anisotropy component for Jovian electrons is larger at 5 AU than at 1 AU; at 1 AU the radial anisotropy increases from near the equatorial region

towards the poles. Whereas for galactic electrons, the radial anisotropy increases from near the equatorial plane towards the poles at both 1 AU and 5 AU.

- The latitudinal anisotropy follows the behaviour of the latitudinal gradient because of the primary dependence on the polar gradient (G_θ) and the polar diffusion coefficient ($K_{\perp\theta}$); the polar gradient at 1 AU and 5 AU increases from the equatorial plane to the polar regions for galactic electrons. Whereas for Jovian electrons at 1 AU the polar gradient increases from the equatorial regions to the poles. At 5 AU for Jovian electrons, the polar gradient decreases from the equatorial plane to the poles.
- For the galactic azimuthal anisotropy, being dependent on the radial gradient (G_r) and $K_{r\phi}$, decreases from the equatorial plane to the poles at 1 AU, while at 5 AU it increases from the equatorial plane to the poles caused by the dependence on the radial gradient. For Jovian electrons, it increases for both 1 AU and 5 AU from the poles to the equatorial plane; for Jovian electrons the azimuthal gradient plays a major role, especially close to the electron source.

The modulation effect of the different d scenario was illustrated for the spatial dependence of the anisotropy vector components. It was found that:

- The $d = 7$ scenario is the dominant scenario for all three anisotropy components.

The effects of the d scenarios were also illustrated on the magnitude of the 7 MeV total anisotropy vector along the Ulysses trajectory. It was found that:

- A large increase in the anisotropy during the first direct encounter with Jupiter in 1992 is computed that has the same value (38%) as for the close 2004 encounter.
- The maximum anisotropy can be obtained even if only a close encounter of the planet is made but that an equatorial approach produces a much sharper peak when illustrates on a time-scale, a result of the global features of the modulation of 7 MeV electrons in the inner heliosphere.
- The broader peak in the total anisotropy-time profile found for 2004 is indicative of the role of perpendicular diffusion in the latitudinal direction.

It is concluded that:

- Low-energy electrons (< 50 MeV) are mainly modulated by diffusion and convection, adiabatic energy losses and drifts are of less importance.
- The diffusion coefficients such as $K_{\phi\phi}$ and $K_{r\phi}$ which were neglected in the 2D modulation studies play a major role in determining Jovian electron anisotropies (radial and azimuthal) close to the source.
- The Jovian radial and azimuthal anisotropy are mainly determined by G_ϕ close to the source.
- The Jovian electron latitudinal anisotropy is everywhere in the heliosphere determined by the product $G_\theta K_{\perp\theta}$.
- The normal modulation mechanisms, in particular convection, parallel and perpendicular diffusion combine to produce 38% total electron anisotropy close to the Jovian electron source. This implies that the normal anisotropy may contribute as much as 50% of the extra-ordinary anisotropies observed during the 15 electron 'jet' episodes (McKibben et al., 2005).
- It is clear from this work that perpendicular diffusion in the polar direction plays an important role in the modulation of low-energy electrons, in accordance with the work of Ferreira (2002) and Moeketsi (2004).
- The magnitude of the total anisotropy along the Ulysses trajectory dropped below 1% for the periods 1994 to 1997, again during 2001 to 2002. It was above 10% during a short time in 1991, 1992-93, in 1997 and again from 2003 to 2005.

The following aspects of electron modulation, considered to be beyond the scope of this dissertation, deserve to be mentioned and to be studied further:

- What causes the very high electron anisotropy observed during the observed electron 'jet' episodes? The Jovian electron jets are striking examples of tightly guided propagation along the HMF lines over great distances (McKibben et al. 2005). For such as study a different transport equation may be required since Parker's equation is not derived to handle very large anisotropies.
- Whether Coronal Mass Ejections played a role during these episodes, and how the subsequent effects influence electron modulation between Jupiter and Earth.

- Whether frequent large-scale deviations from the Parker magnetic field spiral pattern occur that may have significant implications for understanding of energetic charged particle propagation through the interplanetary medium, and how important cross-field transport (polar diffusion coefficient) is for the propagation of low-energy electrons.
- What are the causes of the other strong peaks in the magnitude of the total anisotropy shown in Figure 7.10?
- What is the contribution to the total anisotropy from solar electrons during time of increased solar activity?

References

Baker, D. N., and J. A. Van Allen, Energetic electrons in the Jovian magnetosphere, *J. Geophys. Res.*, *81*, 617, 1976.

Balogh, A., E. J. Smith, B. T. Tsurutani, D. J. Southwood, R. J. Forsyth, and T. S. Horbury, The Heliospheric Magnetic Field Over the South Polar Region of the Sun, *Science, 268 (5213)*, 1007, 1995.

Balogh, A., R. G. Marsden, and E. J. Smith, (Eds.), The Heliosphere Near Solar Minimum: *The Ulysses Perspective*, 411 pp., Springer-Praxis, London, 2001.

Bieber, J. W., Transport of charged particles in the heliosphere: Theory, *Adv. Space Res.*, *32(4)*, 549, 2003.

Bieber, J. W., and W. H. Matthaeus, Cosmic ray pitch angle scattering in dynamical magnetic turbulence, *Proc 22nd Inter. Cosmic Ray Conf, Dublin*, *3*, 248, 1991.

Bieber, J. W., W. H. Matthaeus, C. W. Smith, W. Wanner, M-B. Kallenrode, and G. Wibberenz, Proton and electron mean free paths: The Palmer consensus revisited, *Astrophys. J., 420(1)*, 294, 1994.

Burger, R. A., On the theory and application of drift motion of charged particles in inhomogenous magnetic fields, *Ph.D. thesis, Potchefstroom University for CHE, South Africa*, 1987.

Burger, R. A., Cosmic-ray modulation and the heliospheric magnetic field, *Adv. Space Res.*, *35*, 636, 2005.

Burger, R. A., and M. Hattingh, Effects of Fisk-type heliospheric magnetic field on the latitudinal transport of cosmic rays, *Proc. 27th Inter. Cosmic Ray Conf. (Hamburg)*, *9*, 3698, 2001.

Burger, R. A., and M. Hattingh, Steady-State Drift-Dominated Modulation Models for Galactic Cosmic Rays, *Astrophysics and Space Science, 230*, 375, 1995b.

Burger, R. A., M. S. Potgieter, and B. Heber, Rigidity dependence of cosmic-ray proton latitudinal gradients measured by the Ulysses spacecraft: Implications for the diffusion tensor, *J. Geophys. Res., 105(A12)*, 27447, 2000.

Chenette, D. L., T. F. Conlon, and J. A. Simpson, Burst of relativistic electrons from Jupiter observed in interplanetary space with time variation of planetary rotation period, *J. Geophys. Res.*, *79*, 3551, 1974.

Classen, H. T., G. Mann, R. J. Forsyth, and E. Keppler, Particle Acceleration at Corotating Interaction Regions, *Am. Inst. Phys. Conf. Series 471*, 625, 1999.

Conlon, T. F., and J. A. Simpson, Modulation of Jovian electron intensity in interplanetary space by co rotating interaction regions, *Astrophys. J., 211*, L45, 1977.

Coroniti, F. V., C. F. Kennel, F. L. Scarf, and E. J. Smith, Whistler mode turbulence in the disturbed solar wind, *J. Geophys. Res.,87*, 6029, 1982.

Davis, L., The interplanetary magnetic field, in Solar Wind, edited by C. P. Sonett, P. J. Coleman, and J. M. Wilcox., Scientific and Technical Information Office, NASA, Washington, 93, 1972.

del Peral, L., R. Gomez-Herrero, M. D. Rodriguez-Frias, J. Gutikez, Müller- Mellin, H. Kunow, Jovian electrons in the heliosphere: new insights from EPHIN on board SOHO, *Astropar. Phys.*, *20*, 235, 2003.

Douglas, J., Alternating direct implicit methods for three space variables, *Numerische mathematik, 4,* 41, 1962.

Dröge, W., Particle scattering by magnetic fields, *Space Sci. Rev.*, *93*, 121, 2000.
Dröge, W., Solar Particle Transport in a Dynamical Quasi-linear Theory, *Astrophys. J., 589*, 1027, 2003.
Dröge, W., Probing heliospheric diffusion coefficients with solar energetic particles, *Adv. Space Res., 35*, 532, 2005.
Earl, J. A., The diffusive idealization of charged-particle transport in random magnetic fields, *Astrophys. J., 193*, 231, 1974.
Eraker, J. H., and J. A. Simpson, Jovian electron propagation close to the Sun (< 0.5 AU), *Astrophys. J., 232(2)*, L131, 1979.
Eraker, J. H., Origins of the low-energy relativistic interplanetary electrons, *Astrophys. J., 257(1),* 862, 1982.
Ferrando, P., R. Ducros, C. Rastoin, and A. Raviart, Jovian electron jets in interplanetary space, *Planet. Space Sci., 41*, 839,1993a.
Ferrando, P., R. Müller-Mellin, H. Sierks, G. Wibberenz, A. Raviart, R. Ducros, and L.Treguer, The Kiel electron telescope onboard Ulysses, *Proc. 22nd Inter. Cosmic Ray Conf, Dublin, 3*, 366, 1991.
Ferrando, P., A. Raviart, L. J. Haasbroek, M. S. Potgieter, W. Droge, B. Heber, H. Kunow, R. Müller-Mellin, H. Sierks, G. Wibberenz, and C. Paizis, Latitude variations of - 7 MeV and >300 MeV cosmic ray electron fluxes in the heliosphere: Ulysses COSPINKET results and implications, *Astron. Astrophys., 316*, 528, 1996.
Ferreira, S. E. S., A study of the modulation of cosmic ray electrons in the heliosphere, *M.Sc. dissertation, Potchefstroom University for CHE, South Africa*, 1998.
Ferreira, S. E. S., The heliospheric transport of galactic cosmic rays and Jovian electrons, *Ph.D. thesis, Potchefstroom University for CHE, South Africa*, 2002.
Ferreira, S. E. S., and M. S. Potgieter, The modulation of 4- to 16-MeV electrons in the outer heliosphere: Implications of different local interstellar spectra, *J. Geophys. Res., 107(A8)*, SSH12-1, 2002.
Ferreira, S. E. S., and M. S. Potgieter, Long-term cosmic ray modulation in the Heliosphere, *Astrophys. J., 603*, 744, 2004.
Ferreira, S. E. S., and M. S. Potgieter, Galactic cosmic rays in the heliosphere, *Adv. Space Res., 34*, 115, 2004a.
Ferreira, S. E. S., and M. S. Potgieter, Long-term cosmic ray modulation in the heliosphere, *Astrophys. J., 603*, 744, 2004b.
Ferreira, S. E. S., and K. Scherer, Modulation of cosmic-ray electrons in the outer heliosphere, *Astrophys. J., 616*, 1215, 2004.
Ferreira, S. E. S, M. S. Potgieter, and D. M. Moeketsi, Modulation effects of a changing solar wind speed on low-energy electrons, *Adv. Space Res.,* 32(4), 675-680, 2003a
Ferreira, S. E. S., M. S. Potgieter, B. Heber, R. Fichtner and R. Kissmann, Solar wind effects on the transport of 3 – 10 MeV cosmic ray electrons from solar minimum to solar maximum, *Astrophys. J., 594*, 552, 2003b.
Ferreira, S. E. S., M. S. Potgieter, R. A. Burger, B. Heber, and H. Fichtner, Modulation of Jovian and galactic electrons in the heliosphere 1. Latitudinal transport of few MeV electrons, *J. Geophys. Res., 106 (A11)*, 24979, 2001a.
Ferreira, S. E. S., M. S. Potgieter, R. A. Burger, B. Heber, H. Fichtner, and C. Lopate, Modulation of Jovian and galactic electrons in the heliosphere: 2. Radial transport of a few MeV electrons, *J. Geophys. Res., 106 (A12)*, 29313, 2001b.

Ferreira, S. E. S., M. S. Potgieter, B. Heber, H. Fichtner, and R. A. Burger, Latitudinal transport of 7 MeV Jovian and galactic electrons, *Proc. 27Th Inter. Cosmic Roy Conf, (Hamburg), 8*, 3702, 2001c

Ferreira, S. E. S., M. S. Potgieter, R. A. Burger, and B. Heber, Modulation effects of anisotropic perpendicular diffusion on cosmic ray electron intensities in the heliosphere, *J. Geophys. Res., 105(A8)*, 18305, 2000.

Fichtner, H. Anomalous cosmic rays: Messengers from the outer heliosphere, *Space Sci. Rev., 95 (3/4)*, 639, 2000a.

Fichtner, H., M. S. Potgieter, S. E. S. Ferreira, and R. A. Burger, On the propagation of Jovian electrons in the heliosphere: transport modeling in 4-D phase space, *Geophys. Res. Lett., 27(11)*, 1611, 2000b.

Fichtner, H., M. S. Potgieter, S. E. S. Ferreira, and B. Heber, Time-dependent 3D modeling of the heliospheric propagation of few-MeV electrons, *Proc. 27th inter. Cosmic Ray Conf., Hamburg, 8*, 3666, 2001b.

Fisk, L. A., B. Koslovsky, and R. Ramaty, An interpretation of the Observed Oxygen and Nitrogen Enhancements in Low-Energy Cosmic Rays, *Astrophys. J., 190*, L35, 1974.

Fisk, L. A., Motion of the footpoints of heliospheric magnetic field lines at the Sun: Implications for recurrent energetic particle events at high heliographic latitudes, *J. Geophys. Res., 101 (A7)*, 15547, 1996.

Forbush, E., Three unusual cosmic ray increases probably due to the charged particles from the Sun, *Physical Rev., 70*, 771, 1946.

Garcia-Munoz, M., G. M. Mason, and J. A. Simpson, The Abundances of Galactic Cosmic-Ray Carbon, Nitrogen, and Oxygen and Their Astrophysical Implications, *Astrophys. J., 184*, 967, 1973.

Gazis, P. R., A. Barnes, J. D. Mihalov, and A. J. Lazarus, Solar wind velocity and temperature in the outer heliosphere, *J. Geophys. Res., 99 (A4)*, 6561, 1994.

Gazis, P. R., A. Barnes, J. D. Mihalov, and A. J. Lazarus, The structures of the inner heliosphere from Pioneer, Venus and IMP observations, in *Solar Wind*, edited by E. Marsch and R. Schwenn, *Pergamon Press., New York*, 183, 1991.

Giacalone, J., and J. R. Jokipii, The Transport of Cosmic Rays across a Turbulent Magnetic Field, *Astophys. J., 520(1)*, 204, 1999.

Gil, A., and M. V. Alania, 27-day variations of cosmic rays for the minima epochs of solar activity: Experimental and 3-D drift modeling results, *Proc. 27th Inter. Cosmic Rays Conf. (Hamburg), 9*, 3725, 2001.

Goldstein, M. J., A. J. Klimas, and G. Sandri, Mirroring in the Fokker-Planck coefficient for cosmic-ray pitch-angle scattering in homogeneous magnetic turbulence, *Astrophys. J., 195*, 787, 1975.

Goldstein, M. J., A nonlinear theory of cosmic-ray pitch-angle diffusion in homogeneous magnetostatic turbulence, *Astrophys. J., 204*, 900, 1976.

Haasbroek, L. J., Modulation of cosmic rays in the heliosphere: A model study for the Ulysses mission (in Afrikaans), *M.Sc. dissertation, Potchefstroom University for CHE, South Africa*, 1993.

Haasbroek, L. J., The transport and acceleration of charged particles in the heliosphere, *Ph.D thesis, Potchefstroom University for CHE, South Africa*, 1997.

Hamilton, D. C., and J. A. Simpson, Jovian electron propagation out of the solar equatorial plane - Pioneer 11 observations, *Astrophys. J., 228(2)*, L123, 1979.

Hasselmann, K., and G. Wibberenz, A note on the parallel diffusion coefficient, *Astrophys. J., 162*, 1049, 1970.

Hasselmann, K., and G. Wibberenz, Scattering of charged particles by random electromagnetic fields, *Zeitschrift für Geophysik, 34*, 353, 1968.

Hattingh, M., The modulation of galactic cosmic rays in a three-dimensional heliosphere, *Ph.D. thesis, Potchefstroom University for CHE, South Africa*, 1998.

Hattingh, M., and R. A. Burger, A new simulated wavy neutral sheet drift model, *Adv. Space Res., 13(9)*, 213, 1995b.

Heber, B., Modulation and propagation of cosmic rays in the inner three-dimensional heliosphere: Ulysses observations, *Habilitation study, Universität Osnabriick, Germany,* 2002.

Heber, B., and R. G. Marsden, Cosmic Ray Modulation over the poles at solar maximum: Observations, *Space Sci. Rev., 97*, 309, 2001b.

Heber B., P. Ferrando, A. Raviart, C. Paizis, R. Müller-Mellin, H. Kunow, Propagation of 3-10 MeV electrons in the inner heliosphere: Ulysses observations, *Adv. Space Res., 27*, 547-552, 2001

Heber B., P. Ferrando, A. Raviart, C. Paizis, G. Sani, A. Posner, G. Wibberenz, R. Müller-Mellin, H. Kunow, M. S. Potgieter, S. E. S. Ferreira, R. A. Burger, and H. Fichtner, Quite-time MeV electron increases at solar maximum: Ulysses COSPIN/KET observations, *Adv. Space Res., 32*, 663, 2003a.

Heber, B., S. E. S. Ferreira, H. Fichtner, M. S. Potgieter, V. K. Henize, R. Kissmann, and D. M. Moeketsi, Out-of-ecliptic quiet time MeV electron increases: Ulysses COSPIN/KET observations, *American Institute Physics Conference Series, 703*, 157, 2004.

Heber B., H. Fichtner, R. Kissmann, M. S. Potgieter, S. E. S. Ferreira, Quiet-time MeV electron increases at solar maximum: Ulysses COSPIN/KET observations, *Astronomosche Nacherichten, 324*, 87, 2003b.

Heber, B., M. S. Potgieter, and P. Ferrando, Solar modulation of galactic cosmic rays: The 3D heliosphere, *Adv. Space Res., 19(5)*, 795, 1997.

Heber, B., G. Wibberenz, M. S. Potgieter, R. A. Burger, S. E. S. Ferreira, R. Müller-Mellin, H. Kunow, P. Ferrando, A. Raviart, C. Paizis, C. Lopate, F. B. McDonald, and H. V. Cane, Ulysses Cosmic Ray and Solar Particle Investigation/Kiel Electron Telescope Observation: Charge sign dependence and spatial gradients during the 1990-2000 A > 0 solar magnetic cycle, *J. Geophys. Res., 107(A10)*, 2002

Hoeksema, J. T., Large scale structure of the heliospheric magnetic field: 1976-1991, In Marsh, E. and R. Schwenn eds. Solar wind seven. *Pergamon press, New York*, 191, 1992.

Hu, Y. Q., S. R. Habbal, Y. Chen, and X. Li, Are coronal holes the only source of fast solar wind at solar maximum? *J. Geophys. Res., 108(A10)*, SSH8-1, 2003.

Hundhausen, A. J., An interplanetary view of coronal holes, in *Coronal Holes and High Speed Streams*, edited by J. B. Zirker, *Colorado Associated Univ. Press., Colorado*, 114, 1977.

Jokipii, J. R., Cosmic-ray propagation. I. Charged particles in a random magnetic field, *Astrophys. J., 146*, 480, 1966.

Jokipii, J. R., Propagation of cosmic rays in the solar wind, *Rev. Geophys. Space Physics, 9*, 27, 1971.

Jokipii, J. R., and J. Kóta, The polar heliospheric magnetic field, *Geophys. Res. Lett.*, *16*, 1, 1989.

Jokipii, J. R, E. H. Levy, and W. B. Hubbard, Effects of particle drift on cosmic ray transport. I – General properties, application to solar modulation, *Astrophys. J.*, *213*, 861, 1977.

Jones, F. C., and D. C. Ellison, The plasma physics of shock acceleration, *Space Sci. Rev., 58(3-4)*, 259, 1991.

Kanekal, S. G., D. N. Baker, J. B. Blake, M. D. Looper, R. A. Mewaldt, and C. A. Lopate, Modulation of Jovian electrons at 1 AU during solar cycles 22 - 23, *Geophys. Res. Lett.*, *30*, SSCl, 2003.

Keppler, E., B. Drolias, M. Fraenz, A. Korth, M.K. Reuss, B. Blake, and J.J. Quenby, The high latitude pass of ULYSSES: energetic particle observations with EPAC, *Astron. Astrophys.*, *316*, 464, 1996.

Kissmann, R., H. Fichtner, and S. E. S. Ferreira, The influence of CIRs on the energetic electron flux at 1 AU, *Astron. Astrophys.*, *419*, 357, 2004.

Kojima, M., H. Washmimi, H. Misawa, and K. Hakamada, Solar wind observed within 0.3 AU with interplanetary scintilation, in *Solar Wind*, edited by E. Marsch, and R. Schwenn, *Pergamon Press., New York*, 201, 1991.

Kóta, J., and J. R. Jokipii, Effects of drift on the transport of cosmic rays. VI – A three-dimensional model including diffusion, *Astrophys. J., 265*, 573, 1983.

Kóta, J., and J. R. Jokipii, The role of corotating interaction regions in cosmic-ray modulation, *Geophys. Res. Lett., 18*, 1797, 1991.

Kóta, J., and J. R. Jokipii, 3D distribution of cosmic rays in the outer heliosphere, *Proc. 24th Inter. Cosmic Ray Conf. (Rome), 4*, 670, 1995.

Kóta , J., and J. R. Jokipii, 3-D simulation of heliospheric transport: A comparison of models, *Proc. 25th Inter. Cosmic Ray Conf. (Durban)*, *2*, 25, 1997.

Kóta , J., and J. R. Jokipii, Cosmic ray modulation and the structure of the heiospheric magnetic field, *Proc. 26th Inter. Cosmic Ray Conf. (Salt Lake City), 7*, 9, 1999.

Koyama, K., R. Petre, E. V. Gotthelf, U. Hwang, M. Matsuura, M. Ozaki, and S. S. Holt, Evidence For Shock Acceleration of High-Energy Electrons in the Supernova Remnant SN:1006, *Nature*, *378(6554/NOV16)*, 255, 1995.

Krieger, A. S., A. F. Timothy, and E. C. Roelof, A Coronal Hole and Its Identification as the Source of a High Velocity Solar Wind Stream, *Solar Physics*, *29*, 505, 1973.

Krüger, T. P. J., The effects of a Fisk-Parker hybrid magnetic field on cosmic rays in the heliosphere, *M.Sc. dissertation, North-West University (Potchefstroom Campus), South Africa*, 2005.

Kunow, H., B. Heber, M. S. Potgieter, S. E. S. Ferreira, R. Müller-Mellin, Ulysses COSPIN/KET Observations of Jovian Electrons during the Distant Ulysses Jupiter Flyby,*Proc. Sol. Wind 11*, 2005.

L'Heureux J., and P. Meyer, Quiet-time increases of low-energy electrons - The Jovian origin, *Astrophys. J.*, *209*, 955, 1976.

Lange, D., Simulation der Modulation Kosmischer Strahlung über einen solaren Zyklus, *Ph.D. thesis, Institut für Thoeretische Physik IV Weltraum- und Astrophysik Ruhr-Universität Bochum, Germany*, 2004.

Lange D., H. Fichtner, and R. Kissmann, Time-dependent 3D modulation of Jovian electrons comparing with Ulysses/KET observations, *Astron. Astrophys., 449*, 401, 2005

Langner, U. W., Effects of different local interstellar spectra on the heliospheric modulation of cosmic rays, *M.Sc. dissertation, Potchefstroom University for CHE, South Africa*, 2000.

Langner, U. W., Effects of termination shock acceleration on cosmic rays in the heliosphere, *Ph.D. Thesis, Potchefstroom University, South Africa*, 2004.

Langner, U. W., O. C. de Jager, and M. S. Potgieter, Proposed local interstellar spectra for cosmic ray electrons, *Proc. 2Th Inter. Cosmic Ray Conf, Hamburg*, 4, 3992, 2001a.

Langner, U. W., O. C. de Jager, and M. S. Potgieter, On the local interstellar spectrum for cosmic ray electrons, *Adv. Space Res., 27(3)*, 517,2001b.

Langner, U. W., M. S. Potgieter, H. Fichtner, and T. Borrmann, Modulation of anomalous protons: Effects of different solar wind speed profiles in the heliosheath, *J. Geophys. Res., 111*, 2006b.

Langner, U. W., and M. S. Potgieter, Heliospheric modulation of cosmic rays computed with new local interstellar spectra, *Proc. 27th Inter. Cosmic Ray Conf, Hamburg, 4*, 3686, 2001c.

Lapidus, L., and G. F. Pinder, Numerical solution of partial differential equations in science and engineering, *Wiley, New York*, 1982.

Lemmer, M., Die invloed van die interpleenitêre magneetveld op die daaglikse variasie van kosmiese strale, *M.Sc. dissertation, Potchefstroom University for CHE, South Africa*, 1982.

Longair, M. S., Cosmic rays and the Galactic radio background emission, in *Low Frequency Astrophysics from Space*, Springer-Verlag, 227, 1990.

Lopate, C., Jovian and galactic electrons (2-30 GeV) in the heliosphere fiom 1 to 50 AU, *Proc. 23rd Inter. Cosmic Ray Conf., Calgary, 3*, 415, 1991.

Marsch, E., Kinetic physics of the solar wind plasma, in *Physics of the Inner Heliosphere*, edited by R. Schwenn and E. Marsch, Springer-Verlag, Berlin, *45*, 1991.

Marsch, E., W. I. Axford, and J. F. McKenzie, Solar wind, in dynamic Sun, edited by B. N. Dwivedi, *Cambridge University Press, Cambridge*, 374, 2003.

Marsden, R. G. (Ed.), The High Latitude Heliosphere, *Space Sci. Rev., 72(1/2)*, 1995.

Marsden, R. G. (Ed.), The 3-D Heliosphere at Solar Maximum, *Space Sci. Rev., 97(1-4)*, 2001.

Marsden, R. G., The intrepid heliospheric explorer, *Physics World*, 6(11), 36, 1993.

McComas, D.J., S. J. Bame, B. L. Barraclough, W. C. Feldman, H. 0. Funsten, J. T. Gosling, P. Riley, R. Skoug, A. Balogh, R Forsyth, B. E. Goldstein, and M. Neugebauer, Ulysses return to the slow solar wind, *Geophys. Res. Lett., 25*, 1, 1998.

McComas, D. J., Ulysses observations of the three-dimensional solar wind over the solar cycle and their implications for the outer heliosphere, *EOS, 81*, F983, 2000.

McComas, D. J., H. A. Elliot, and R. Von Steiger, Solar wind from high-latitude coronal holes at solar maximum, *Geophys. Res. Lett., 29*(9), 28, 2002a.

McComas, D. J., H. A. Elliot, J. T. Gosling, D. B. Reisenfield, R. M. Skoug, B. E. Goldstein, M. Neugebauer, and A. Balogh, Ulysses' second fast-latitude scan:

Complexity near solar maximum and the reformation of polar coronal holes, *Geophys. Res. Lett.*, *29(9)*, 4, 2002b.

McDonald, F. B., T. L. Cline, and G. M. Simnett, Multifarious temporal variations of low-energy relativistic cosmic ray electrons, *J. Geophys. Res.*, *77*, 2213, 1972.

McKibben, R. B., Three-dimensional Solar Modulation of Cosmic Ray and Anomalous Components in the Inner Heliosphere, *Space Sci. Rev., 83*, 21, 1998.

McKibben, R. B., Cosmic-ray diffusion in the inner heliosphere, *Adv. Space Res., 35*, 518, 2005.

McKibben, R. B., J. J. Connell, C. Lopate, M. Zhang, J. D. Anglin, A. Balogh, S. dalla, T. R. Sanderson, R. G. Marsden, M. Y. Hofer, H. Kunow, A. Posner, and B. Heber, Ulysses COSPIN observations of cosmic rays and solar energetic particles from the South Pole to the North Pole of the Sun during solar maximum, *Ann. Geophys., 21*, 1217, 2003

Mewaldt, R. A., E. C. Stone, and R. E. Vogt, Observations of Jovian electrons at 1 AU, *J. Geophys. Res.*, *81*, 2397, 1976.

Minnie J., An ab initio approach to the heliospheric modulation of galactic cosmic rays, *Ph.D. Thesis, North-West University, South Africa*, 2006.

Moeketsi, D. M., Modelling of galactic and Jovian electrons in the heliosphere, *M.Sc. dissertation (Potchefstroom Campus), South Africa*, 2004.

Moeketsi, D. M., M. S. Potgieter, S. E. S. Ferreira, B. Heber, H. Fichtner, and V. K. Henize, The heliospheric modulation of 3-10 MeV electrons: Modeling changes in the solar wind speed in relation to perpendicular polar diffusion, *Adv. Space Res., 35(4)*, 597, 2005.

Morioka, A., F. Tsuchiya, and H. Misawa, Modulation of Jovian electrons by solar wind, *Adv. Space Res., 20*, 209, 1997.

Moses, D., Jovian electrons at 1 AU: 1978-1984, *Astrophys. J., 313*, 471, 1987.

Ndiitwani, D. C., A study of the modulation of galactic time-dependent cosmic rays in the heliosphere, *M.Sc. dissertation, North-West University (Potchefstroom Campus), South Africa,* 2005.

Ndiitwani, D.C., S.E.S. Ferreira, M.S. Potgieter, and B. Heber, Modelling cosmic ray intensities along the Ulysses trajectory, *Ann. Geophys., 23*, 1061, 2005.

Neugebauer, M., P. C. Liewer, E. J. Smith, R. M. Skoug, and T. H. Zurbuchen, Sources of the solar wind at solar activity maximum, *J. Geophys. Res., 107*, SSH13-1, 2002.

Neugebauer, M., and P. C. Liewer, Creation and destruction of transitory coronal hole and their fast solar wind streams, *J. Geophys. Res., 108*, SSH3-1, 2003.

Nolte, J.T., Coronal holes as source of solar wind, *Solar Physics., 46*, 303, 1976.

Odstrcil, D., Modeling 3-D solar wind structure, *Adv. Space Res., 32(4)*, 497, 2003.

Parker, E. N., Cosmic ray modulation by the solar wind, *Physical Rev., 110*, 1445, 1958.

Parker, E. N., Dynamics of the interplanetary space and magnetic fields, *Astrophys. J., 128*, 664, 1958.

Parker, E. N., The passage of energetic charge particles through interplanetary space, *Planet. Space Sci., 13*, 9, 1965.

Philips, J. L., A. Balogh, S. J. Bame, B. E. Goldstein, J. T. Gosling, J. T. Hoeksema, D. J. McComas, M. Neugebauer, N. R. Sheeley, and Y. M. Wang, Ulysses at 50^0 south: constant immersion in the high-speed solar wind, *Geophys. Res. Lett., 21(12)*, 1105, 1994.

Philips, J. L., S. J. Bame, B. L. Barraclough, W. C. Feldman, B. E. Goldstein, J. T. Gosling, G. W. Hoogeveen, D. J. McComas, M. Neugebauer, and S. T. Suess, Ulysses solar wind plasma observations from pole to pole, *Geophys. Res. Lett., 22(23)*, 3301, 1995.

Potgieter, M. S., The modulation of galactic cosmic rays as described by a three-dimensional drift model, *Ph.D thesis, Potchefstroom University for CHE, South Africa*, 1984.

Potgieter, M. S., and H. Moraal, A drift model for the modulation of galactic cosmic rays, *Astrophys. J., 294*, 425, 1985.

Potgieter, M. S., The heliospheric modulation of galactic electrons: consequences of new calculations for the mean free path of electrons between 1 MeV and 10 GeV, *J. Geophys. Res., 101*, 24411, 1996.

Potgieter, M. S., The modulation of galactic cosmic rays in the heliosphere: Theory and models, *Space Sci. Rev., 83 (1/2),* 147, 1998.

Potgieter, M. S., and H. Moraal, A drift model for the modulation of galactic cosmic rays, *Astrophys. J., 294*, 425, 1985.

Potgieter, M. S., L. J. Haasbroek, and B. Heber, The modelling of the latitude dependence of cosmic ray protons and electrons in the inner heliosphere, *Adv. Space Res., 19* (6), 917, 1997.

Potgieter, M. S., S. E. S. Ferreira, and B. Heber, The heliospheric modulation of cosmic ray electrons: Rigidity dependence of the perpendicular diffusion coefficient, *Proc. 26th Inter. Cosmic Ray Conf. (Salt Lake City)., 7*, 57, 1999a.

Potgieter, M. S., S. E. S. Ferreira, B. Heber, P. Ferrando, and A. Raviart, Implications of the heliospheric modulation of cosmic ray electrons observed by Ulysses, *Adv. Space Res., 23(3)*, 467, 1999b.

Potgieter, M. S., G. S. Nkosi, S. E. S. Ferreira, B. Heber, and D. M. Moeketsi, Electron anisotropies in the inner heliosphere: A theoretical perspective, *Proc. 29th Inter. Cosmic Ray Conf, Pune: 2,* 109, 2005

Rastoin, C., Jovian and galactic electrons in the heliosphere: Observations of the KET experiment on board the Ulysses spacecraft, *Ph.D. Thesis, Universify of Paris VII, France*, 1995.

Richardson, J. D., C. Wang, and K. I. Paularena, The solar wind: From solar minimum to solar maximum, *Adv. Space Res., 27(3)*, 471, 2001.

Roelof, E. C., G. M. Simnett, and S. J. Tappin, The regular structure of shock-accelerated ~ 40-100keV electrons in the high latitude heliosphere, *Astron. and Astrophys., 316*, 418, 1996.

Scherer, K., and S. E. S. Ferreira, A heliospheric hybrid model: Hydrodynamic plasma flow and kinetic cosmic ray transport, *ASTRA, 1*, 17, 2005.

Schlickeiser, R., On the interplanetary transport of solar cosmic rays, *J. Geophys. Res., 93,* 2725, 1988.

Schlickeiser, R., Cosmic ray Astrophysics, Springer, Germany, 2002.

Schwenn, R., The average solar wind in the inner heliosphere: Structures and slow variations, in *Solar Wind five*, edited by M. Neugebauer, *NASA CP-2280*, 489, 1983.

Sheeley, N. R., Y. M. Wang, S. H. Hawley, G. E. Brueckner, K. P. Dere, R. A. Howard, M. J. Kooman, C. M. Korendyke, D. J. Michels, S. E. Paswaters, D. G. Socker, O. C. St. Cyr, D. Wang, P. L. Lamy, A. Llebaria, R. Schwenn, G. M. Simnett, S. Plunkett,

and D. A. Biesecker, Measurements of Flow Speeds in the Corona between 2 and 30 R_{sun}, *Astrophys. J., 484*, 472, 1997.

Simpson, J. A., Cosmic radiation: Particle astrophysics in the heliosphere, in Frontiers in cosmic physics: Symposium in memory of Serge Korff, edited by R. B. Mendell, and A. J. Mincer, *New York Academy of Sciences, New York*, 97, 1992.

Simpson, J. A., The cosmic radiation: Reviewing the present and future, *Proc. 29th Inter. Cosmic Ray Conf, Durban*: Invited, Rapporteur & Highlighted Papers, 4, 1997.

Simpson, J. A., D. Hamilton, G. Lentz, R. B. McKibben, A. Mogro-Campero, M. Perkins, K. R. Pyle, A. J. Tuzzolino, and J. J. O'Gallagher, Protons and electrons in Jupiter's magnetic field: Results from the university of Chigago experiment on Pioneer 10, *Science, 183(4122)*, 306, 1974.

Simpson, J. A., J. D. Anglm, A. Balogh, J. R. Burrows, S. W. H. Cowley, P. Fenando, B. Heber, R. J. Hynds, H. Kunow, and R. G. Marsden, Energetic charged-particle phenomena in the Jovian magnetosphere - First results from the ULYSSES COSPIN collaboration, *Science, 257(5076)*, 1543, 1992a.

Simpson, J. A., J. D. Anglin, A. Balogb, M. Bercovitcb, J. M. Bouman, E. E. Budzinski, J. R. Burrows, R. Carvell, J. J. Connell, R. Ducros, P. Ferrando, J. Firth, M. Garcia-Munoz, J. Henrion, R. J. Hynds, B. Iwers, R. Jacquet, H. Kunow, G. Lentz, R. G. Marsden, R. B. Mckibben, R. Müller-Mellin, D. E. Page, M. Perkins, A. Raviart, T. R. Sanderson, H. Sierks, L. Treguer, A. J. Tuzzolino, K. P. Wenzel, and G. Wibberenz, The Ulysses cosmic ray and solar particle investigation, *Astron. Astrophys. Supp. Series, 92(2)*, 365, 1992b.

Smith, C. W., and J. W. Bieber, Solar cycle variation of the interplanetary magnetic field spiral, *Astrophys. J., 370*, 435, 1991.

Smith, E. J., The Sun, solar wind and magnetic field. I, in *Proceeding of the International School of Physics "Enrico Fermi" Course CXLII*, edited by B. Coppi, A. Ferrari, and E. Sindoni, *IOS Press., Amsterdam,* 179, 2000.

Smith, E. J., The heliospheric current sheet, *J. Geophys. Res.,106*(A8), 15819, 2001.

Smith, E. J., R. G. Marsden, A. Balogh, G. Gloeckler, J. Geiss, D. J. McComas, R. B. McKibben, R. J. MacDowall, L. J. Lanzerotti, N. Krupp, H. Krueger, and M. Landgraf, The Sun and heliosphere at solar maximum: Review, *Science, 302*, 1165, 2003.

Snodgrass, H. B., Magnetic rotation of the solar photosphere, *Astrophys. J., 270*, 288, 1983.

Stawicki, O., On solar wind magnetic fluctuations and their influence on the transport of charge particles in the heliosphere, *Institut für thoeretische Physik IV Ruhr-Universität Bochum*, 2003.

Stone, E. C., A. C. Cummings, and W. R. Webber, The distance to the solar wind termination shock in 1993 and 1994 from observations of anomalous cosmic rays, *J. Geophys. Res., 101(A5)*, 11017, 1996.

Stone E. C., A. C. Cummings, F. B. McDonald, B. C. Heikkila, N. Lal, and W. R. Webber, Voyager 1 Explores the Termination Shock Region and the Heliosheath Beyond, *Science, 309*, 2017, 2005.

Suess, S .T., J. L. Phillips, B. E. Goldstein, M. Neugebauer, and S. Nerney, The solar wind-Inner heliosphere, *Space Science Rev., 83*, 75, 1998

Tanimori, T., T. Hayami, S. Kamesi, S. A. Dezeley, P. G. Edwards, S. Gunji, S. Hara, T. Hara, J. Holder, A. Kawachi, T. Kifune, R. Kita, T. Konishi, A. Masaike, Y. Matsubara, T. Matsuoka, Y. Mizumoto, M. Mori, M. Moriya, H. Muraishi, Y. Muraki, T. Naito, K. Nishijima, S. Oda, S. Ogio, J. R. Patterson, M. D. Roberts, G. P. Rowell, K. Sakurazawa, T. Sako, Y. Sato, R. Susukita, A. Suzuki, R. Suzuki, T. Tamura, G. J. Thornton, S. Yanagita, T. Yoshida, and T. Yoshikoshi, Discovery of TeV Gamma Rays from SN 1006: Further Evidence for the Supernova Remnant Origin of Cosmic Rays, *Astrophys. J., 497,* L25, 1998.

Teegarden, B. J., F. B. McDonald, J. H. Trainor, W. R. Webber, and E. C. Roelof, Interplanetary MeV electrons of Jovian origin, *J. Geophys. Res., 79,* 3615, 1974.

Teufel, A., and R. Schlickeiser, Analytic calculation of the parallel mean free path of interplanetary cosmic rays I. Dynamical magnetic slab turbulence and random sweeping model, *Astron. Astophys., 393*, 703, 2002.

Tsuchiya, F., A. Moroika, and H. Misawa, Jovian electron modulations by the solar wind interaction with the magnetosphere, *Earth Planets Space, 51*, 987, 1999.

Thomas, B. T., and E. J. Smith, The structure and dynamics of the heliospheric current sheet, *J. Geophys. Res., 86,* 11105, 1981.

van Niekerk, Y., An investigation into the causes and consequences of north-south asymmetries in the heliosphere, *M.Sc. dissertation, Potchefstroom University for CHE*, South Africa, 2000.

Wenzel, K. P., Ulysses - it's status and prospects, *Adv. Space Res., 13(6)*, 275, 1993.

Whang, Y. C., and L. F. Burlaga, Anticipated Voyager crossing of the termination shock, *Geophys. Res. Lett., 27(11),* 1607, 2000.

Wilcox, J. M., and N. F. Ness, Quasi-stationary co rotating structure in the interplanetary medium, *J. Geophys. Res., 70*, 5793, 1965.

Williams, T., The influence of the wavy heliospheric neutral sheet on the modulation of cosmic rays (in Afrikaans), *M.Sc. dissertation, Potchefstroom University for CHE, South Africa*, 1990.

Zirker, J. B., Coronal holes: An overview, in coronal holes and high speed wind streams, edited by J. B. Zirker, *Colorado Associated Univ. Press., Colorado,* 1, 1977.

Acknowledgements

I wish to thank the following:

- Prof. Marius Potgieter (my supervisor) for his leadership, motivations and assistance. I would like to thank him for giving me more insight on this field.
- Dr. Stefan Ferreira (my assistant supervisor) for his useful discussions and assistance on various occasions.
- Mr. Donald Ngobeni and Mr. Chris Ndiitwani for their friendship and useful discussions.
- Mr. Mathew Holleran for his assistance on computer related problems and queries.
- Mrs. Anne Mans and Dr. Ulrich Langner for their assistance to enable me to use the IBM RS/6000 SP computer.
- The Unit for Space Physics at North-West University (Potchefstroom Campus), the South African National Research Foundation and the Department of Labour of South Africa for financial support.
- Mrs. Petro Sieberhagen and Mrs. Lizelle le Roux for all their administrative assistance.
- Miss. Ntobeko Dladla for the understanding, motivation and believing in me.
- Mr. Daniel Moeketsi, Freddy Rathai, Mr Golden Nyambuya, Mr Isak Davids, Mandla Nkosi and Oscar Monama for their friendship and motivation.

A special thanks to:

- My parents John and Esther for everything
- My sisters Ntombifuthi and Nonhlanhla for being there during hard times.
- God, for letting me study a small portion of his magnificent creation.

Acknowledgements

I wish to thank the following:

- Prof. Marius Potgieter (my supervisor) for his leadership, motivations and assistance. I would like to thank him for giving me more insight on this field.
- Dr. Stefan Ferreira (my assistant supervisor) for his useful discussions and assistance on various occasions.
- Mr. Donald Ngobeni and Mr. Chris Ndiitwani for their friendship and useful discussions.
- Mr. Mathew Holleran for his assistance on computer related problems and queries.
- Mrs. Anne Maas and Dr. Ulrich Langner for their assistance to enable me to use the IBM RS/6000 SP computer.
- The Unit for Space Physics at North-West University (Potchefstroom Campus), the South African National Research Foundation and the Department of Labour of South Africa for financial support.
- Mrs. Petro Siebenhagen and Mrs. Lizelle le Roux for all their administrative assistance.
- Miss. Nkobeko Dlada for the understanding, motivation and believing in me.
- Mr. Daniel Mocketsi, Freddy Ratlai, Mr Golden Nyambuya, Mr Isak Davids, Mandla Nkosi and Oscar Monama for their friendship and motivation.

A special thanks to:

- My parents John and Esther for everything
- My sisters Nkombiluth and Nonhlanhla for being there during hard times.
- God, for letting me study a small portion of his magnificent creation.